UNIVERSITY OF NAIROBI

FACULTY OF ENGINEERING

DEPARTMENT OF ENVIRONMENTAL AND BIOSYSTEMS ENGINEERING

Shear Strength Behaviour of Vertisols : Case of Rice Growing in Mwea Irrigation Scheme

F56/76900/2009

Gordon Ochieng Nyakiti - Bsc. (Hons.), Agric.Eng., UoN, (1998)

A Thesis submitted in partial fulfillment for the award of the Degree of Master of Science in the Department of Environmental and Biosystems Engineering of the University of Nairobi.

November 2022

DECLARATION

I hereby declare that this thesis is my original work and to the best of my knowledge has not been presented in any other university for examination.
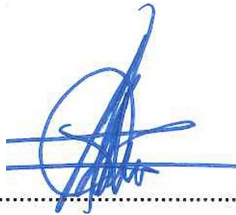
22nd November 2022

....
F56/76900/2009   Date
Gordon Ochieng Nyakiti

This thesis has been submitted for examination with our approval as University supervisors.

22-11-2022

....
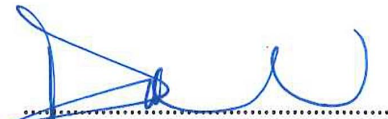Eng. Prof. Ayub N. Gitau (PhD)   Date

Department of Environmental and Biosystems Engineering,

University of Nairobi.

22nd November 2022

....
Eng. Daniel A. Mutuli (M.Phil)   Date

Department of Environmental and Biosystems Engineering,

University of Nairobi.

DEDICATION

This thesis work is dedicated to my Wife, Elizabeth and daughters who kept my spirit alive during the challenging moments of being a student, parent and a professional worker.

ACKNOWLEDGEMENT

TABLE OF CONTENTS

LIST OF TABLES

LIST OF FIGURES

LIST OF APPENDICES

ACRONYMS AND SYMBOLS

a.   Letters and Numbers

w   Soil Water Content, %

H   Thrust Force, N

A   Contact Area, m2

C   Cohesion, kPa

W   Load/Weight, N

V   Volume, m3

q   Deviatoric Stress, kPa

K   Darcy's Coefficient of Permeability, m/s

R^2 Coefficient of determination/correlation

i   Hydraulic Gradient

Fn   Normal Force, N

X,Y&Z Coordinates in Three Directional Axes

E   Modulus of Elasticity/Young's Modulus, N/m^2

p   Mean Normal Stress, kPa

u   Pore Pressure, kPa

C_c Compression Index, %

b.   *Subscripts*

n   Normal

x   X Direction

y   Y Direction

z   Z Direction

1   Top Layer

2   Middle Layer

3   Bottom Layer

c.   *Greek Notations*

Φ   Angle of internal friction, ᵒ

ρ_t Density of soil mass, kg/m^3

Ϥ   Shear Stress, kPa

σ_n Normal Stress, kPa

ε_x Linear Strain in X Direction

ε_y Linear Strain in Y Direction

ε_z Linear Strain in Z Direction

Δ Change

υ Poisson's Ratio

γ_{zx} Angle of distortion, Radians

ε_{zx} Pure Shear Strain

σ_1 Major Principal Stress, kPa

σ_2 Intermediate Principal Stress, kPa

σ_3 Minor Principal Stress, kPa

θ Angle of Inclination, $^{\circ}$

ß   Angle of obliquity

LIST OF ABBREVIATIONS

AASHO	American Association of State Highway Officials
AL	Atterberg Limits
ASAE	America Society of Agricultural Engineers
ASTM	America Society for Testing and Materials
CD	Consolidated Drained
CU	Consolidated Undrained
FMRC	Farm Mechanization Research Centre
ILCA	International Livestock Centre for Africa
ISRIC	International Soil Reference and Information Centre
JICA	Japan International Cooperation Agency
KRD	Karaba Disturbed
KRU	Karaba Undisturbed
KSS	Kenya Soil Survey
MWD	Mwea Disturbed
MWU	Mwea Undisturbed
LL	Liquid Limit
MOA	Ministry of Agriculture
NCPB	National Cereals and Produce Board
NIA	National Irrigation Authority
NIB	National Irrigation Board
NICHE	Netherlands Initiative for Capacity Development in Higher Education
PI	Plasticity Index
PL	Plasticity Limit
TBD	Tebere Disturbed
TBU	Tebere Undisturbed

THD	Thiba Disturbed
THU	Thiba Undisturbed
USCS	Unified Soil Classification System
USDA	United States Department of Agriculture
WMD	Wamumu Disturbed
WMU	Wamumu Undisturbed

ABSTRACT

Rice growing vertisol soils at Mwea Irrigation Scheme in Kenya are routinely subjected to dry ploughing prior to establishment of a new crop. During ploughing, the soil experiences varying levels of induced shear stress emanating from the weight of the working machinery which are mostly self-propelled tractors as well as soil engaging plough components. Characteristics response/behaviour of the vertisols under these loading variabilities is not only significant in influencing resultant traction developed but also tillage operation performances.

The objective of this research study was to assess the shear stress behaviour of rice growing vertisols at Mwea Rice Irrigation Scheme with a view to manipulating resultant shear stress parameters at empirically established magnitudes for optimal tillage and traction operations. Collected samples (disturbed and undisturbed) from the study field were triaxially tested through successive three phases of saturation, isotropic consolidation and shearing based on critical state soil mechanics principles. Deviatoric stress – strain plots to establish shear strengths of samples from three profile depths (0 - 20, 20 – 40 and 40 – 60 cm) over varied water contents were developed. The study established that three patterns deformation characteristic occurred in vertisols when subjected to loading from working tillage machinery. A predictive exponential model satisfactorily correlated deviatoric stress – strain response pattern of the the study soil. Cohesive strength that is believed to represent maximum cohesive force holding soil particles together was established at 70 kPa with a corresponding frictional angle of 3^0. Thus, maximum traction with optimal tillage performances on vertisols at Mwea Irrigation Scheme are likely to be achieved by operating tillage machinery at a cohesive force and frictional angle just above 70 kPa and 3^0 respectively. Consequently, any tillage tractor with a tractive effort above 70 kPa is optimal for use by farmers and tractor hire service providers on rice growing vertisols in Mwea Irrigation Scheme.

Key Words: Vertisol; Stress – strain; Traction; Tillage; Working machinery; Isotropic consolidation; Critical state; Deviatoric stress; Profile depth

1.0 INTRODUCTION

1.1 Background

In Kenya, rice is the third staple crop after maize and wheat. Its consumption rate has been growing steadily with a likelihood of overtaking wheat in the near future. Local annual production is estimated at between 230,000 – 250,000 metric tons against estimated consumption of 620,000 metric tons as per National Irrigation Authority (NIA) Annual Report (2021). The deficits is met through imports.

About 95% of the rice in the country is grown under irrigation in paddy schemes managed by the NIA. The rest is rainfed and found in Kwale, Kilifi and Tana River Counties at the Coast as well as Teso Sub - Counties in Western Kenya. The 95% of paddy rice under NIA is grown on vertisol soils that occur on very gentle undulating to flat topography in Kenya (KSS, 2009). This is characteristic of Mwea, Ahero and West Kano Irrigation Schemes. Due to the heavy nature of these rice growing vertisol soils, workability and trafficability on the soil is difficult. Besides, enormous amounts of water is required under wet rice tillage (paddy system) as is practized. Previous studies by Bhagat *et al*., (1996) reported that more than 5,000 litres of water is used to produce a unit kg of rice. Out of this amount, a significant portion is used in land preparation during land soaking phase as huge water losses occur through cracks inherent in the vertisols before saturation level is attained.

The variabilities in the behaviour of vertisol soil at Mwea present formidable challenges under wet (puddling) and dry ploughing activities. During puddling or wet tillage, porosity distribution markedly changes with both storage and residual porosity increasing at the expense of transmission porosity (Bhagat, 2003). On the one hand, the scenario is different in dry ploughing that usually precedes puddling. During dry ploughing , the soil is subjected to vertical (normal stress) arising from the weight of the working machinery whereas the soil engaging plough component that moves within the dry soil experience horizontal resistance/stress attributable to interparticle friction and grain interlocking of the contact soil. According to Holtz and Kovacs (1981) the interactions between the resultant vertical and horizontal stresses within the soil mass produce a non-hydrostatic stress state that contains the all-important shear stress. This shear stress is critical as it determines traction (driving force) developed by the working machinery whose tyres/tracks are in contact with the soil. Further, the contact pressure acting on such tyre bearing surface reflects the relationship between the tyre and the soil in terms of the soil stress from the tractor wheels (Bauer *et al.,* 2022).

Rice growing vertisol soils at Mwea Irrigation Scheme are routinely subjected to dry ploughing prior to establishment of a new crop. As a result, they experience varying levels of induced shear stresses

depending on the weight of the operating machinery. Since there is a limit to how much shear stress a particular soil can support without failing/deforming, this study intends to establish these critical limits for the rice growing vertisol soils within Mwea Irrigation Scheme. Further, establishment of these limits shall ensure that full advantage of the strength of study soil is taken at a certain level of slip (soil displacement) where traction is optimum hence maximum work output in terms of dry ploughing (Bryan *et al*., 1986). Overall, the information obtained will also form a useful basis upon which appropriate vertisol soil management regime relating to good tillage and traction practices will be made.

1.2   Statement of Problem
Identification of the shear stress parameters influencing traction and tillage on vertisol will provide critical data that will inform selection of appropriate machinery (by weight) for use in tillage operations. Appropriate machinery here infers land preparation units that will develop maximum traction hence optimum work output when working on vertisol without creating detrimental slip. Presently, there is lack of empirically proven data on suitable weights of land preparation machinery in use on vertisol at Mwea. Consequently, this has led to the current phenomenon where heavy machinery or light ones are in use thus resulting in high draft power requirements coupled with damage to soil structure and low work output respectively.

1.3   Justification
The importance of vertisols for growth of rice crop cannot be gainsaid considering that it forms 95 % of the rice cropland under the management of NIA. Every crop season, the vertisols are subjected to external loading arising from machinery used in land preparation. Ideally, 87 % of land preparation in rice production is done by tractors while the remaining 13 % is accomplished by animal and manual labour (Tilakaratna, 2000). With a wide range of tractors of different sizes available in the market, the challenge facing farmers is how to select the most appropriate ones that will give greatest work output in terms of tillage and traction efficiency without destroying the soil structure. Similarly, the selected tractor unit should have optimum fuel consumption as well as field capacity.

As found out by Hua and Zhai (1985), fundamental shear strength parameters of soil which in this case is vertisol play a significant role in determining the desired thrust hence necessary traction required in tillage operations. It is therefore paramount that before selection of appropriate tillage machinery is made, knowledge on pertinent shear strength parameters i.e. cohesion, angle of internal friction, weight of the selected machinery amongst others be available. Inturn, proper understanding

of shear strength parameters of the vertisol shall enable their manipulation for attainment of efficient and optimal traction without damage to the soil physical structure.

1.4   Objectives

The broad objective of the study was to assess the shear stress behaviour of rice growing vertisols at Mwea. The specific objectives were to:

    i.   Develop analytical relationships between field tractors weights and the resultant/induced shear stress parameters in vertisols soils

    ii.   Analyse shear strength parameters of vertisols that influence tillage and traction

    iii.   Apply a mathematical model in correlating shear stress parameters in (i) and (ii) above.

1.5   Hypothesis

On the basis of above research objectives, the following two hypothesis were postulated for the study;

"Tillage and Traction are a function of pertinent vertisols parameters" and

"Shear strength parameters of vertisols influence the resultant tillage and traction".

1.6   Scope of Study

The scope of study was limited to triaxial analysis of shear stress parameters that influenced shear stress behavioural response of vertisols soil under varying loading conditions. Further, mathematical analysis was done on the generated parameters to make inferences on the extent of their influences on resultant traction and tillage operational performances.

2.0   LITERATURE REVIEW

2.1   Occurrences of Vertisols

2.1.1   Global Scale

According to International Soil Reference and Information Centre (ISRIC) Annual Report of 2020 – 21, vertisols occupy about 335 million ha (2.42 % of ice-free land) of land on earth out of which 150 million ha (48%) is potential cropland (Figure 2.1). They occur mainly in the tropics covering about 200 million ha (4 %) of land. Globally, 177 million ha (56 %) of the 335 million ha have ustic soil moisture regime and 89 million ha (27 %) have aridic soil moisture regime, frequently occurring on desert fringes. The largest deposits (more than 75 %) of Vertisols in the world occur in the humid tropics mainly in the Deccan plateau of India (79 million ha or 24 %), the Murray Darling basin of South East Australia (70 million ha or 21 %), the Gezira plain of Sudan (50 million ha or 15 %), the Blacklands of Texas (18 million ha or 6%), the East African Rift Valley and the Ethiopian Plateau region (13 million ha or 4 %), China (13 million ha or 4 %) and in Rio Plasta Basin of North Argentina (6 million ha or approx 2%). However, uncertainty of these estimate remain high since many countries are yet to be included in the inventory and some areas under Vertisols are often too small to resolve at the scale of a map
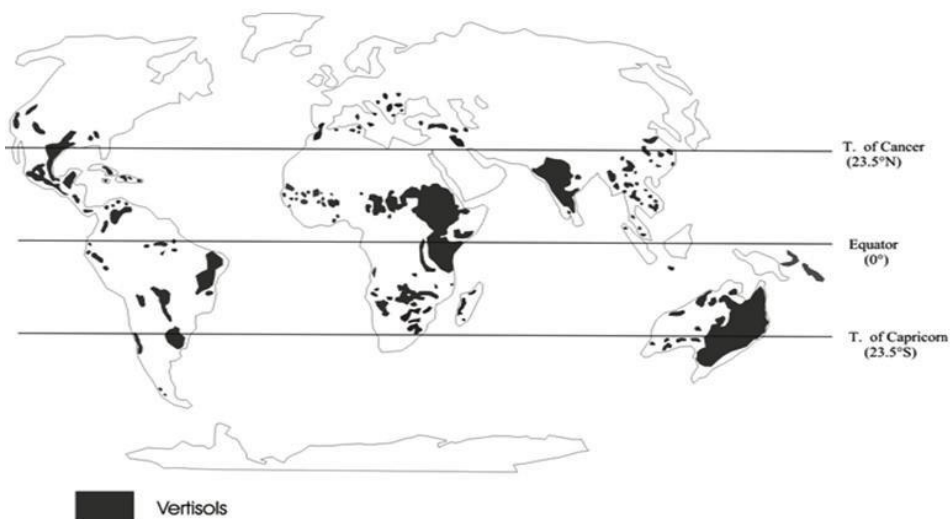
Figure 2-1: Global distribution of vertisols

2.1.2   National Distribution

In Kenya, vertisols and associated soils occupy approximately 2.8 million hectares or 4.9 % of the total land area (Figure 2.2). They are commonly referred to as ''black cotton soils'' or ''black

cracking clay soils''. They occur from the sea level to altitudes of about 2100 m and are scattered all over the country. In particular, vertisols occur extensively in the Athi Plains around Nairobi, Kano Plains in Kisumu County, Mwea in Kirinyaga County and North Eastern Kenya as reported by Scabroek *et al., (*1982) and Muchena and Pouns (1982).
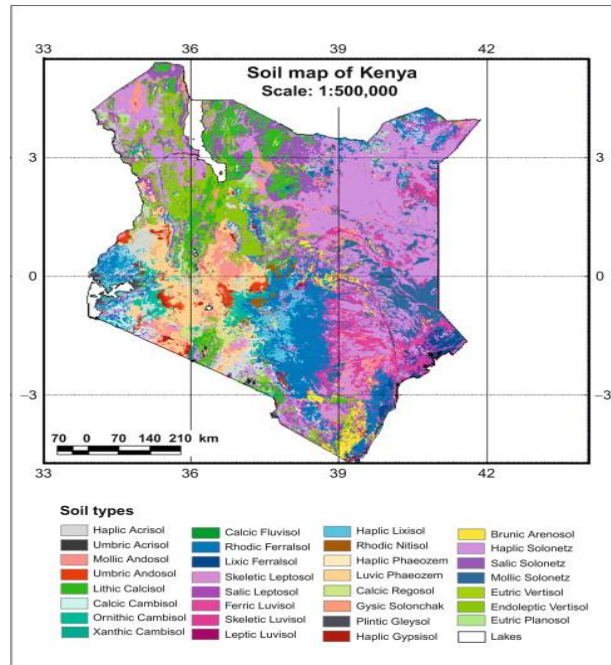
Figure 2-2: Major soil and data types in Kenya

2.1.3   Vertisols in Mwea

Like elsewhere in Kenya, vertisols at Mwea Rice Irrigation Scheme are generally suited for paddy rice production. The usual vertisol problems include impeded drainage, water – logging hence late post rain planting, run off and soil erosion, difficult tillage and unsuitable implements and low organic carbon and nitrogen (Macharia *et al.,* 2013). Within the scheme that has a about 30,350 acres of gazetted area, vertisols is the predominant soil (NIA Report, 2021). However, only 26,000 acres of the total gazetted area has been developed for paddy rice production. The remaining is used for settlement, public utilities, subsistence and horticultural crops farming. Meanwhile, the Kenyan Government in partnership with Japanese Government through its development arm Japan International Cooperation Agency (JICA) has successfully implemented a Ksh. 13 billion Mwea Irrigation Development Project from March 2018 to September 2022 (NIA Report, 2021). This is one of Kenyan Vision 2030 Flagship Projects that involved construction of 40 m tall and 1 km long Thiba Dam. The construction of the Dam has resulted in the expansion of scheme irrigable area by

5

another 22,000 acres within Kandongu and Mutithi Sections. With the completion of this project, vertisol soil coverage area within the scheme has increased tremendously.

2.2 Physical Properties of Vertisol Soils

Vertisol soils are mainly dark in colour, fine in texture, low in organic matter and alkaline or near alkaline in reaction (Dudal, 1965). They swell and shrink on alternate wetting and drying, and this results in distinct vertical cracking and a specific structure in which oblique slickensides define wedge shaped structural aggregate. In terms of particle size distribution, the soil particles have less than 0.002 mm diameter. Cracks formed on these soils run from the surface down into the profile, sometimes up to 1 metre. However, the soils lack distinct horizons in their profile and are generally described as AC – profiles.

According to Lambe's Hypothesis for structure in clays, if net electrical forces between adjacent soil particles at the time of deposition are attraction, a flocculated structure is obtained. Alternatively, if the net forces are repulsion, then a dispersed soil structure is formed. For fresh water clays like the case in Mwea Irrigation Scheme, the tendency towards flocculation is reduced with the particles assuming a higher degree of orientation (dispersed structure) hence relatively denser and less permeable. Meanwhile, the void ratios of dispersed clay are roughly in the range of 0.5 to 2 (Singh and Chowdhary, 2007).

Thus, while it is easy to have a direct observation of particles arrangement in coarse grained soils, the structure of clays (fine grained soils) can only be hypothesized. This implies that the structure of clays can only be inferred from other soil characteristics such as particle size, shape, nature and magnitude of forces operating in soil – water systems, and empirical relationships between soil structure and other soil properties such as density, compressibility, permeability and shear stress.

Soil density is computed as expressed in equation 2.1 below.

$$\rho_t = W/V \qquad\qquad [2.1]$$

Where W is total weight of soil mass, V is total volume of soil mass and ρ_t is density of the soil mass.

Meanwhile, permeability which is rate of water flow through the soil is given by Darcy Weisbach equation in 2.2.

$$q = AKi \qquad\qquad [2.2]$$

6

q – Rate of flow, A – Cross sectional area, i – Hydraulic gradient and K is Darcy's Coefficient of permeability or permeability of soil.

Similarly, compressibility property of the soil is expressed as in equation 2.3.

$$\text{av} = \frac{\Delta e}{\Delta p} \qquad\qquad\qquad [2.3]$$

Where av is co – efficient of compressibility, Δe is change in void ratio and Δp is change in pressure.

On shear stress which is a mechanical property of the soil, computation is obtained by Coulomb – Mohr equation in 2.4.

$$\tau = C + \sigma n \tan \Phi \qquad\qquad\qquad [2.4]$$

Where τ is shear stress, C is effective cohesion, σn is normal stress on failure plane and Φ is the angle of internal friction.

2.3 Tillage and Traction Practices on Vertisol Soils

Owing to characteristic behaviours of vertisol soils, tillage and traction practices should be undertaken in such away that there is less soil damage (less slip) while developing the requisite maximum traction (driving force).

2.3.1 Tillage

Tillage is the physical manipulation of soil with appropriate implements to loosen the surface soil layer. Igor *et al.,* (2019), further defined tillage as mechanical manipulation of physical conditions of soils. Its main objectives are to provide an ideal environment for plant growth, and specifically to prepare a seedbed which permits soil – water – air balance, provide good physical conditions for early root penetration and proliferation, incorporate preceeding crop residues and organic manures, destroy weeds and hibernating pest and disease organisms and facilitate proper soil chemical and microbial activities. However, soil water content at the time of tillage influences the particle sizes distribution of the resulting soil as found out by Ojeniyi and Dexter (1978). This occurs due to the fact that water changes in the soil significantly affects the strength of the soil and the mode of failure.

During tillage operations, the soil yields or moves. According to Gill and Van Berg (1967), the dominating parameters of the force system are cohesion, friction and adhesion. These are very useful parameters when predicting soil resistance of a drawn tillage tool (Kooen and Kuipers, 1983).

Additionally, the weight of the heavy tillage machinery compresses the soil, causing it to loose pore/void space. While the commonest causes of compaction on the soil is due to external loading (tillage machinery, grazing animals, draft animals, man, etc), lack of water in the soil may also induce compaction. Nevertheless, and as highlighted by Thomas *et al.,* (2019), soil compaction caused by vehicular traffic adversely affects key soil function and ecosystem services that soil provides.

Puddling or wet tillage for rice as practised in Mwea decreases total soil porosity only slightly, but markedly changes porosity distribution with both storage and residual porosity increasing at the expense of transmission porosity. In turn, rice response to tillage varies with soil texture and climatic water balances. Depending on the soil texture, tillage may induce again or loss in soil permeability. Sharma and Bhagat (1993) found out that in soils with less than 70 % sand, puddling as well as compaction are equally effective in decreasing water percolation to satisfactory levels for growing a good rice crop.

On drying after harvest of a rice crop, the Mwea vertisol soils shrink, become compact, hard and produce surface fissures of varying size and shape. Ploughing the dry and hard soil results in the formation of large clods having high breaking strength (Sharma and Bhagat, 1993) and consequently requiring large amounts of tillage energy and time before establishment of subsequent crop. Interactions among energy intenstive inputs tillage, irrigation and nutrients can be gainfully exploited to combat soil and management related stresses for improved crop performance. Bhagat *et al.*, (2003) indicated that energy inputs in a conventional tillage was about 276 kwh more than that in a no tillage system. Nonetheless, the former system produced more grains per unit of energy consumed. From the foregoing, it is imperative that an understanding on the shear stress and possibe deformation characteristics of vertisols is not only critical in explaining its mechanical behaviour but more importantly on selection of appropriate, optimal and specific tillage system to be adopted.

2.3.2   Traction

Traction refers to the driving force developed by the wheels or tracks in contact with soil. It largely depends on the shear strength of the soil in contact with the traction devices (wheels or tracks). Thus, puddled rice growing vertisol soils which are essentially wet do not have much strength hence traction/force is poor. On the other hand, when dry, these soils are stronger hence have better traction.

The shear strength of agricultural soil is derived from a combination of its cohesive strength and internal friction as reported by Bryan *et al.,* (1986). Wet clays have no internal friction but have cohesion which is not dependent on the load applied. Pure sand, derive their strength only from

internal friction which increases with the load applied to them. In most instances, agricultural soils do not fall simply into either classification (clay and sand) but are a mixture of each with sandy soils tending to respond to loading to increase their strength, and the strength of clay soils depending more on area that can be sheared.

During the conversion of soil strength into traction, some displacement of the soil particles by the tyre or track occurs. This displacement is referred to as slip and is dependent on the overall traction developed. The relationship between traction (force) and soil displacement (slip) for three categories of soils is presented in Figure 2.3.
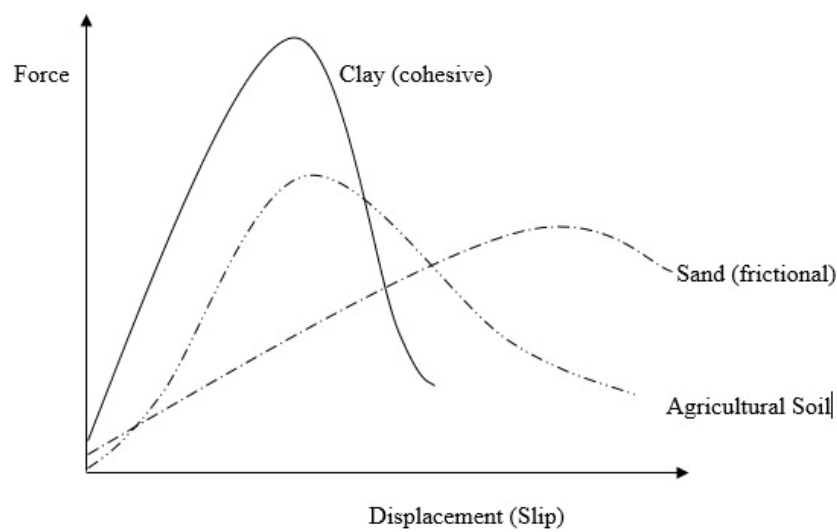
Figure 2-3: Relationship between force (traction) and displacement (slip)

Source: BRYAN, *et al.(1986)* Soil Management, 4th Edition, pg 109.

Figure 2.3 shows that full advantage of strength of the soil can only be taken at a certain amount of slip, and an increase in slip beyond this point reduces the traction that can be developed. It is therefore prudent that tractors in the field should certainly never be operated anywhere near the level of slip at which the traction declines, and compaction and shearing damage to the soil occurs well below this level.

A study conducted on farm mechanization in rice cultivation in Sri Lanka that compared performances of tractors of different engine sizes revealed distinct characteristics with respect to fuel consumption and field capacity as presented in the table below.

Table 2-1:Field capacity and fuel consumption of tractors vis-a-vis horse power
Source: FMRC 2000

Tractors' Power (HP)	Fuel Consumption (l/h)	Field Capacity (ha/08 hr day)	Field Capacity (ha/l of fuel)	Remarks
07	1.0	0.4	0.05	Walking Type – Two Wheel Tractor
12	1.4	1.0	0.09	Riding Type – Two Wheel Tractor
35	4.5	1.4	0.04	Four Wheel Tractor

From Table 2.1, the riding type – two-wheel tractor gives maximum work output per litre of fuel consumption thereby recommending its selection compared to the other two categories.

Apart from fuel consumption basis upon which the above illustrative selection is made, a more imperative selection is guided by vertisol properties. This arises from the fact that mobility and tractive efficiency of machinery or implements are influenced by shearing strength of the soil (Hua and Zhai, 1985), which ultimately determines the drawbar forces i.e. the difference between horizontal thrust and rolling resitance.

Whereas calculation of the soil thrust is difficult, the thrust force (H) under a given load (W) can be expressed as in equation 2.5;

$$H = Ac + W \tan \Phi \qquad\qquad [2.5]$$

Where, A is the contact area, c is cohesion (where it is 0 in cohesionless soils) and Φ is angle of internal friction

From equation 2.5, it follows that fundamental shear strength parameters of soil which in this case is vertisol play a significant role in determining the desired thrust hence necessary traction required in tillage operations. It is therefore paramount that before selection of appropriate tillage machinery is made, knowledge on pertinent shear strength parameters i.e. cohesion, angle of internal friction, weight of the selected machinery amongst others be available. Inturn, proper understanding of shear

strength parameters of the vertisol shall enable their manipulation for attainment of efficient and optimal traction without damage to the soil physical structure.

2.4   Shear Stress Behaviour of Soils
The response of any soil to applied loads denotes its behaviour. When loaded, soil produces reactionary internal forces/stresses of varied magnitude that may result in excessive deformation termed failure stresses. Since soil is a particulate material, occurrence of failure is primarily due to rolling and slipping of grains and not via simple tension or compression. Because of this failure mode, the stresses of interest are shear stresses while the soil resistance or soil strength of interest is the shear strength.

While most efforts to predict soil response to applied loads have relied on both elasticity and plasticity theories, the major limitation has been that the two theories are for elastic continuum whereas soil is an aggregation of particulate material (Feda,1982). Besides, soil is state dependent that is, it changes in volume with changes in water content and under stress (Brink *et al*., 1980). Any of these state changes produces a different material from what was started with. With the foregoing, it is apparent that a high degree of success in predicting soil deformation is a challenge (Scott, 1989).

Meanwhile, the complexities of soil behaviour have led to the development of a number of mathematical models to explain the different patterns of response to different combinations of stress (Srinivasa Murthy *et al*., 2008). The original elasto – plastic model for predicting soil behaviour/response under stress path was developed by Roscoe *et al*., (1958) and Schofield and Wroth (1968) and was called Original Cam – Clay Model. Since then, several versions of elasto – plastic models, which are essentially modifications or improvements of the original model have been developed. Nonetheless, the fundamental theory behind all these models remains the same. The only notable difference between the present modified/revised cam -clay models and the original cam – clay model is that the latter needed only five soil parameters while the former require a range of 25 – 35 parameters, most of which do not have physical meaning (Srinivasa Murthy *et al*., 2008).

A review of some background in understanding contemporary soil mechanics theory is presented herebelow:

2.4.1   Normal Stress

Brink *et al., (*1980) defined stress as the intensity of force per unit area. A normal stress is that which acts at right angle to any face or plane whereas shear stress on the other hand act parallel to the face. Thus, a normal stress therefore forces particles closer together or changes their state of packing or spatial distribution i.e. it compresses the fabric.

The normal stress is computed by equation 2.6 below.

$$\sigma_n = \frac{Fn}{A} \qquad\qquad [2.6]$$

where Fn - Normal Force acting on the plane

A - Area of the plane

σ_n - Normal Stress

Meanwhile, the normal linear strain along x direction (ε_x) is given by equation 2.7

$$\varepsilon_x = \frac{\Delta x}{X} \qquad\qquad [2.7]$$

Where X - Original length

Δx - Change in length

Strain in other directions (z and y axes) would be $\varepsilon_z = \Delta z /Z$ and $\varepsilon_y = \Delta y/Y$. From the two strains along x and z axes, a proportionality factor between the strains i.e. ε_x and ε_z that lies at right angle to each other gives the Poisson's Ratio (υ) expressed as equation 2.8 below;

$$\nu = {\varepsilon x}/{\varepsilon z} \qquad\qquad [2.8]$$

For incompressible materials like saturated clay i.e. puddled vertisol soils at Mwea which cannot drain immediately under initial application of a load, the theoretical value of $\nu = 0.5$. In non saturated, compressible soils, ν may be nearer 0.3. However, this ratio is often assumed to remain constant and independent of the magnitude of stress when soil is in elastic range. Also, Modulus of Elasticity (Young's Modulus) E links normal stress in one direction i.e. (σz) with strain in the same direction (εz) as presented in equation 2.9:

12

$$E = \frac{6z}{\varepsilon_z} \qquad\qquad\qquad [2.9]$$

E is also assumed to remain independent of magnitude of the stress in the elastic range i.e. deformation of the soil fabric in the direction of the normal stress is linearly related to the magnitude of the stress. Thus, it is assumed that the stress – strain behaviour of a soil in the elastic range is defined by Young's Modulus and Poisson's ratio.

2.4.2   Shear Stress

The strain produced by shear stress that acts parallel to the face or plane is manifested in the movement of particles over each other, which changes the orientation of domains and distorts the soil fabric (Alam, S. 2002). It also affects the volume. The *Engineers's Shear Strain* expressed in equation 2.10 refers to the angle of distortion γ_{zx} (in radians).

$$\gamma_{zx} = \frac{6x}{\triangle z} \qquad\qquad\qquad [2.10]$$

For some theoretical purposes, pure shear strain ε_{zx} is more convenient and is obtained from equation 2.11.

$$\varepsilon_{zx} = \frac{1}{2}\gamma_{zx} \qquad\qquad\qquad [2.11]$$

On the whole, it is evident from the foregoing that the effects of normal and shear stresses are quite different and produce different strains in the fabric with corresponding changes in soil volume. Whereas the normal stress forces particles closer together and thus enhances stability, shear stress on the other hand determines the resultant traction/ driving thrust/force developed by the operating tillage machinery.

2.5   Mohr's Strength Theory

According to Singh and Chowdhary (2007), Mohr's strength theory can be expressed in terms of three fundamental statements as follows:

(a)   Ultimate strength of a material is determined by the stresses in the planes of slip

(b)   The failure of a material is essentially by shear but the critical shear stress is governed by the normal stress on the potential failure plane and properties of the material

(c)   In a three-dimensional stress system, the magnitude of the intermediate principal stress has no effect on the strength of a material, or in other words, the failure criterion is independent of the intermediate principal stress.

On the basis of Mohr's strength theory therefore, shear stress (Υ) on any plane is given by equation 2.12.

$$\Upsilon = \sigma \tan \beta \qquad\qquad [2.12]$$

Where: σ is Normal Stress and β is angle of Obliquity.

2.6   Shear Strength of Soils

The shear strength of a soil refers to its maximum resistance to shearing stresses. In most cases, it is taken to be equal to the shear stress at failure on the failure plane. It is a function of :

(a)   Internal Friction or the resistance due to interlocking of particles and friction between individual particles at their contact points

(b)   Cohesion i.e. the resistance due to interparticle forces which tend to hold the particles together in a soil mass.

It can be represented by Coulomb – Mohr equation in 2.13:

$$\Upsilon_f = C + \sigma \tan \Phi \qquad\qquad [2.13]$$

Where σ is total normal stress on the failure plane, C is cohesion, Φ is angle of internal friction and Υ_f is the shear strength. While equation 2.13 assumes that the total normal stress governs the shear strength of soil, this is not always true. Thus, the strength (deformation) characteristics of soil are best governed by the principle of effective stress as postulated by Terzaghi. Terzaghi effective stress principle may be stated in the form of two propositions as follows:

Effective stress is the best available parameter to express certain aspects of the soil behaviour particularly the shear strength and compression

(a)   The effective stress σ' in a soil is equal to total applied stress σ minus pore pressure u.

2.7   Stress Patterns in Vertisols at Mwea

The stresses induced in the vertisols at Mwea Rice Irrigation Scheme emanate from the weights of tractors and soil engaging machinery working on the soil. These stresses are essentially transferred

14

to the soil through the tyres in contact with it. Past studies by Bryan *et al., (*1986) have experimentally verified and calculated the stress effects of tyres on the soil. Figure 2.4 shows stress distribution in the soil beneath tractor tyres of varying weights but same tyre inflation pressure.

From Figure 2.4, it appears that stress tends to concentrate under the center line of the tyres i.e. load axis and the tendency is greater with increased moisture and reduced cohesion. This implies that the tendency becomes greater as the soil becomes weaker.
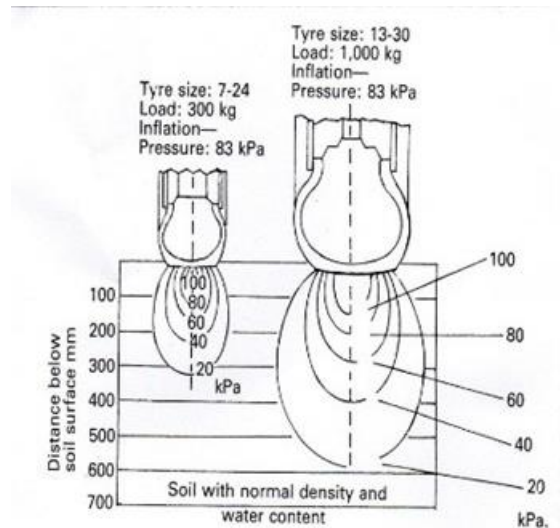
Figure 2-4: Stress distribution patterns in soil below tractor tyres
Source : *ASAE 1958*

Meanwhile, the region of maximum stress is not immediately at the tyre face but is some distance below the soil surface. The actual depth at which this maximum stress occurs increases chiefly with increasing moisture content but also with surface pressure and total wheel load. Further, Xuewen *et al.,* (2019) reported that increment in soil water content resulted in the reduction of loading time for the soil to reach critical limit. Also, while ground pressure is important for the maximum level of compaction involved, the depth to which compaction takes place depends on total wheel load i.e. tractor weight (Bryan *et al.,* 1986). Similarly, Dorthe *et al*., (2018), while determining the in-situ stress input and propagation due to tractors and harvesters wheeling on two South Brazilian soils established that lower tyre pressures strongly diminished contact pressure and principal stress in the soil. This trend is in agreement with the findings made by Loraine *et al.,* (2020) that in order to reduce soil stress, tyre design and use should allow for a large contact area and low inflation pressure. Besides tyre design, Frantisenk *et al.*, (2022) added that proper suspension of the plough during tillage can achieve sustantial changes in the contact pressure under the rear wheels of a plough tractor.

The implication of these observed phenomenon is that tyre sizing alone cannot fully eliminate the load effects (tractor weights) on soil thereby necessitating the need for synchronization of tractors weights with requisite vertisol shear stress parameters in order to achieve optimal but nondestructive traction and tillage practices during rice cultivation.

2.8   Summary of Literature Review

In line with Mohr's strength theory, failure of a material is essentially by shear stress and this occurs when the resultant induced stresses reach critical state or limiting value. Consequently, for effective and optimal management of traction and tillage practices on paddy rice growing vertisols at Mwea, knowledge and determination of the magnitudes of these shear stresses are pre-requisites in understanding the soil behaviour hence prevention of undesired failures or soil deformation during cultivation. Since internal friction or the resistance due to interlocking of particles as well as friction between individual particles at their contact points is proportional to the normal force which tends to push the particles together, an increment in normal force will lead to a corresponding increment in the shear force.

Application of varying axial loads comparable to tractor weights on vertisol specimens under triaxial compression tester will yield test data such as axial strain, volume strain, deviator stress, etc for each level of axial load. Analysis of the test data in turn will generate the desired shear stress parameters and subsequently interpretation of their influence on traction and tillage practices. This information shall guide selection of tillage machinery with appropriate weights that result in maximum traction and work output without high draft power requirements or detrimental slip. Presently, data on these selection guide parameters are not available.

3.0   THEORETICAL FRAMEWORK

3.1   Shear Stress Parameters

The vertisol soil at Mwea are essentially contractive. As the soil contracts due to confining pressures, it becomes denser and thus acquire greater peak strength. However, the rate of contraction decreases until a critical void ratio (e) is achieved beyond which no more contraction occurs. In line with Mohr's Strength Theory, at the critical state (void ratio), the shear stress on the failure plane (Υ_{crit}) is determined by the effective normal stress on the failure plane (σ_n) and critical state friction angle (Φ_{crit}) and expressed by the equation 3.1 below:

$$\Upsilon_{crit} = \sigma_n \tan \Phi_{crit} \qquad\qquad [3.1]$$

On the other hand, the peak strength of the soil may be greater due to interlocking of soil grains and expressed as in equation 3.2

$$\Upsilon_{peak} = \sigma'_n \tan \Phi'_{peak} \qquad\qquad [3.2]$$

Notwithstanding the two equations above, Coulomb proposed that the shear strength (Υ_f) of soil may be expressed as a combination of cohesion (C) and internal angle of friction (Φ) as indicated in equation 3.3

$$\Upsilon_f = C + \sigma'_n \tan \Phi' \qquad\qquad [3.3]$$

Whereby C and Φ parameters are not fundamental soil properties but are dependent on soil type, water content, laboratory testing and field loading conditions. While equation 3.3 above infers that total normal stress determines the shear strength of the soil, this inference does not always hold. Accordingly, the strength characteristics of soil are best governed by the Principle of effective stress as formulated by Karl Terzaghi and expressed in equation 3.4

$$\Upsilon_f = C' + (\sigma - u) \tan \Phi' \qquad\qquad [3.4]$$

Where: C' = Effective Cohesion Intercept

                Φ' = Effective internal angle of friction

                σ = Total applied stress

                u   = Pore pressure

3.2   Three Dimensional Stress State Analysis

Normally, under field conditions, soil is subjected to stresses in three dimensions. Consider stresses that surround a small cube within the soil mass. Forces acting on each face of the imaginary cube can be resolved into normal and shear stresses as shown in Figure 3.1. It is however, possible to define a particular cube with its axes oriented such that no shear stresses act on any of its faces. The planes

of these faces are known as the *Principal Planes* in the soil mass and the normal stresses acting on them are termed *Principal Stresses* designated as *σ_1, σ_2 and σ_3*.
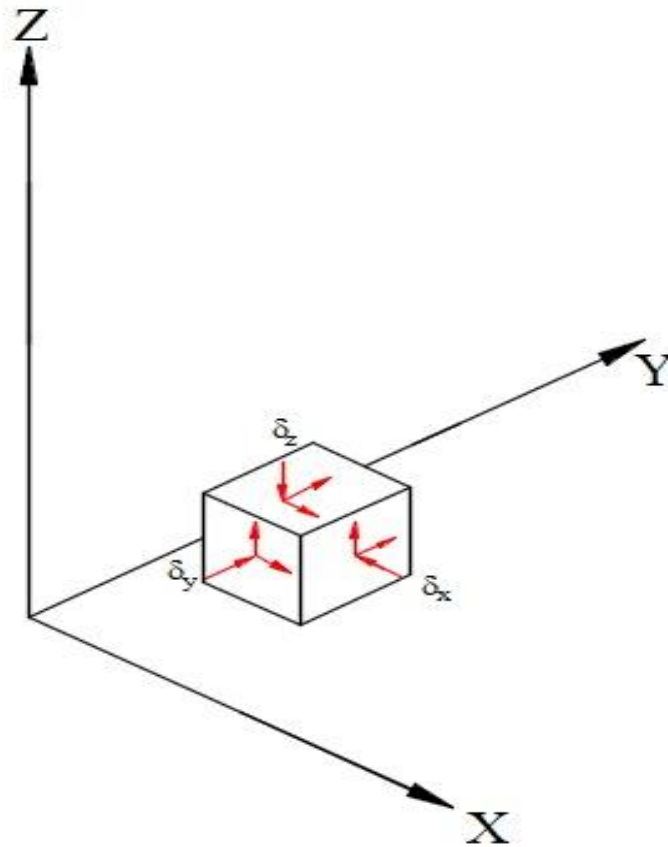
Figure 3-1: Three-dimensional stress state

Where:

      σ_1 is the Major Principal Stress,

      σ_2 is Intermediate Principal Stress and

      σ_3 is Minor Principal Stress.

The above three principal stresses are illustrated in Figure 3.2.

Z

Y

σ_1

σ_2

σ_3

X
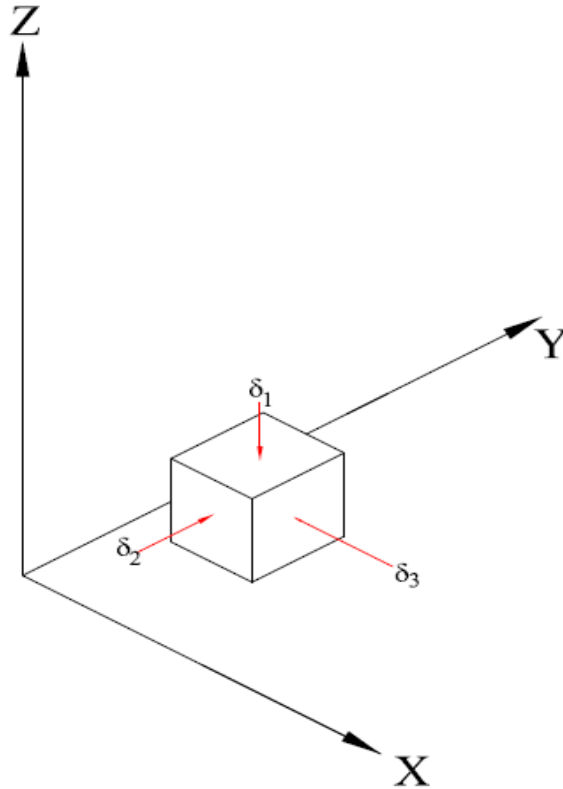
Figure 3-2: Principal stresses acting on a body

A corresponding matrix notation of the three principal stresses is given in equation 3.5.

$$\begin{vmatrix} \sigma_{11} & \sigma_{12} & \sigma_{13} \\ \sigma_{21} & \sigma_{22} & \sigma_{23} \\ \sigma_{31} & \sigma_{32} & \sigma_{33} \end{vmatrix} \qquad [3.5]$$

The major and minor principal stresses are the largest and smallest in magnitude of the three normal stresses and the difference between them is deviator stress (q) expressed in equation 3.6;

$$q = \sigma_1 - \sigma_3 \qquad [3.6]$$

The deviator stress in equation 3.6 is proportional to the maximum shear stress in the soil mass. In addition, the mean stress (p) is the average of the three principal stresses presented in equation 3.7.

$$p = \tfrac{1}{3}(\sigma_1 + \sigma_2 + \sigma_{3)} \qquad [3.7]$$

For differentiation between interparticle and total stresses, a notation of p, q or σ are used to represent effective stresses hence equations 3.6 and 3.7 become:

$$q = \sigma_1 - \sigma_3 \qquad\qquad p = \frac{1}{3}(\sigma_1 + \sigma_2 + \sigma_{3)}$$

3.3 Shear Stress Analysis by Mohr Circle

Mohr (1882) devised a graphical method for finding the normal and shear stresses on a plane perpendicular to the intermediate principal plane and inclined at an angle θ to the major principal plane as indicated in Figure 3.3.
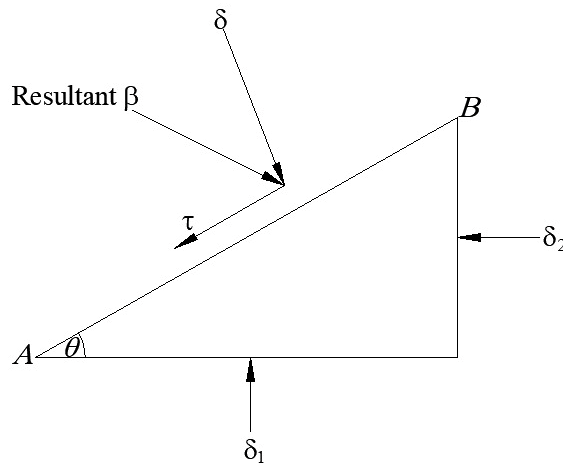
Figure 3-3: Two-dimensional stress systems

In line with Mohr's method of stress analysis, a system of coordinates axes shown in Figure 3.4 is established in which x – axis represents the normal stress while y axis represent shear stress.
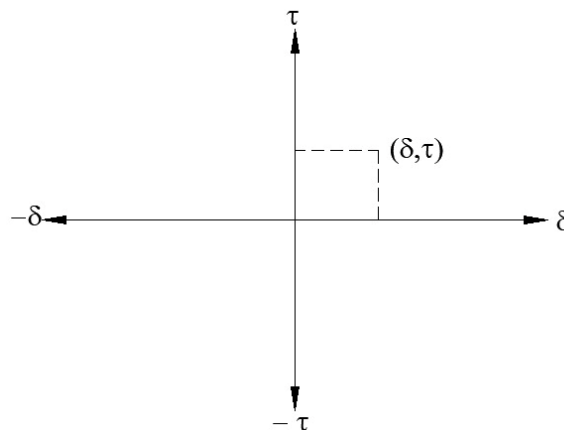
Figure 3-4: Mohr's Coordinates

In the coordinate system, the origin of stress is 0. Compressive normal stress is conventionally taken as positive and tensile stress negative. When principal stresses σ_1 and σ_3 are plotted on the x-axis as shown in Figure 3.5, a circle can be drawn with its centre F on the x-axis and cutting the x – axis at the abscissae of σ_1 and σ_3. The drawn circle has a radius of $\frac{(\sigma_1 - \sigma_3)}{2}$ and it usually suffices to draw only the upper half of the circle. Tangential lines drawn to the circles and intersecting the

shear strength/y – axis and inclined at angle to the horizontal will yield the shear strength parameters of cohesion and angle of internal friction. The intersection value on the y – axis will be the cohesion while angle of inclination to the horizontal line with be the angle internal friction,
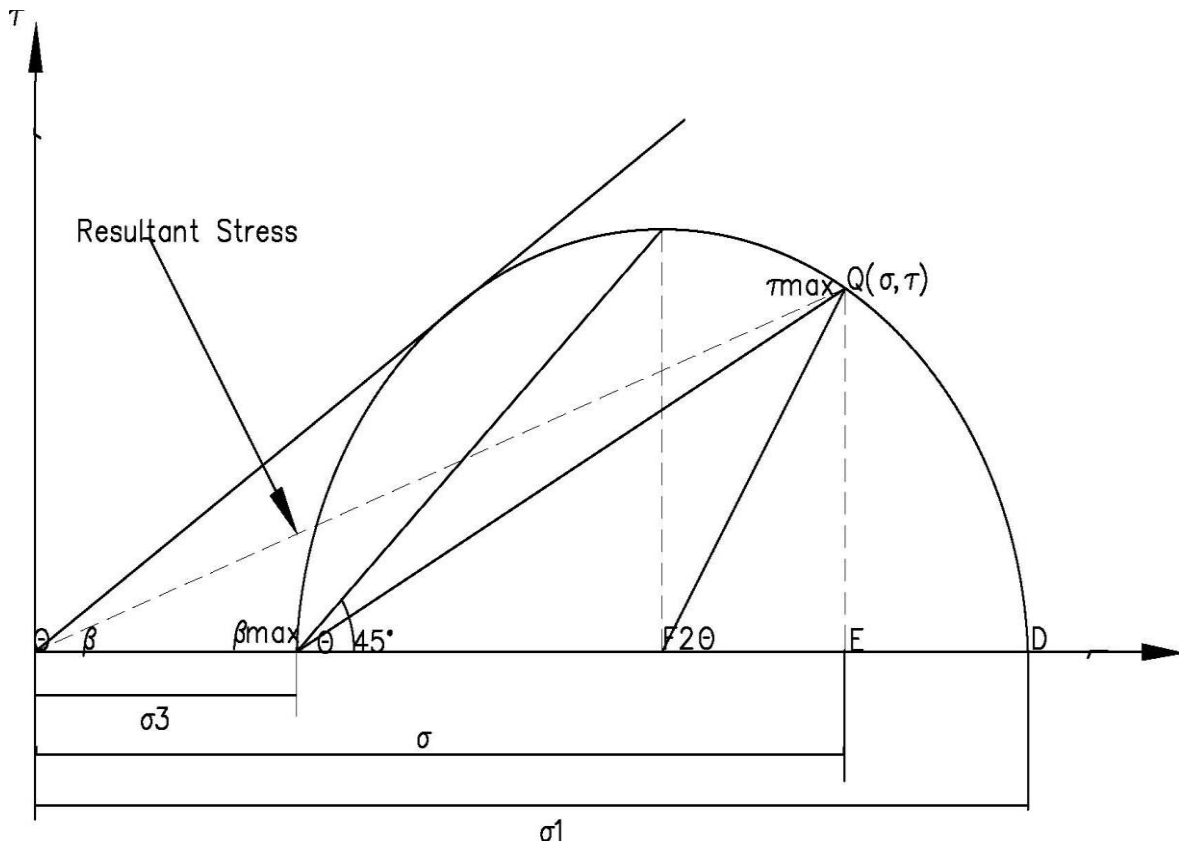
Figure 3-5: Mohr Circle
Source: Venkatraman,C*(2006)* Geotechnical Engineering, 3rd Edition, pg 257.

3.4   Triaxial Tester Data Relationships

Triaxial compression of test specimens simulated the actual field loading conditions on paddy rice growing vertisol at Mwea Irrigation Scheme. The generated data from triaxial testing were axial stress (σ_1), confining stress (σ_3), strain(ε) and Mohr's circles for every samples tested from which shear strength parameters of cohesion (c) and angle of internal friction (Φ) were evaluated and subsequently presented as in equation 3.3. Axial stress on the test specimen due to axial load applied represented the major principal stress while confining stress arising from all round fluid in triaxial cell denoted minor principal stress. The difference between the major and minor principal stresses was deviatoric stress (q) as illustrated in equation 3.6. The shapes of deviatoric stress – strain plots denoted shear stress behaviour of the tested soil specimens. Meanwhile, in triaxial conditions, the minor principal stress is taken to be equal to intermediate principal i.e. intermediate principal stress does not affect failure conditions

4.0 METHODOLOGY

4.1 Overview

The scope of the research study entailed experimental analysis of the shear strength parameters of paddy rice growing vertisols at Mwea Irrigation Scheme. Specifically, the desired shear strength parameters empirically tested and evaluated were internal angle of friction (Φ) and cohesion (C). Although simulating actual in situ soil conditions (undisturbed) status was difficult, great efforts were made to obtain sample specimens as close as possible to the undisturbed state during collection at the selected sites. Similarly, disturbed (remoulded) soil sample specimens were also collected and subjected to laboratory testing procedures.

Actual sample collections was done in every one hectare piece of land from the five sections of the scheme. The sections were Mwea, Tebere, Wamumu, Thiba and Karaba. A typical representative experimental sample collection lay out site is presented in Figure 4.1. Within the lay out site, two points were traversely located for sample collections – one point for undisturbed samples and the other for disturbed samples. Samples were collected from three profile depth zones ranging from 0 – 20 cm (top profile depth), 20 – 40 cm (middle profile depth) and 40 – 60 (bottom profile depth) as illustrated in Figure 4.2. In each depth profile, three samples were collected to produce a total of nine samples from each collection point for both disturbed and undisturbed samples using auger and stainless-steel tubes respectively.
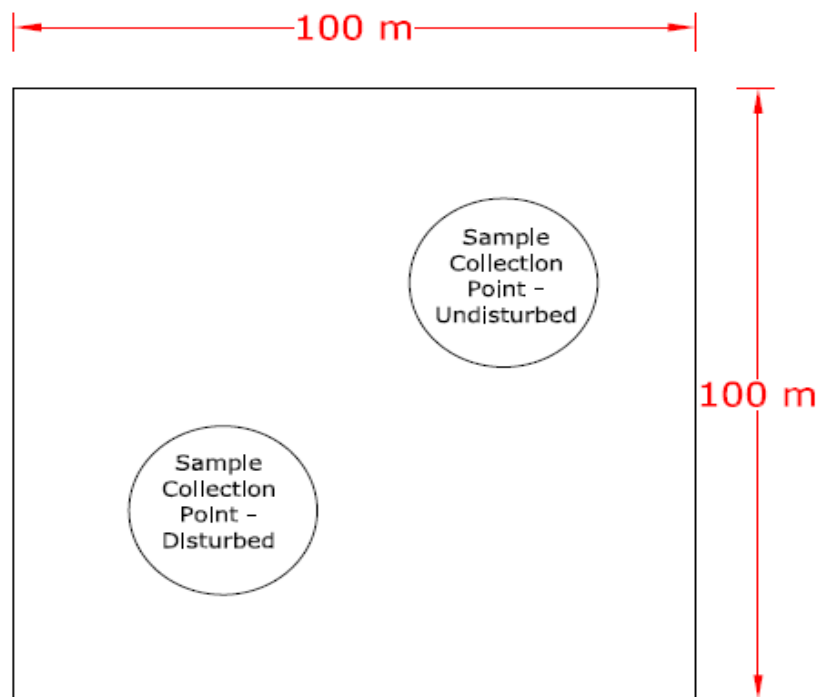
Figure 4-1: Experimental lay out of representative sample collection site
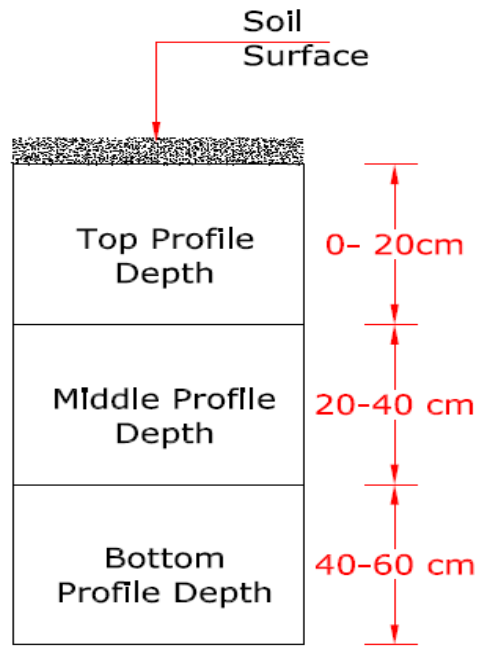
Figure 4-2: Soil profile depth zones

4.2 Experimental Procedure

4.2.1 Experimental Condition

Drainage conditions to which vertisol sample specimens are subjected during testing significantly influenced the test results. Therefore, test results obtained are as good and reliable as the correct drainage conditions used. For this study, consolidated undrained test was performed as it simulated closely the natural response of vertisols when exposed to external loading under operating tractors. This was attested to by the fact that distribution of stresses in the soil under tractor tyres occurred in decreasing magnitude upto a depth of 60 cm as illustrated in Figure 2.4. Thus, any void water within this depth would naturally be drained under the effect of normal stress emanating from tractor load until full consolidation was achieved. This informed the selection of the consolidated undrained test for the experiment.

4.2.2 Experimental Method

Four commonly used methods for determining shear strength parameters of soils are (i) Direct Shear Test (ii) Triaxial Compression Test (iii) Unconfined Compression Test and (iv) Vane Shear Test. Among these four methods, the most preferred one is the Triaxial Compression Test due to several merits over the rest. The merits include complete control over the drainage of specimens and performing all the three test conditions on all soil types, ability to precisely measure pore and volume changes during the test, uniform stress distribution on the failure plane and its adaptability to special

23

requirements as dictated by reasearch purposes. Nevertheless, its major drawback is its complexity. Owing to the highlighted strong attributes, Triaxial Compression Test in a Triaxial Tester was used in the study to analyse shear strength parameters of the rice growing vertisol soil specimens.

4.2.3   Triaxial Compression Tester

A triaxial compression tester equipment was used to obtain stress, strain and volume change data for soil sample specimens tested. Specifically, soil specimens of 38 mm diameter with a length twice this diameter was enclosed in a rubber membrane of about 0.1 to 0.4 mm in thicknesses. Since the membrane was thought to act as a reinforcing shell by slightly increasing the apparent strength of the specimen, this effect was corrected by subtracting from the compressive strength (deviator stress) of the test specimen. Meanwhile, vertical strains of the test specimens in the tester were measured from downward movement of the pistons thereby producing piston friction which was a source of error. To compensate for this error, the piston was lifted above the specimen when the cell pressure had built up while setting the dial gauge on the proving ring zero. A schematic diagram of the Triaxial Compression Tester is presented in Figure 4.3.
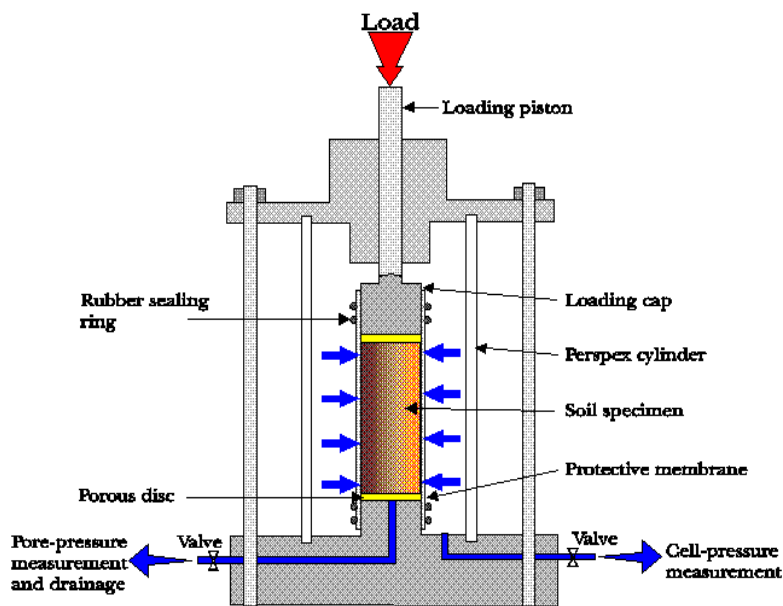
Figure 4-3: Triaxial compression tester

4.2.4   Sample Design

According to NIA Report (2021) , the study area had a total of 26,000 acres of irrigated paddy rice fields. This total area was therefore taken as the population/universe for the research study. The area was further divided into five sections namely Mwea, Thiba, Tebere, Wamumu and Karaba. Thus, the

sampling criteria adopted for this case was Area Random Sampling considering the five sections into which the scheme was divided as Clusters. From each of the five sections, a one ha piece of rice field was selected randomly from which requisite sample specimens for laboratory testing were obtained. This method of sample selection was preferred due to the homogenity in the spread of vertisols soils within the entire scheme as well as effectiveness in terms of cost and time.

4.2.5   Soil Specimens Collection

Soil specimens sampling was done from the selected rice fields identified in 4.2.4 within Mwea Irrigation Scheme. Since the ploughing depth averaged between $0 - 60$ cm, profiles sampled were obtained within this range. A total of five samples profiles from different sites within the selected fields were collected while ensuring that the chosen sites were atleast 10 m from the boundaries to prevent edge effects (due to the boundaries and human traffic) and 30 m from each other. Figure 4.4 presents a map of Mwea Irrigation Scheme with various sections from which study samples were collected.
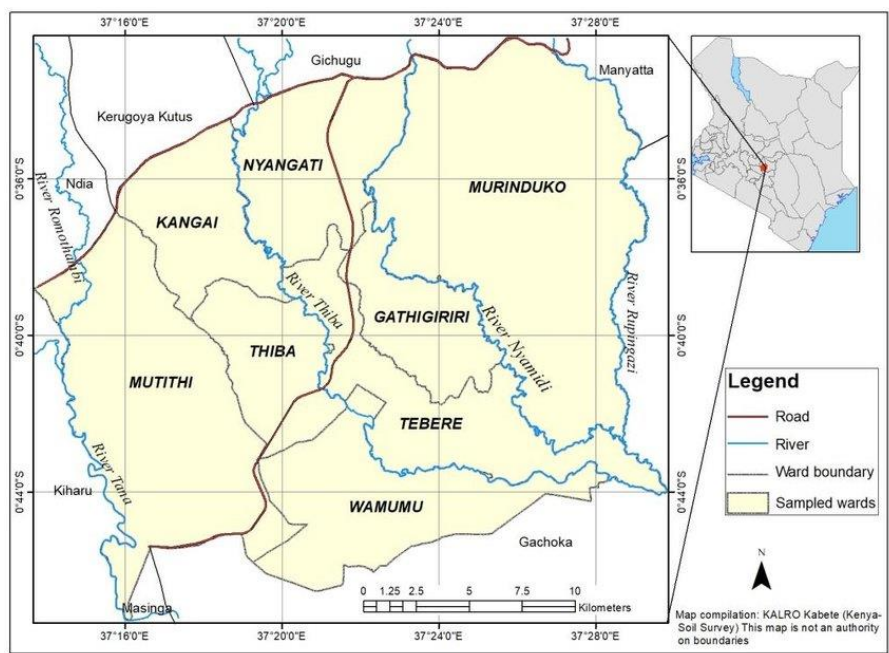
Figure 4-4: Map of Mwea Irrigation scheme with samples collection sections

Actual sample excavations were done by an auger using traverse method from the five profiles sites. This yielded 45 disturbed sample specimens i.e. 3 specimens per profile depth for three depths per profile site. Each augered sample was placed and sealed in a polythene sheeting to prevent moisture loss. On the polythene sheeting enclosure, the samples were well labelled with appropriate

25

abbreviations denoting the collection site section name, profile depth and number. These data were also entered into a common sampling sheet before placing all the polythene sealed samples into a clearly labelled sampling bag for onward delivery at the test laboratory.

Meanwhile, a similar number (45 specimens) for undisturbed samples were also obtained by use of sample rings as shown in Figure 4.5. These rings were made from stainless steel (SS) tubes and had 38 mm internal diameter and a height of 200 mm. They were driven vertically into the vertisol soils upto a depth of 60 cm. Afterwards, the rings were removed, trimmed, covered with plastic lids and sealed to prevent water loss. Nine rings were used for every sample site to cover the full soil profile lying within the average ploughing depth of 60 cm.

Figure 4-5: Undisturbed sample field collection

4.3   Laboratory Experiments

4.3.1   Soil specimens' preparation

For the collected undisturbed sample specimens, they were trimmed using a thin-walled tube to form the desired cylindrical vertical orientation. The cylindrical vertical specimen was then sized to the required diameter and height of 38 and 76 mm respectively. The masses were measured to the nearest 0.1 g followed by enclosure in the membrane ready for triaxial testing. Meanwhile, the remoulded (disturbed) collected sample specimen were compacted at the required condition of moisture/density in a suitable split mould. This was followed by cutting the ends plane

to form an upright cylindrical specimen orientation whose length, diameter and mass were measured to the nearest 0.5 mm and 0.1 g respectively.

4.3.2 Classification of the Study Soils

Physical characterization and classification of the soil was undertaken in terms of Consistency/Atterberg Limits and Particle Size Distribution using sedimentation analysis (Hydrometer Method). The use of these two methods is premised on the fact that in the latter method (Particle Size Distribution), soils with almost identical grain size distribution may widely differ in other physical properties hence the need to use Atterberg Limits (AL) to distinctly and comprehensively classify the soils. More importantly, AL are quite significant in respect to the behaviour of soils under load thus qualifying its use in classification of cohesive soils besides grain size distributioin.

i.   Soil Classification by Particle Size Distribution (Hydrometer Method)

Particle Size Distribution Method is essentially a Soil Textural Classification system that is based on the relative proportions of the different particle sizes in the soil mass. The respective percentages of the various particle sizes in the study soil and their corresponding textural classes according to United States Department of Agriculture (USDA) soil classification system using soil texturial triangle was determined.

ii.   Soil Classification by Consistency Limits

Plasticity tests was carried out on the tested soil samples in order to classify them using consistency limits/Atterberg limits. Using Unified Soil Classification System (USCS) plasticity criteria, the soils were classified accordingly.

4.3.3 Triaxial Testing of Sample Specimens

The consolidated undrained (CU) triaxial compression used in the study was performed in several successive stages as per ASTM D4767 – 04 Standard Test Method Procedures for cohesive soils. These stages are saturation, consolidation and shearing which were done for all the sample specimens. Each of the prepared sample specimens were encased in a rubber membrane using a membrane stretcher. Any air that was trapped between the membrane and specimen was sucked out before sealing the top cap by means of rubber O rings.

With the test specimen well placed in the cell chamber, de – aired water was admitted into the chamber while securing the loading ram by tightening the gland. The de-aired water provided the requisite confining pressure (6_3) - minor principal stress as the test was run. The machine however did not have provision for measuring pore pressures.

To simulate machinery field loading on vertisols during ploughing, compression of the soil specimens was done by setting the loading machine into action. The loading machine applied axial

compressions comparable to varying weights of different field working machinery i.e field tractors for the study. The axial loads were applied on the test specimens at a speed of 0.5 mm per min. For each subsequent cell pressures applied, simultaneous readings of axial deformation, axial stress (σ_1) were recorded. Meanwhile, cell /confining pressure (σ_3) and back pressure were raised in increment of 10 kPa and done in such away that the cell pressure always remained 5 kPa higher than the specimen back pressures.

At every level of cell pressure applied, the deviator stress (σ_d) was calculated for the 45 sample specimens in each category i.e. disturbed and undisturbed.

4.3.4   Constitutive Relations

Constitutive relations define mechanical behaviour of soil such as stress – strain and consequent effect due to their changes (Alam, 2002). Since real stress – strain relations for soils are normally complicated, often simplified models are used to describe these relations for a better understanding. In Triaxial tests, measured relations between stress and deformation are not all linear as found out by Koolen and Kuipers (1983).

4.4   Data Analysis

Analysis of experimental data obtained were done to make inferences of the relationsip that existed between various established parameters. Basically, the analysed data were of stress - strain relationships, shear strength parameters (obtained from mohr cirles) and critical state elastic and plastic parameters from modified cam clay model. To investigate the relationships phenomenon between these data, R statistical computing software program was used in the analysis and generation of the predictive models for deviatoric stress – strain relationships within elastic, shear strength and residual/failure stress deformation zones. Within the first elastic/recoverable deformation zone, a predictive model developed by Gitau et al., (2006) and expressed in equation 4.1 was chosen to correlate deviatoric stress (*q)* with strain *(ε).*

$$q = A\left[1 - \exp(-B\varepsilon)\right] \qquad\qquad [4.1]$$

A and B are the model parameters established for all the 30 experimental graphs while applying non linear regression principle when running the model in R programming language. Earlier researchers such as Bailey and Johnson (1989) and Zhang et al., (1998) used comparable models on different agricultural materials with satisfactory predictions.

5.0 RESULTS AND DISCUSSIONS

5.1 Physical Characteristics of the Study Soils

Physical characterization and classification was done for all the 15 soils samples obtained from 5 different profile sites at depths ranging from 0 – 20 , 20 – 40 to 40 – 60 cm and lying within A – horizon by particle size distribution (hydrometer method) as well as consistency /Atterberg limits.

5.1.1 Particle Size Distribution (Hydrometer Method)

All the profile depths i.e. (0 -20, 20 – 40 and 40 – 60 cm) had high average means of clay particles at 74 %, 75.2% and 73 % respectively (Table 5.1). Overall profiles mean for clay content was also high at 74.1 %. Silt particles within the soil mass accounted for 23.8%, 22.4 % and 23.8 % means for the three depths in increasing order. Meanwhile, sand contents were generally low at 2.2 %, 2.4 %, 3.2 % for the profile depths and 2.6 % for the overall profile depth. When all the 15 soil sample profiles contents (sand, clay and silt) were marked in the textural triangle, they all fell within the clay texture class region thereby confirming the soil as clay. From the foregoing findings, it is imperative to note that the soil has high clay content with many medium and small void spaces hence poor drainage potentials. It is due to this poor drainage phenomenon that Consolidated Undrained Triaxial Test was adopted in the experimental set up.

Table 5-1: Soil classification by particle size distribution (Hydrometer Method)

Samples Section Profiles	Sand (%)	Clay (%)	Silt (%)	Soil Textural Class/Grade
KR$_1$	2	78	20	Clay
KR$_2$	2	75	23	,,
KR$_3$	3	77	20	,,
MW$_1$	2	74	24	,,
MW$_2$	2	75	23	,,
MW$_3$	2	74	24	,,
TB$_1$	2	75	23	,,
TB$_2$	3	77	20	,,
TB$_3$	5	78	17	,,
WM$_1$	3	68	29	,,
WM$_2$	2	75	23	,,
WM$_3$	3	68	29	,,
TH$_1$	2	75	23	,,
TH$_2$	3	74	23	,,
TH$_3$	3	68	29	,,
Section Profiles Means				
1	2.2	74.0	23.8	Clay
2	2.4	75.2	22.4	Clay
3	3.2	73	23.8	Clay
Overall Profile Mean				
(0 - 60 cm)	2.6	74.1	23.3	Clay

USDA Soil Classification System – Using Soil Texture Triangle

NB: 1.   -   Represents Profile Depth Range of   0 – 20 cm
 2.   -   ,,   ,,   ,,   ,,   20 – 40 cm
 3   -   ,,   ,,   ,,   ,,   40 – 60 cm

5.1.2   Consistency Limits

Table 5.2 shows results of plasticity tests carried out on the tested soil samples under consistency/Atterberg limits. All the soils from section profiles exhibit high liquid limit (LL) with the profile means being 99.30%, 99.52 % and 100.80 % for the respective profile depths. In line with Unified Soil Classification System (USCS) developed in 1957, soils with more than 50 % LL are considered to be of high plasticity as the case in point here.

In particular, the soils were on average found to have plasticity indices (PI) of 51 %, 52.04 % and 53.96 % for the three profile depth ranges of between 0 – 20 cm, 20 – 40 % and 40 – 60 cm respectively. These findings conform to those established by Burmister (1947) where he classified any soil with more than 40 % PI as possessing very high plasticity. Meanwhile, Casagrande (1942) developed a plasticity chart that was later redesignated as the USCS in 1957 for correlating principal soil physical characteristics with the Atterberg Limits.

When the soils from the three different profiles depths are plotted on the Casagrande's plasticity charts as shown in Figures 5.1, 5.2 and 5.3, they are all found to fall well beyond the LL mark (50 %) but below the A Line within the region representing OH (Organic Clay) soil group. Consequently and in tandem with USCS, the study soils are therefore classified as fine grained Organic Clays of medium to high plasticity (OH) with colour. This is in agreement with the findings of Temga et al., (2022) while working on vertisols under seasonally contracted climate in Lake Chad Basin.

Table 5-2: Soil classification by consistency/atterberg limits

Samples Section Profiles	LL (%)	PL (%)	PI	C_c
KR$_1$	105.0	48.4	56.6	0.855
KR$_2$	105.3	47.0	58.3	0.858
KR$_3$	106.9	48.5	58.4	0.872
MW$_1$	93.4	44.3	49.1	0.751
MW$_2$	91.1	43.3	47.8	0.730
MW$_3$	93.4	42.1	51.3	0.751
TB$_1$	102.4	48.0	54.4	0.832
TB$_2$	105.9	49.5	56.4	0.863
TB$_3$	105.3	50.0	55.3	0.858
WM$_1$	103.8	52.6	51.2	0.844
WM$_2$	103.8	51.8	52.0	0.844
WM$_3$	104.4	50.0	54.4	0.850
TH$_1$	91.9	48.2	43.7	0.737
TH$_2$	91.5	45.8	45.7	0.734
TH$_3$	94.0	43.6	50.4	0.756
Section Profiles Means				
1	99.30	48.30	51.00	0.804
2	99.52	47.48	52.04	0.806
3	100.80	46.84	53.96	0.817
Overall Profile Mean (0 - 60 cm)	99.87	47.54	52.33	0.809

Where: LL – Liquid Limit, PL – Plastic Limit, PI - Plasticity Index and C_c – Compression Index

NB: 1 - Represents Profile Depth Range of 0 – 20 cm
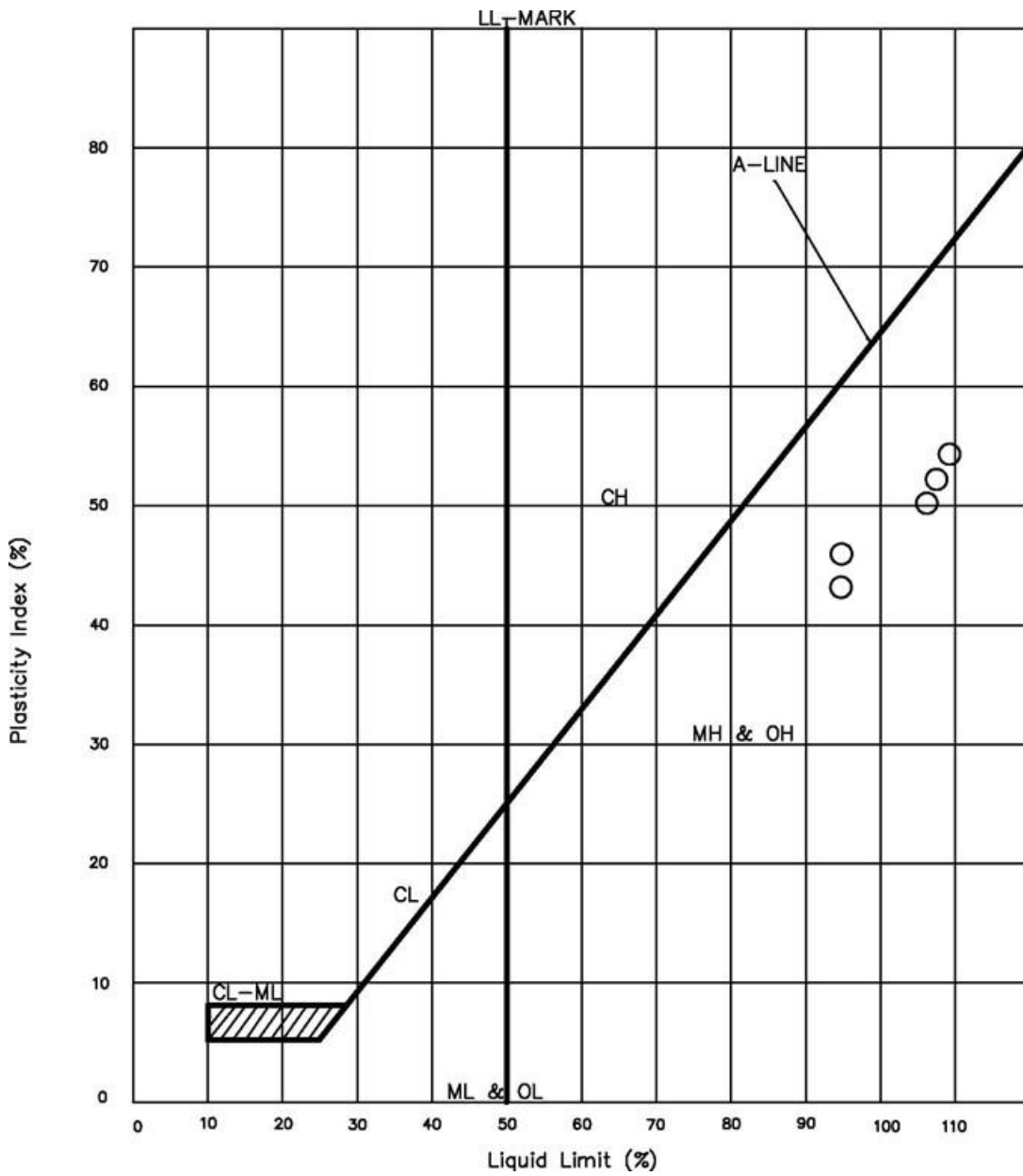
2 -   '' ''   ''   ''   '' 20 – 40 cm

3 -   ''   ''   ''   ''   '' 40 – 60 cm

Figure 5-1: Soil classification for samples from 0 – 20 cm profile depth
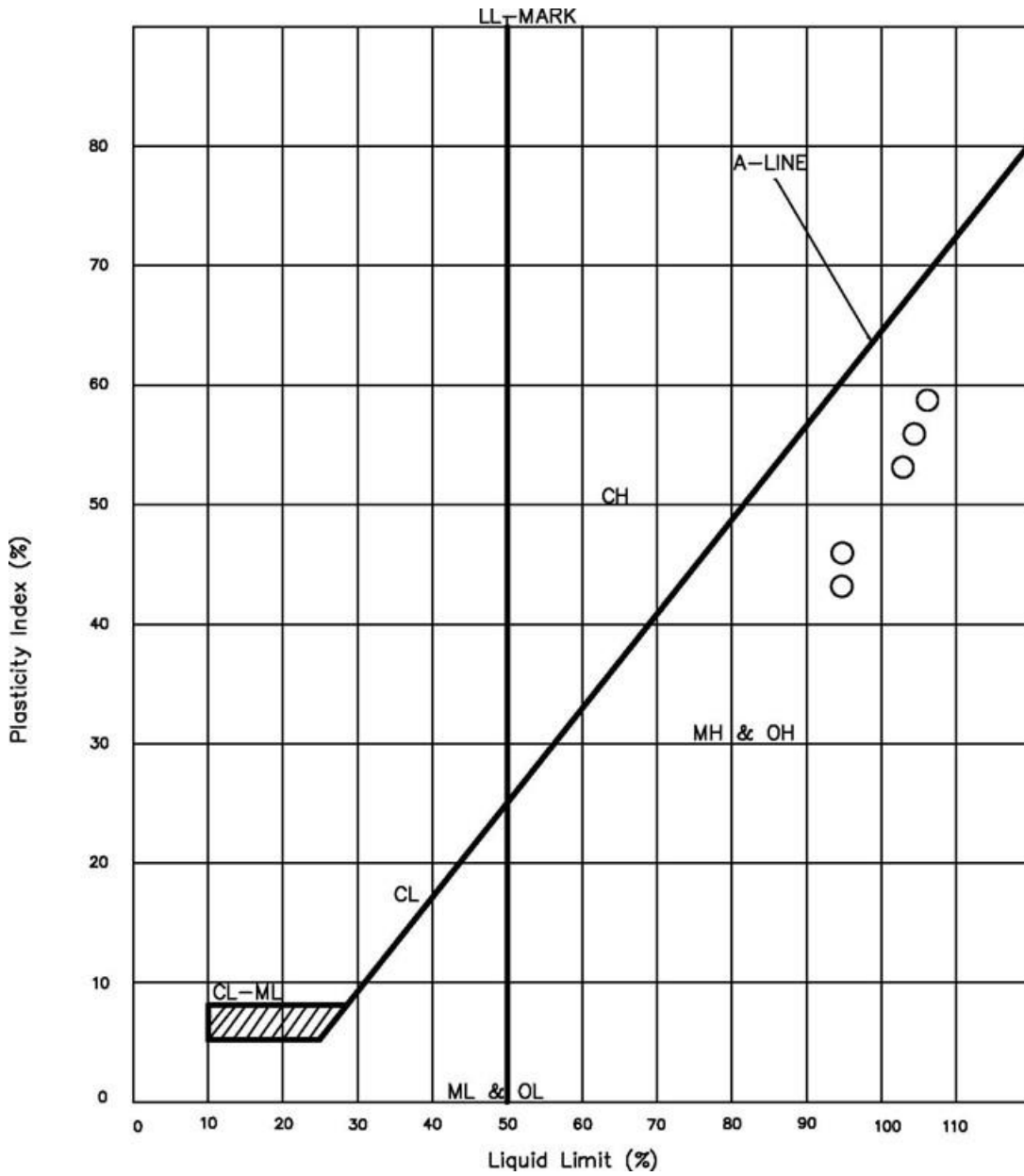
Figure 5-2: Soil Classification for Samples from 20 - 40 cm profile depth
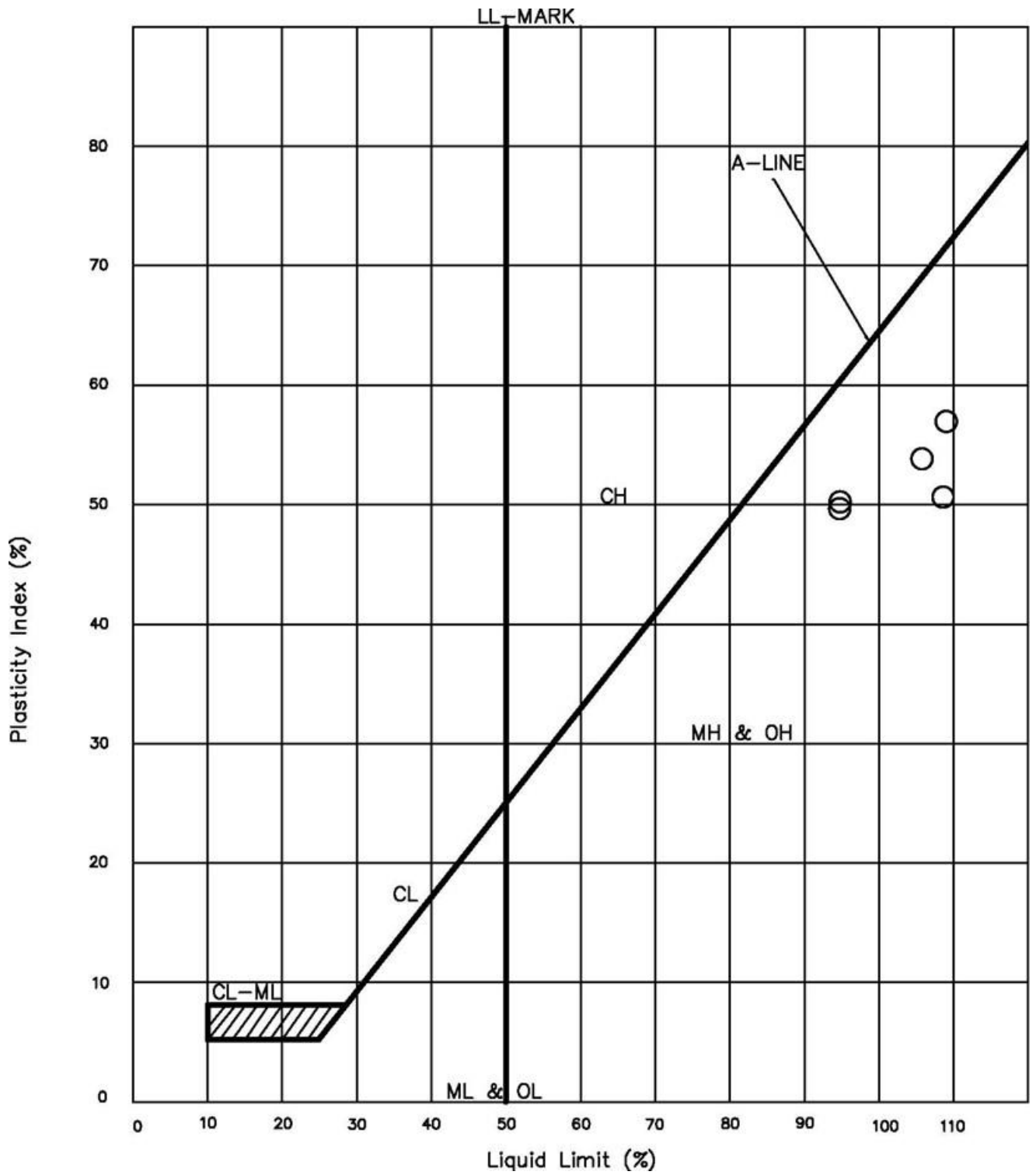
Figure 5-3: Soil classification for samples from 40 - 60 cm profile depth

34

Compression index (C_c) values for all the tested soil specimens we computed using equation 5.1. The soils exhibited high compression indexes averaging 0.804, 0.806 , 0.817 for the three profile depths and an overall profile mean value of 0.809. These values show that the soils have high compressibility and attendant water holding capacity, a typical characteristic of clays soils as established by Terzaghi and Peck (1948).

$$C_c = 0.009 \ (LL - 10 \ ) \qquad\qquad [5.1]$$

5.2   Stress – Strain Relations

Stress – strain relationships experimental results carried out on the test samples at varying axial loads, confining pressures and water contents have been presented in tables and graphical format. Since the samples were tested under consolidated undrained (CU) Triaxial Compression procedures without pore pressure measurement, the resulting parameters are in total rather than effective terms. The succeeding sections present discussions on the obtained test results on basis of disturbed and undisturbed (in situ) samples states.

5.2.1   Deviatoric Stress – Strain Results for Disturbed Samples

Graphical presentations of deviatoric stress – strain experimental data for disturbed soil samples (KRD_1, KRD_2 and KRD_3) tested at total confining stresses of 100, 200 and 300 kPa are illustrated in Figure 5.4.
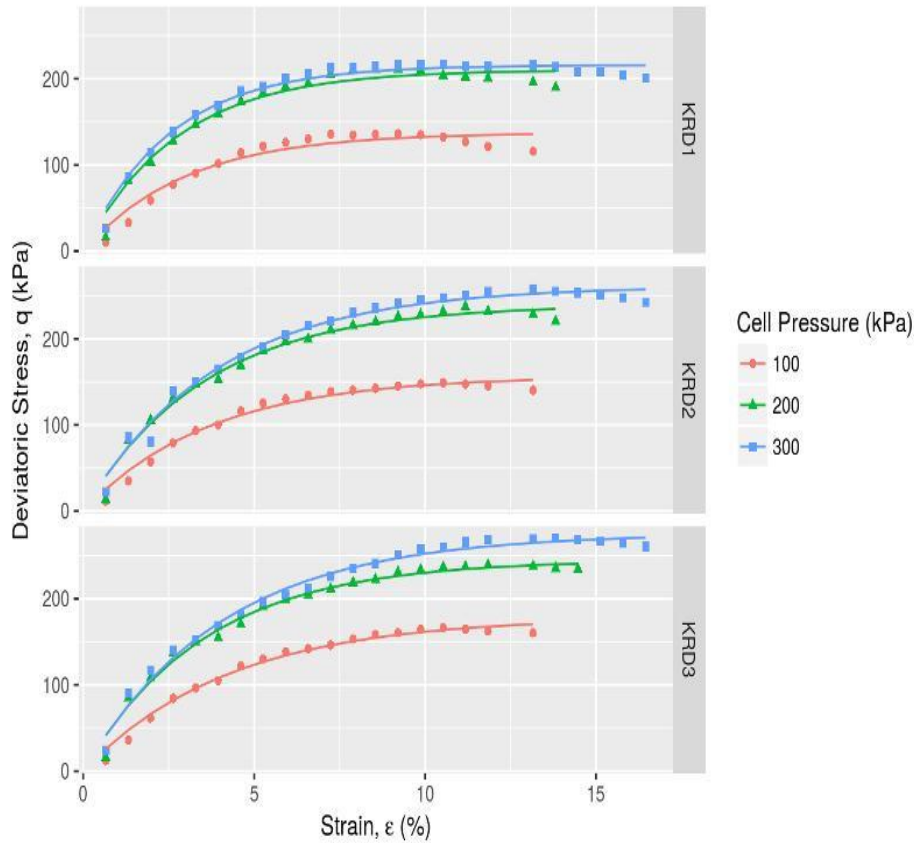
Figure 5-4: Deviatoric stress – strain relationships for disturbed soil samples (KRD1, KRD2 and KRD3(

Isotropic Compression Tests under Consolidated Undrained (CU) conditions were performed on the samples from three distinct profile depths i.e. 0 – 20 cm, 20 – 40 cm and 40 – 60 cm. These varying profile depths are denoted by 1, 2 and 3 as subscripts to the samples abbreviated names respectively.

A common characteristic feature observed in the three deviatoric stress – strain curves in Figure 5.4 is a linear increase in deviatoric stress with strain at an increasing rate upto 5 % strain. This trend denotes elastic recoverability within the zone. It is followed by a region of an increasing deviatoric stress with strain but at a decreasing rate until it reaches maximum shear stress. This region occurs within a strain range from 5 – 10%. After reaching the maximum shear stress levels, the region with continuous deformation (critical state) without corresponding increase in stress sets and extends onwards from 10 % strain . This observed typical three pattern deformation characteristics i.e elastic/recoverable zone, maximum shear stress zone and continuous deformation/failure stress zone can be modelled using a tested and suitably proven model.

For the first elastic/recoverable deformation zone, a predictive model of the form in equation 4.1 was chosen to correlate deviatoric stress (*q)* with strain *(ε)*. A and B are the model parameters established

36

for all the 30 experimental graphs while applying non linear regression principle when running the model in R programming language, a statistical computing software. Earlier researchers such as Bailey and Johnson (1989) and Zhang et al. (1998) used comparable models on different agricultural materials with satisfactory predictions. Temesgen *et al.,* (2022) while working on vertisols in Southern Ethiopia also used comparable model.

The same three patterns deformation trends were observed in sample specimens (MWD_1, MWD_2 and MWD_3) as shown in Figure 5.5. Notably, rapid rise in deviatoric stress within 0 to 5 % span of strain was recorded. This was quickly followed by a gentle rise in deviatoric stresses with corresponding strains and reaching peak strength values between 10 and 15 % strains. The third stage was characterized by a fall in deviatoric stresses with increment in strains until residual/failure stress values were reached. Most of the specimens approached failure states between 11 and 15 % axial strains.
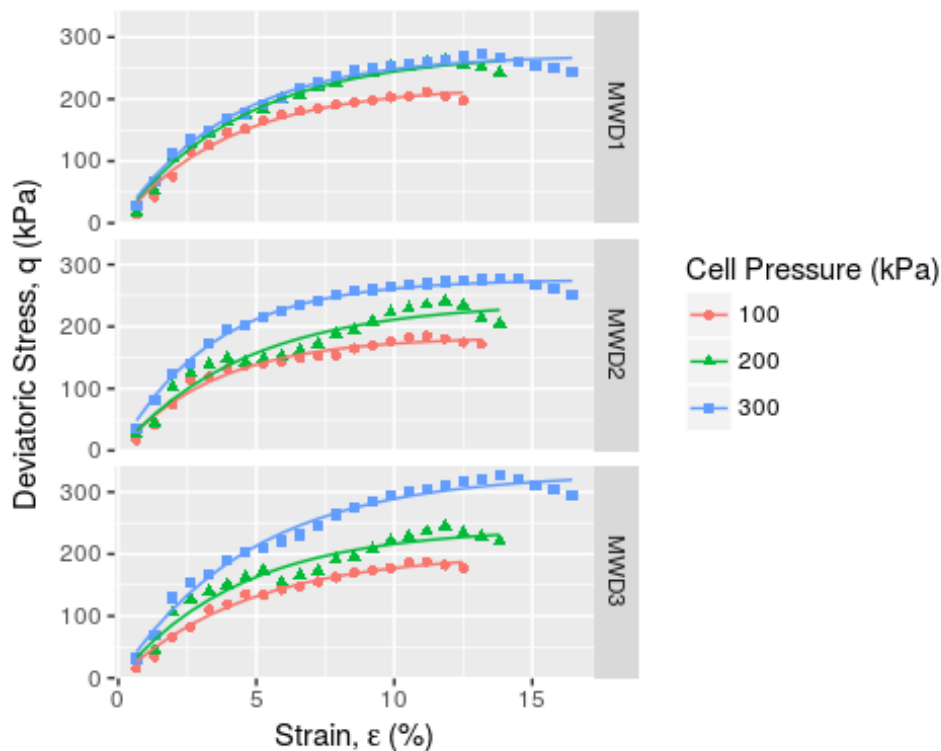
Figure 5-5: Deviatoric stress – strain relationships for disturbed soil samples - MWD1, MWD2 and MWD3

More importantly, specimen failures was observed through bulging on the lower sides that pointed to a possible attainment of plastic flow mode failure pattern. A similar finding of this failure pattern was reported by Rajaram and Gee – Clough (1998) while working on a clay – loam soil.

In all the samples tested at profile depths (0 – 20 cm), (20 – 40 cm) and (40 – 60 cm), the resultant deviatoric stresses increased with each subsequent increment in the confining stresses. This observation is attributed to the development of greater shearing resistance within the test specimens at every increase in the magnitude of the applied cell pressures as found out by Venkatraman, C. (2006). The constitutive predictive equation (4.1) defining the deviatoric stress – strain relationships within the top soil profile (0 – 20 cm), middle soil profile (20 – 40 cm) and bottom soil profile (40 – 60 cm), reasonably modelled the resultant soil behaviour. This is attested to by the high coefficients of determination/correlation (R^2) ranging between 0.947 and 0.989 for all top profiles samples as indicated in Table 5.3, 0.932 and 0.992 for all middle profiles samples as in Table G1 and 0.944 and 0.989 for all bottom profiles samples as shown in Table G2.   Coefficient of determintion/correction (R^2) is important as it indicates the extent to which the independent variable strain (ε) accounts for deviatoric stress (q) in model equation 4.1.

Table 5-3: Deviatoric stress – axial strain curves with model parameters A and B for disturbed top profile samples

Samples in (0-20cm Depth) Top Profile	Total Confining Stresses (kPa)	Non-linear recoverable deformation zone			Peak shear strength (kPa)	Residual/failure stress (kPa)
		A (kPa)	B	r^2		
KRD	100	137 (4.74)	0.336 (0.039)	0.947	140	130
WMD	100	140 (3.97)	0.315(0.029)	0.971	140	140
MWD	100	220 (5.77)	0.249(0.018)	0.985	200	200
TBD	100	231(13.25)	0.169(0.020)	0.962	210	200
THD	100	240(11.19)	0.158(0.014)	0.979	200	200
KRD	200	210(4.26)	0.366(0.028)	0.969	200	190
WMD	200	267(4.89)	0.255(0.014)	0.986	260	250
MWD	200	273(5.81)	0.223(0.013)	0.987	250	240
TBD	200	306(7.75)	0.214(0.014)	0.981	295	260
THD	200	328(7.58)	0.186(0.010)	0.989	295	295
KRD	300	215(2.39)	0.398(0.019)	0.980	220	210
WMD	300	266(3.80)	0.274(0.014)	0.980	275	240
MWD	300	270(3.99)	0.248(0.012)	0.982	270	250
TBD	300	325(8.49)	0.212(0.016)	0.964	325	280
THD	300	303(7.84)	0.192(0.013)	0.973	300	300

Meanwhile, the shear strength values obtained for KRD$_1$ samples ranged from 136.16 to 216.29 kPa. Similarly, shear strength values established for WMD$_1$, MWD$_1$,TBD$_1$ and THD$_1$ specimens varied from 135.76 to 271.20 kPa, 211.55 to 274.27 kPa, 213.12 to 321.12 kPa and 213.12 to 307.22 kPa respectively under the three total confining stresses (100, 200 and 300 kPa) as indicated in Tables D1 to D5.

The mean water content for tested specimens from the top profile (0 – 20 cm) ranged from 34.60 and 35.62 %. Comparatively, these water contents are fairly low to the mean liquid limit (LL) of the subject samples at 99.3 % (See Table 5.2). Consequently, the samples recorded reasonable shear

strength values from 135.76 to 321.12 kPa. Usually, the magnitude of the shear strengths of the clay becomes negligible as its water content approach the liquid limit (Allan and Chowdhary, 2007). Similar observation had also been made by Yates *et al*., (2017) who indicated that small increases in moisture content lead to large reductions in shear strength.

For middle profiles (20 – 40 cm), the shear strengths varied from 148.8 to 258.31 kPa for KRD_2 and 184.91 to 276.75, 184.91 to 277.66, 180.21 to 284.99 and 184.91 to 288.92 for WMD_2, MWD_2, TBD_2 and THD_2 tested samples respectively under three total confining stresses (100, 200 and 300 kPa) as contained in Tables D6 to D10.

The mean water contents for the middle profiles samples varied from 35.9 to 36.76 %. As noted in top profile samples earlier, moisture contents within the middle profiles also fell well below the liquid limit (LL) of the study soil thus indicating shear strength values above that at LL.

Meanwhile, shear strength values for specimens from the bottom profile varied from 146.39 to 255.49 kPa for KRD_3 and 175.65 to 270.87, 180.05 to 240.42, 179.86 to 282.50 and 182.60 to 286.54 kPa for WMD_3, MWD_3, TBD_3 and THD_3 respectively under the three total confining stress (See Tables Tables D11 to D15). On water content, it was found out that the bottom profile specimens had between 36.40 and 37.65 % . Although the water contents in this lowest profile was more than those recorded in the middle (20 – 40 cm) and top (0 – 20 cm) profiles, it was still nonetheless quite lower than the Liquid Limit (LL) of the study soil.

The overall mean water content in the top profile (0 – 20 cm) was 35.17 % while that in the middle profile (20 – 40 cm) was 36.43 %. In the bottom profile, the mean water content was established to be 37.18%. On the other hand, the overall mean shear strength in the top profile was 242.43 kPa whereas those in the middle and bottom profiles were 233.23 kPa and 226.22 kPa respectively. This observation is in agreement with that made by Bilson and Ugarte (2021) while working on medium and coarse textured soils where they reported an increase in soil strength was more pronounced in the top profile zone of 0 – 30 cm depth.

Essentially, the moisture contents within the three profile depths ranging from 35.17 to 37.18 % compare well with those established by Johnson *et al*., (1982), Cooper and Georges (1982) and Paul (1982) of 28 – 40 % and 32 – 46 % for vertisols and some clay soils elsewhere. There was an observed reduction in shear strength values in all the samples tested with increasing water contents. This was perhaps due to the weakening of the cohesive bonds (mutual attractive forces) between fine

clay particles by more water hence increased volume with consequent reduction in density as well as shear strength.

5.2.2   Deviatoric Stress – Strain Results for Undisturbed Samples

Deviatoric Stress – Strain graphical relationships for undisturbed sample specimens are presented in Figures 5.6 and 5.7. As the foregoing case in the disturbed samples, the undisturbed samples were equally subjected to three total confining stresses (100, 200 and 300 kPa) and isotropically compressed under Consolidated Undrained (CU) conditions. The test specimens profile depths also remained the same at top layer (0 – 20 cm), middle layer (20 – 40 cm) and lowest layer (40 – 60 cm).
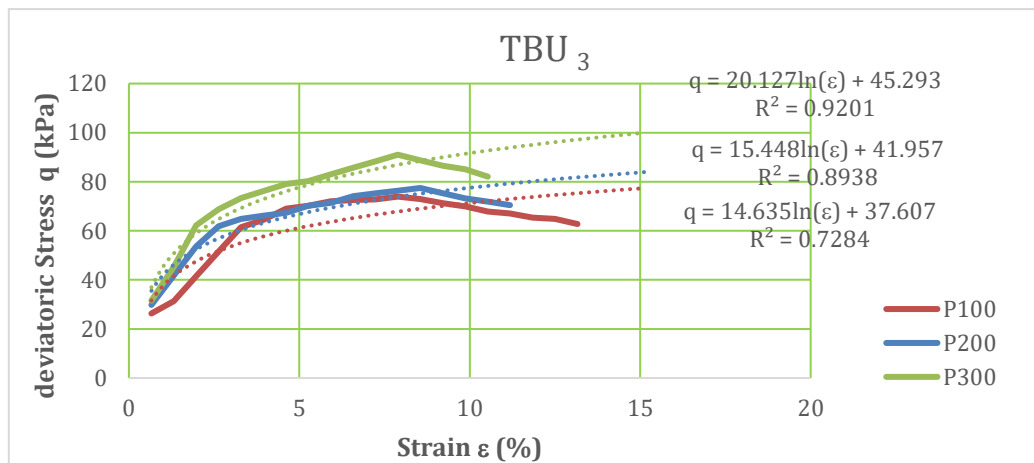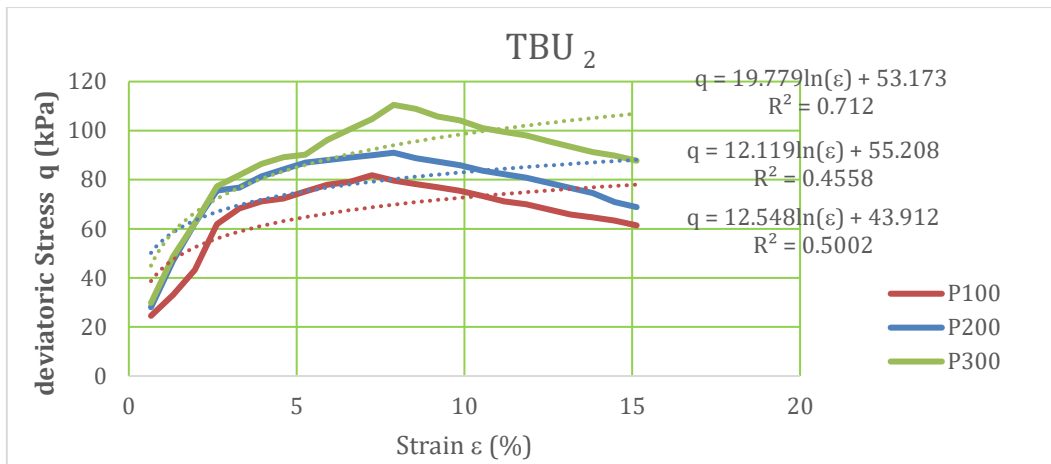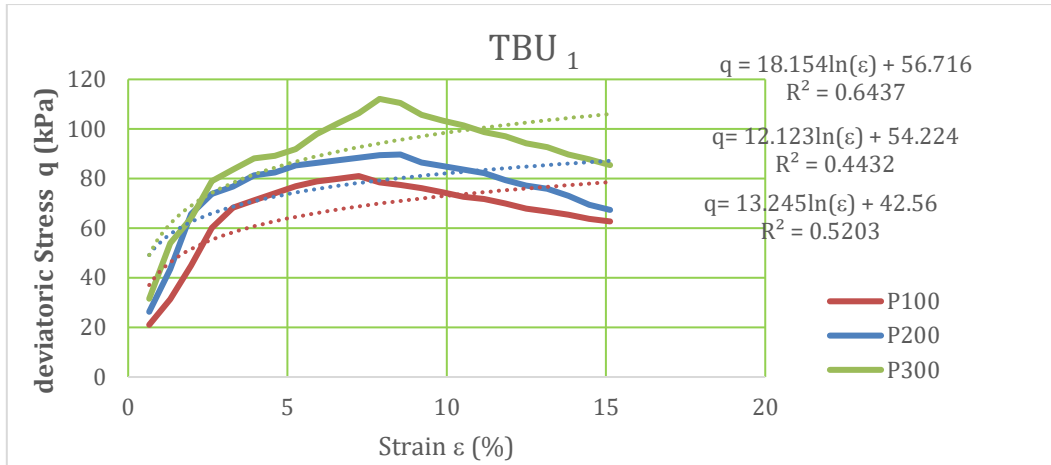
Figure 5-6: Deviatoric stress – strain relationships for undisturbed soil samples -TBU1, TBU2 and TBU3

$q = 19.993\ln(\varepsilon) + 54.41$
$R^2 = 0.6666$

$q = 17.445\ln(\varepsilon) + 43.156$
$R^2 = 0.6254$

$q = 15.464\ln(\varepsilon) + 36.89$
$R^2 = 0.5821$

$q = 20.681\ln(\varepsilon) + 56.713$
$R^2 = 0.726$

$q = 18.786\ln(\varepsilon) + 54.739$
$R^2 = 0.6708$

$q = 12.266\ln(\varepsilon) + 46.452$
$R^2 = 0.4701q$

$q = 27.594\ln(\varepsilon) + 43.871$
$R^2 = 0.9647$

$q = 19.562\ln(\varepsilon) + 43.07$
$R^2 = 0.9314$

$q = 13.46\ln(\varepsilon) + 40.061$
$R^2 = 0.6577$
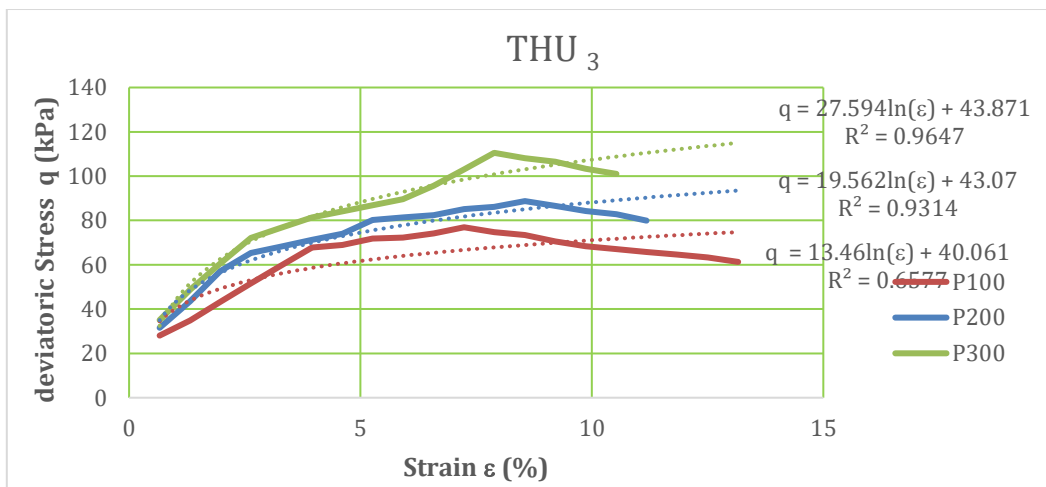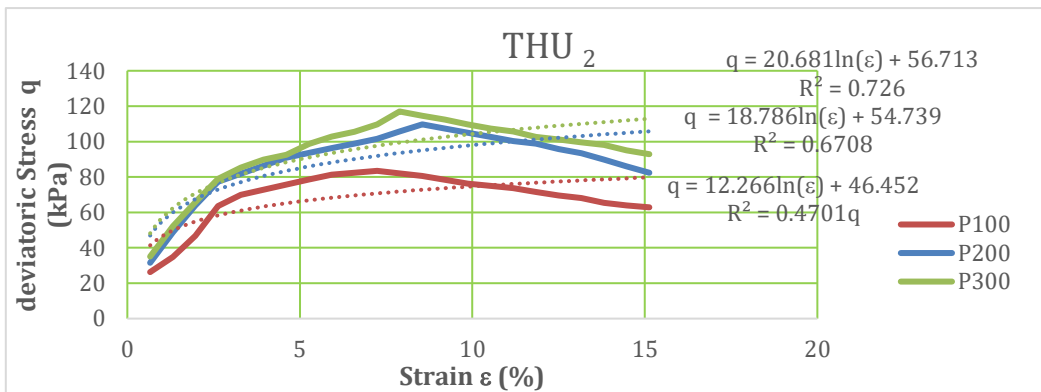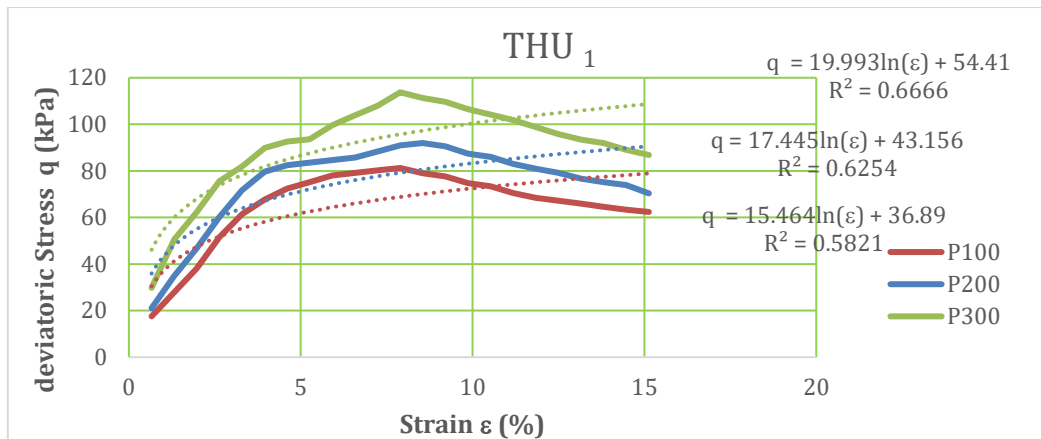
Figure 5-7: Deviatoric stress – strain relationships for undisturbed soil samples -THU1, THU2 and THU3

Both samples i.e. TBU and THU exhibited near similar patterns of deformation at various depths. The deformations observed appears to take three characteristic trends. A near linear rise in stress with strain upto 4 % characterized the first part of deformation. This linearity denoted elastic deformation tendencies within this region. It is then followed by a phase in which further increment of stress with strain occurs but at a decreasing rate until it peaks (deviatoric stress) at a strain value of 8.0 % and thus manifesting elasto – plastic deformation characteristics. After the peak point, there

42

is a sudden drop in all subsequent stress values with increasing magnitudes of strain perhaps pointing at failure occurrence.

The foregoing three steps deformation characteristics of the disturbed samples can be modelled using a predictive model in equation 4.1. As already stated, several researchers such as Bailey and Johnson (1989) and Zhang et al. (1998) used comparable models on different agricultural materials with satisfactory level of predictions. Similar deformation trends were observed in other samples i.e. MWD, KRD and WMD.

On shear strength values, it was found out that KRU_1 sample specimens had between 24.83 and 39.72 kPa. On the other hand, WMU_1, MWU_1, TBU_1 and THU_1 specimens had strength values ranging from 65 to 78.35, 80.20 to 110.51, 81.02 to 112.13 and 81.25 to 113.76 kPa respectively under the three cell pressures. Meanwhile, the average water contents within the top profile specimens varied from a low of 44.9 to a high of 72.79 %. Generally, these water contents are lower than the established profile mean of 99.3 % as contained in Table 5.2. The implication of this phenomenon is that the shear strength values reported are higher than that of the soil at LL.

The foregoing experimental shear strengths values in the top profile compare well with model generated ones in maximum shear strength and residual/failure stress deformation zones as illustrated in Table G3. Coefficient of correlation (R^2) values ranged from 0.702 to 0.966 thus signifying high degree of correlation between shear strength and strain.

The deviatoric stress – strain curve for representative tested samples from the middle profile layer (20 – 40 cm) are presented in Figures E and F . The curves are for WMU_2 and KRU_2 tested samples. In both curves, a typical linear rise in deviatoric stressess over a small span of strain is observed. This is followed by gradual rise over a long span of strain until peak deviatoric stress value is attained. Peak deviatoric stress values occurred between 7.5 and 10 % strain.

A general drop in the value of deviatoric stresses followed immediately after the specimens reached their peak strength/failure point. Thus, further additional axial strains occurred at decreasing magnitudes of deviatoric stresses. Shear strength values ranged from 37.38 to 65 kPa for KRU_2 specimens under total confining pressures of between 100 and 300 kPa. On the other hand, strength values for WMU_2, MWU_2, TBU_2 and THU_2 specimens under the same restraining pressures varied from 69.72 to 81.83, 75.82 to 83.47, 81.83 to 110.51 and 83.47 to 117.01 kPa respectively. The observed trend of shear strength values was that of an increasing magnitude with a reduction in mean water content. This scenario is perhaps attributable to the weakening of the cohesive bonds (mutual

attractive forces) between fine clay particles by more water hence expansion of soil volume with attendant decline in shear strength.

Overall mean water content for all the specimens within the middle layer was 47.95% which is way below the LL of 99.52 % at a corresponding PI of 52.04 % (See Table 5.2). Mehdi et al., 2014 while working on plastic clay in Central Queensland of Australia, established PI at 47 % which compares well with that of the study sample.

Typical characteristic curves (deviatoric stress – strain) for specimens obtained from the bottom profile depth (40 – 60 cm) and isotropically compressed under consolidated undrained conditions are illustrated in Figures 5.6 and 5.7 for representative specimens TBU_3 and THU_3 at 39.23% and 38.64% water content respectively. In both curves, a three stage pattern was evident in the variation of stress vis-a-vis strain. The first stage was marked with a sudden linear rise in stress over a small range of strain thus illustrating elastic or recoverable deformation zone. Subsequent region was characterized by an increase in stress magnitudes with corresponding increment in strain values but at a decreasing rate upto peak strength. Beyond the peak strength, a rapid drop in subsequent deviatoric stresses occurred thereby signifying achievement of critical state or region of plastic deformation. In this region, the deviatoric stresses required to produce additional axial strains decreases since the interlocking forces are being gradually diminished (Horn, 1993; Gitau et al., 2006).

The transition to critical state or failure status was observed in the specimens through lateral bulging at their lower sides without noticeable shear faultline thus indicating plastic failurre. Specimen failures occurred between 7.24 and 8.55 % axial strains and at water content between 38.64 and 39.23 %. The observed plastic failure mode is in agreement with the findings of Rajaram and Gee – Clough (1988) who reported four distinct failure patterns at four different moisture contents while working on a clay soil. They reported that at 5.2 % moisture content, the soil was modified by a collapse mode, at 18.3 % by fracture mode, at 28.6% by chip – forming mode and at 42 % it was characterized by plastic flow mode as the case herein the study soil.

The predictive model in equation 4.1 for deviatoric – strain relationships for samples within the bottom/lower profile depth (40 – 60 cm) is satisfactorily applicable in modelling the resultant soil behaviour due to high values of coefficient of correlation (R^2 above 86%) as indicated in Table G4.

While classical theory of plasticity evolved from careful observations of the behaviour of ductile metals, it should be noted that soil as opposed to metals, experience irrecoverable volumetric as well as irrecoverable shear strains (Houlsby and Wroth, 1982). Further, the deviatoric stress/shear strength of soil cannot be tabulated in codes of practice since a soil can significantly exhibit differrent shear strengths under different field and engineering conditions as established by Venkatraman, C. (2006). Owing to the foregoing, it is imperative that critical parameters constituting and limiting shear strengths magnitudes i.e. cohesion and internal angle of friction be evaluated.

5.3   Mohr – Coulomb Strength Theory

Mohr - Coulomb strength theory is about failure or rupture of a material undergoing loading. Any stress condition falling within the Mohr's circle represents a state of material stability whilst a condition tangent to the circle indicates incipient or imminent failure. Essentially, the theory is basically a functional relationship between the normal stress on any plane within a soil and the shearing strength occuring within the plane. Since failure will occur upon attainment of the critical state, the Mohr – Coulomb criterion provided a valuable means through which actual strength parameters i.e. cohesion (c) and internal angle of friction (Φ) were obtained.

Graphs of shear stress vis-a-vis normal stress were drawn to form what are known as Mohr Circles. Thereafter, tangential lines to the Mohr's Circles representing failure/Coulomb envelopes or critical state lines were drawn to intersect the shear stress axis (y – axis) as illustrated in Figure 5.8 for sample THD$_2$.
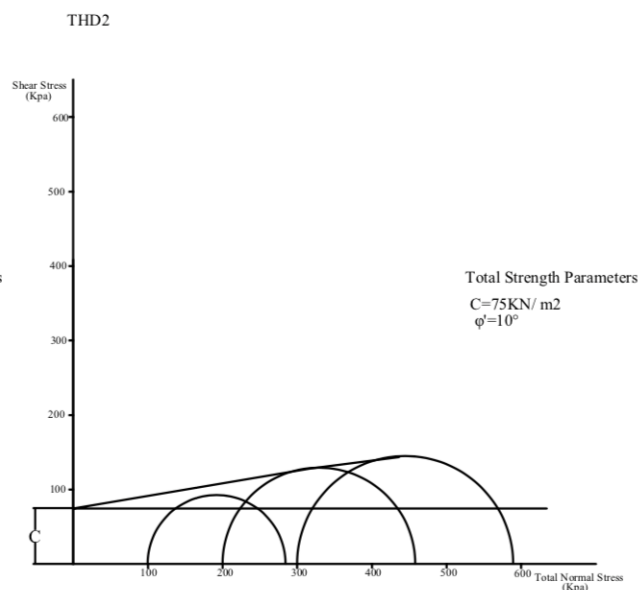
Figure 5-8: Failure envelopes for sample THD2

The point of intersection denoted the cohesive strength magnitude (c) of the subject sample specimen with the angle to the horizontal line drawn becoming the respective angle of internal friction (Φ). Ideally, angle of internal friction is not a true angle of friction as such but simply the gradient of the strength/failure envelope. Physically, it represents a measure of resistance of a soil matrix to sliding along its plane.

A representative sample data i.e at failure condition for sample THD_2 from which Mohr – Coulomb – Failure envelope in Fig. 5.8 is generated from is presented in Table 5.4.

Table 5-4: Failure conditions for THD2

Moisture Content (w) %	36.55	36.39	36.91	36.62 (Mean)
Failure Conditions Data	**Thiba disturbed$_2$(i)**	**Thiba disturbed$_2$(ii)**	**Thiba disturbed$_2$(iii)**	
Cell Pressures σ_3 (kPa)	100	200	300	
Deviator Stress σ_d (kPa)	184.91	258.20	288.92	
Axial Stress σ_1(kPa)	284.91	458.20	588.92	
Axial Strain ε (%)	11.18	11.84	13.82	
Shear Strength Parameters				
Cohesion (C) kPa/kN/m^2	75			
Internal Angle of Friction (φ)	10^0			
Failure Mode:	Lateral Bulging on the lower side			

5.3.1 Mohr – Coulomb Relations for Disturbed Samples

Tables 5.5 and 5.6 present typical shear strength parameters generated from Mohr 's circles (Figures 5.9 and 5.10) with failure envelopes for disturbed soil sample specimens MWD_1 and TBD_3 in top and bottom profile layers respectively.
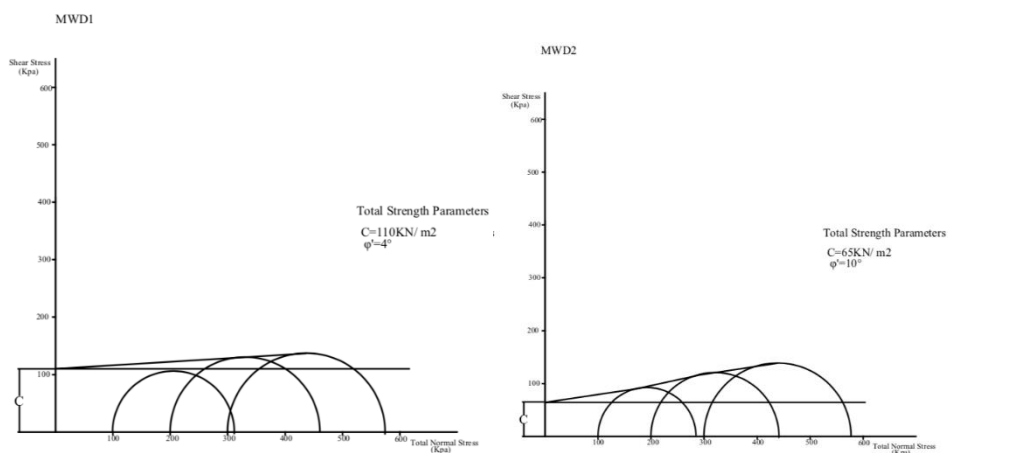
Figure 5-9: Failure envelopes for sample MWD1 and MWD$_2$

Within the top profile (0 – 20 cm) depth, the shear strength parameters i.e. cohesion and angles of internal friction were found to range from 109 to 153 kPa and 0^0 to 7^0 respectively. KRD_1, WMD_1 and THD_1 specimens all had angles of internal friction as zero thus exhibiting pure clay or purely cohesive characteristics. Similarly, corresponding cohesive strengths of the three samples were 110 kPa, 131 kPa and 153 kPa respectively.

Table 5-5: Failure conditions for MWD1

Moisture Content (w) %	35.01	35.62	35.47	35.37 (Mean)
Failure Conditions Data	**Mwea Disturbed $_1$(i)**	**Mwea Disturbed $_1$(ii)**	**Mwea Disturbed $_1$(iii)**	
Cell Pressures σ_3 (kPa)	100	200	300	
Deviator Stress σ_d (kPa)	211.55	261.31	274.27	
Axial Stress σ_1 (kPa)	311.55	461.31	574.27	
Axial Strain ε (%)	11.18	11.84	13.16	
Shear Strength Parameters				
Cohesion (C) kPa/kN/m^2	110			
Internal Angle of Friction (φ)	4^0			
Failure Mode:	Lateral Bulging on the lower side			

For MWD_1 and TBD_1 specimens, angles of internal friction were 4^0 and 7^0 respectively with cohesive strengths being 110 and 109 kPa. Meanwhile, the water contents for the KRD_1, WMD_1, THD_1, MWD_1 and TBD_1 specimens within the profile were 34.6, 34.8, 35.48, 35.37 & 35.62 % respectively. Although the water contents in all the specimens in the top profile were well above 30 % , which is fairly considerable and expected to influence the resultant cohesive strength, this was not the case. This was due to the fact that at above 30 %, the water content was still way below the liquid limit of the soil (99.30%) hence minimal destruction of the cohesive bonds between the clay particles hence retention of the reported cohesive strengths.
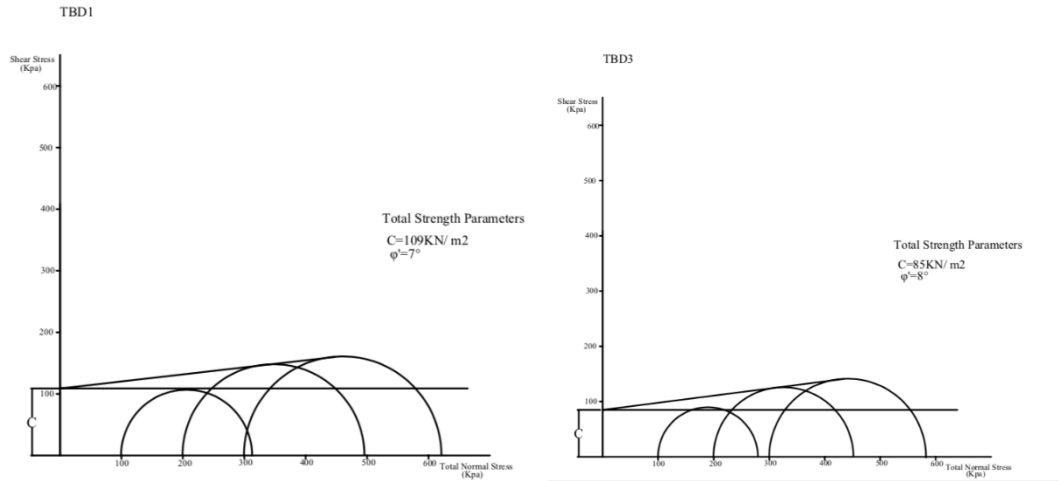
Figure 5-10: Failure envelopes for sample TBD1 and TBD₃

For middle profile (20 – 40 cm) disturbed specimens, sample shear strength parameters for KRD_2 are presented in Table 5.6. The cohesive strength for KRD_2 specimen sample was 94 kPa at 5^0 angle of internal friction and 35.9 % water content. For WMD_2, MWD_2, TBD_2 and THD_2 specimens , the cohesion recorded were 50, 65, 90 and 75 kPa respectively. Similarly, the corresponding angles of internal friction were 10, 10, 7 and 10^0. The water contents for the foregoing four sample specimens were fairly of close range at 36.43, 36.42, 36.76 & 36.62 %.

Table 5-6: Failure conditions for KRD2

Moisture Content (w) %	35.9	35.9	35.9	35.9 (Mean)
Failure Conditions Data	**Karaba Disturbed ₂(i)**	**Karaba Disturbed ₂(ii)**	**Karaba Disturbed ₂(iii)**	
Cell Pressures σ_3 (kPa)	100	200	300	
Deviator Stress σ_d (kPa)	148.80	237.12	258.31	
Axial Stress σ_1(kPa)	248.80	437.12	558.31	
Axial Strain ε (%)	10.53	11.18	13.16	
Shear Strength Parameters				
Cohesion (C) kPa/kN/m^2	94			
Internal Angle of Friction (φ)	5^0			
Failure Mode:	Lateral Bulging on the lower side			

In the lower/bottom profile (40 – 60 cm), sample strength parameters are given in Tables 5.7. The cohesion vary from 45 kPa in MWD_3 to 85 kPa in TBD_3 and at 13^0 and 8^0 angles of internal friction respectively.

Table 5-7: Failure conditions for KRD₃

Moisture Content (w) %	36.4	36.4	36.4	36.4 (Mean)
Failure Conditions Data	**Karaba Disturbed 3(i)**	**Karaba Disturbed 3(ii)**	**Karaba Disturbed 3(iii)**	
Cell Pressures σ_3 (kPa)	100	200	300	
Deviator Stress σ_d (kPa)	146.39	235.15	255.49	
Axial Stress σ_1(kPa)	246.39	435.15	555.49	
Axial Strain ε (%)	10.53	11.84	13.82	
Shear Strength Parameters				
Cohesion (C) kPa/kN/m^2	75			
Internal Angle of Friction (φ)	8^0			
Failure Mode:	Lateral Bulging on the lower side			

Overall, the mean cohesion for specimens within the top , middle and bottom/lower profile depths were 122.6 , 74.8 and 67 kP respectively. On the other hand, mean angles of internal friction increased from 2.2^0 at the top profile to a high of 9.6^0 at the bottom profile. The same trend was observed on mean water contents that increased with the increment in profile depth. At the top most profile, the mean water content was 35.17 % which subsequently increased with the depths to 37.17 % at the bottom profile. In general, the mean cohesive strengths of all the sampled specimens decreased with increase in mean water contents. This observation is in agreement with the findings of Liu *et al*., 2005 who attributed this phenomenon to thickening of water films around the particles and at some point, the effect of the water changes from cohesion to lubrication, making it easier for soil particles to slip past each other. They further postulated that the decrease in cohesion could perhaps arise from water dissolving salts or other materials that help to cement particles together.

Although cohesion was the major shear strength parameter at play in the study soil sample specimens, frictional component was also in place as exemplified earlier. However, the magnitudes of the frictional components as manifested in angles of internal friction reported were small. In particular, among the five sample specimens tested from the top profile, three of them were completely cohesive soils (c soils/pure clay) with zero frictional component. The same trend was noted in the middle and bottom profiles whose mean frictional components were slightly lower than 10^0 at 8.4^0 and 9.6^0 respectively.

Figure 5.11 illustrates graphically the variation of the cohesive characteristics of the disturbed sample soil specimens with water contents of between 34 and 38 %. The graph indicates that the magnitude

of the soil cohesion decreases with increasing water contents upto 37.5 % where it levels off and appears constant with any further increment of water. Kamara (1990) and Haque (1990) while working on different vertisols in Ethiopia highlands established a moisture content range of between 29 and 39 % as optimum for tillage operations.

Meanwhile, the observed trend is attributable to reduction in the cohesive bonding between fine clay particles in the soil mass by water. Once these bonds are broken by water, the mutual attraction that exists and tend to hold these fine particles is dissipated as particles become dispersed. Results of regression analysis showed a decay/exponential relationships between cohesion and water content with an coefficient of determinaton/correlation of $R^2 = 0.4844$.

The chart contains the equation and values:
$$C = 981028e^{-0.259w}$$
$$R^2 = 0.4844$$
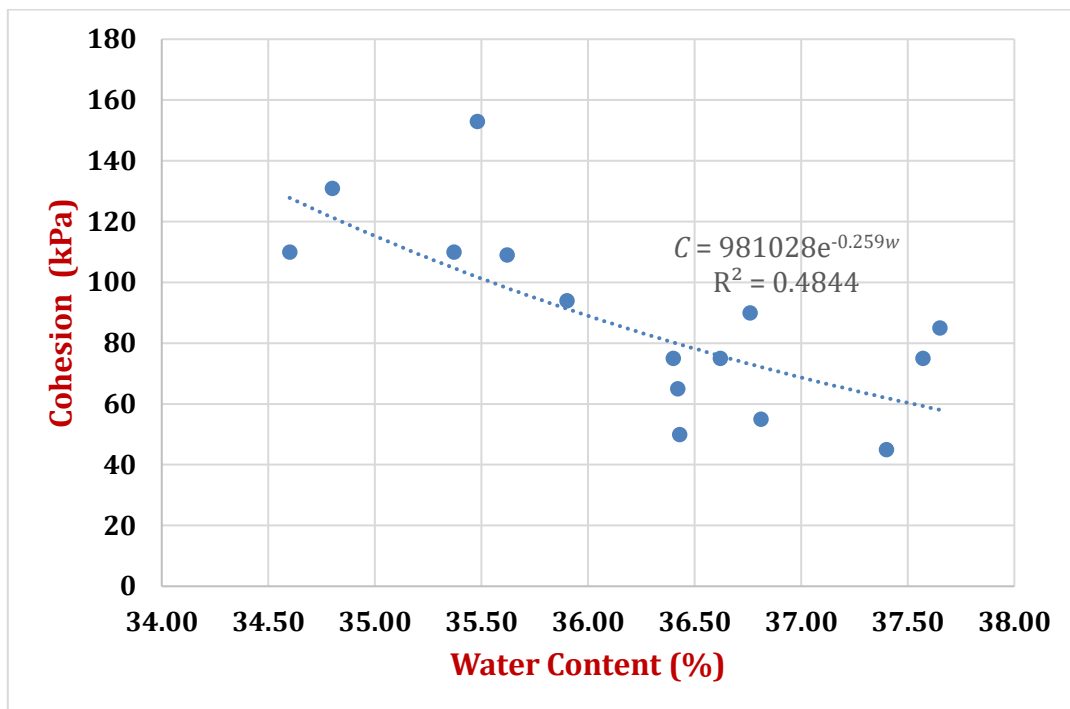
Figure 5-11: Influence of water content on soil cohesion

Mathematical relationships between angle of internal friction and water contents is also graphically presented in   Figure 5.12. The resultant mathematical model of correlation/predictive equation between the friction component of the soil and the water content is a quadratic polynomial type relationship with a R^2 value of 0.7755 with a positive asymptote. Girma (1989) and McKeys (1989) while working on different types of soils also reported a quadratic relationship trend with a positive asymptote. An attempt was made to use either linear or logarithmic models to correlate internal angle of friction and water content. In both models, there was a continuous increase in internal angle of friction with increment in water content. Consequently, apolynomial model for correlating friction

and water content was chosen as it exhibited reduction in friction with increment in water content.

Figure with scatter plot showing water content (%) on x-axis from 34.00 to 40.00 and Angle of Internal Friction (°) on y-axis from -4 to 14. Trendline equation: $\varphi = -1.2924w^2 + 97.048w - 1812$, $R^2 = 0.7755$.
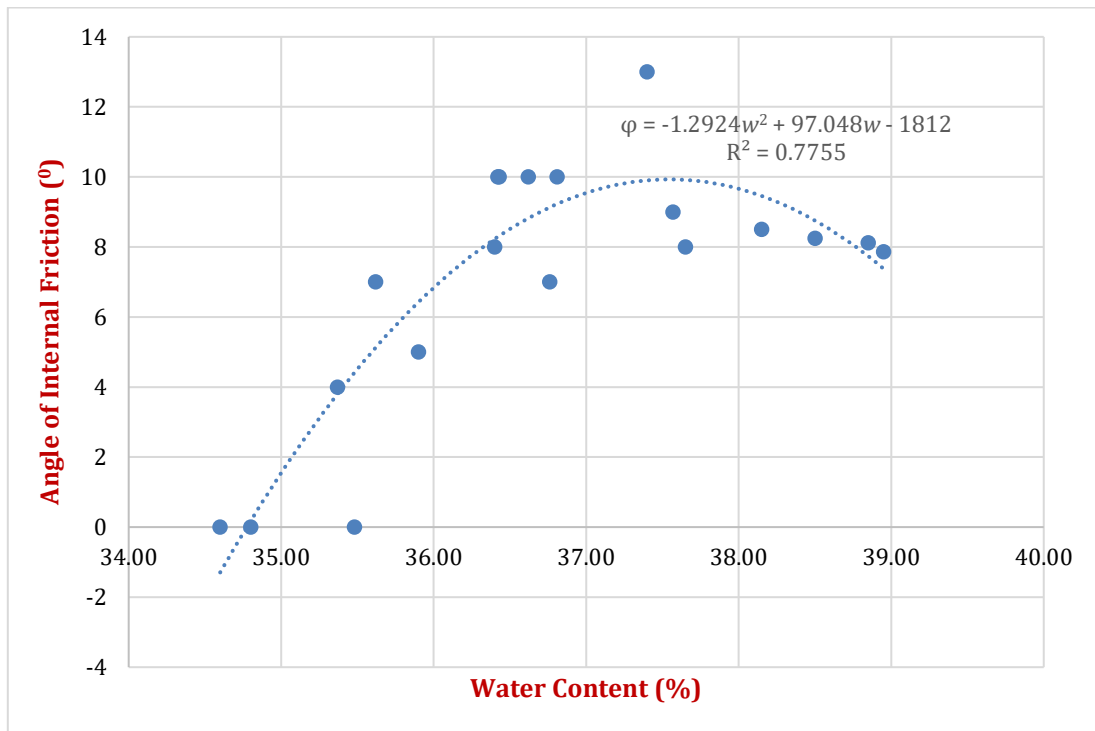
Figure 5-12: Effects of water content on soil angle of internal friction

The frictional component of the soil increased with water content upto a maximum of 10^0 at a corresponding water content of 37.5 %. With constitutive nature of soil, this observation does not appear valid. With internal friction and cohesion being elements of shear strength in vertisol, any increase in water content has tendency of loosening the interlocking bonds holding the particles together as well as friction between individual particles at their contact points thus reduction in angle of internal friction against the observation made. It is likely that this observation may have been due to an experimental error.

Beyond 37.5 % water content, a decline in angle of internal friction was noted. As reported by Kamara (1990) and Haque (1990) while working on different vertisols in Ethiopia highlands, optimum tillage operations on the soil is achieved at water content values between 29 and 39 %. Consequently and for this study soil, the water content at 37.5% appears to represent the point at which tillage intervention on the vertisols will achieve maximum friability at optimal traction during land preparation. Corresponding internal angle of friction at 37.5% water content was 10^0.

From equation 2.5, the angle of internal friction is a major variable in influencing the resulting traction developed by a tillage machinery. Thus, for the disturbed study soil specimens, it is believed that 10^0 angle of internal friction denotes the optimum friction magnitude at which desired maximum traction will be developed by subject machinery working on the soil.

Similarly, the magnitude of cohesion that would maximize the tractive force developed, without compromising the requisite frictional force would be that corresponding to 37.5 % moisture content. From Figure 5.11, the equivalent cohesion magnitude at 37.5 % moisture content is 70 kPa. Thus, maximum traction accompanied by optimal tillage operation (without destruction of soil physical matrix/slip) on disturbed vertisols at Mwea Irrigation would be achieved at shear strength parameters of 70 kPa and 3^0 for cohesion and angle of internal friction respectively.

5.3.2 Mohr – Coulomb Relations for Undisturbed Samples

Sample Mohr – Coulomb shear strength critical parameters for undisturbed soil specimens are presented in Tables 5.8, 5.9 and 5.10 for soils from top , middle and bottom profiles respectively. Similarly, representatives Mohr – Coulomb failure envelopes from which the critical strength parameters are generated are presented in Figures 5.13 and 5.14.

Table 5-8: Failure conditions for KRU1

Moisture Content (w) %	83.41	67.56	67.40	72.79 (Mean)
Failure Conditions Data	**Karaba Undisturbed $_1$(i)**	**Karaba Undisturbed $_1$(ii)**	**Karaba Undisturbed $_1$(iii)**	
Cell Pressures σ_3 (kPa)	100	200	300	
Deviator Stress σ_d (kPa)	24.83	23.51	39.72	
Axial Stress σ_1(kPa)	124.83	223.51	339.72	
Axial Strain ε (%)	13.33	11.18	6.08	
Shear Strength Parameters				
Cohesion (C) kPa/kN/m^2	12.5			
Internal Angle of Friction (φ)	1^0			
Failure Mode:	Lateral Bulging on the lower side			

Figure 5-13: Failure envelopes for sample WMU1 and WMU2

The cohesion parameters within the top profile (0 – 20 cm) varied from 12.5 to 40 kPa with a mean profile value of 28 kPa. Over the same profile, the water contents ranged from 44.9 to 72.79 %. Highest amount of water content was recorded in sample specimen KRU_1 while the lowest amount was for THU_1. The profile mean water content was 57.29 % .

Meanwhile, the lowest angle of internal friction within the top profile was recorded in sample specimen KRU_1 at 1^0. Papacharisis et al., 1999, while working on fine clays established comparable friction angles ranging from 1.5 to 6 degrees. The highest value for angle of internal friction in this profile was 4^0 for both TBU_1 and THU_1 specimens. Specimens WMU_1 and MWU_1 had 2^0 and 2.5^0 internal angles of friction respectively. Within the top profile, the angles of internal friction reduced with increasing amount of water contents. A similar observation was made by Yanrong (2017). Further, Liu *et al.*, (2005) explained that the reduction in internal friction with increasing water content arose from water films thickening around particles with the effect of water changing from cohesion to lubrication thus making particles slip past each other. Zhang *et al.,* (2018) additionally attributed this phenomenon to dissolution of salts and other materials that help to cement the soil particles together thus not only leading to decline in frictional magnitude but also the soil shear strength.

Table 5-9: Failure conditions for TBU$_2$

Moisture Content (w) %	43.97	45.51	44.96	44.81 (Mean)
Failure Conditions Data	**Tebere Undisturbed $_2$(i)**	**Tebere Undisturbed $_2$(ii)**	**Tebere Undisturbed $_2$(iii)**	
Cell Pressures σ_3 (kPa)	100	200	300	
Deviator Stress σ_d (kPa)	81.83	91.01	110.51	
Axial Stress σ_1(kPa)	181.83	291.01	410.51	
Axial Strain ε (%)	7.24	7.89	7.89	
Shear Strength Parameters				
Cohesion (C) kPa/kN/m^2	30			
Internal Angle of Friction (φ)	4^0			
Failure Mode:	Lateral Bulging on the lower side			

Table 5.9 presents typical shear strength parameters of cohesion (c) and angles of internal friction (Φ) of sample specimen TBU$_2$ i.e. from the middle soil profile. The profile mean cohesion value was 30.7 kPa spread between 8 to 47 kPa limits. Similarly, the average value for angle of internal friction was 2.9^0 and varied from a low value of 1.5^0 for WMU$_2$ specimen to a high of 5^0 for KRU$_2$ sample. As noted in the top profile, the frictional resistance in the middle profile also depicted a reduction trend with increasing magnitudes of water contents.
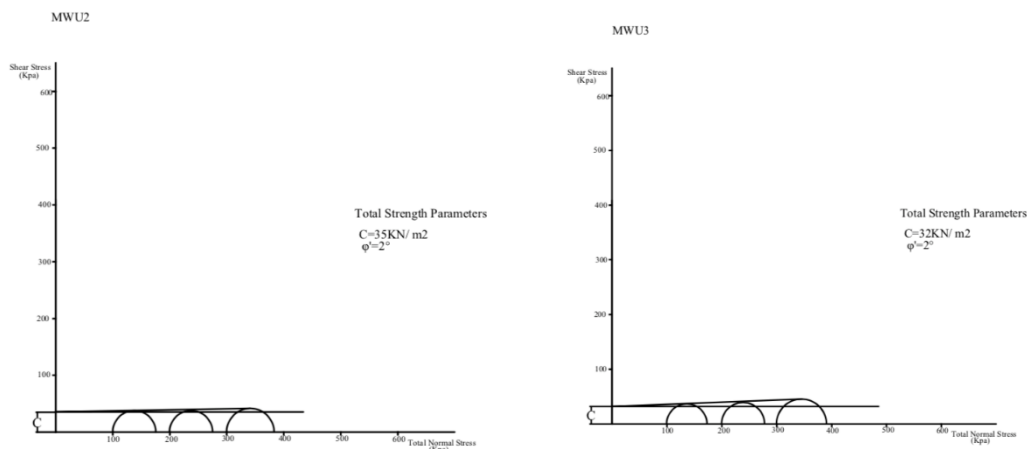
Figure 5-14: Failure envelopes for sample MWU2 and MWU3

The lowest profile occurring at between 40 and 60 cm depth had critical shear strength parameters (C and Φ) close to those in the immediate layer above. Specifically, the mean profile cohesion was 29.6 kPa while that of angle of internal friction was 2.9^0. Table 5.10 presents critical shear stress parameters for specimen THU$_3$. The pattern exhibited in all the profiles was that of a reduction in the magnitude of water contents with increasing profile depths. As earlier explained, this phenomenon accounted for the increased cohesive strength with increasing profile depth.

Table 5-10: Failure conditions for THU3

Moisture Content (w) %	39.56	38.67	37.69	38.64 (Mean)
Failure Conditions Data	**Tebere Undisturbed 3(i)**	**Tebere Undisturbed 3(ii)**	**Tebere Undisturbed 3(iii)**	
Cell Pressures σ_3 (kPa)	100	200	300	
Deviator Stress σ_d (kPa)	76.92	88.74	110.51	
Axial Stress σ_1(kPa)	176.92	288.74	410.51	
Axial Strain ε (%)	7.24	8.55	7.89	
Shear Strength Parameters				
Cohesion (C) kPa/kN/m^2	27			
Internal Angle of Friction (φ)	5^0			
Failure Mode:	Lateral Bulging on the lower side			

Meanwhile, mathematical models of correlation between the resultant shear strength parameters (c and Φ) and water contents for the undisturbed soil specimens were generated in Figures 5.15 and 5.16. From Figure 5.15, a rise in cohesive strength with water contents was noted. A similar trend was reported by Singh and Thompson (2016) while working on grassy waterway (loam) and in agricultural field (loam). Le Bissonnais (1996) explained that as the antecedent soil moisture content increased, the volume of trapped air and the resulting gradient in matric potential decreased thereby leading to decreased slaking hence rise in cohesive strength. Cohesion peaked at water content of about 45 % before dropping markedly with increasing water content. A generated quadratic predictive equation of correlation between cohesion and water content had a very low value of R^2 i.e at 0.1827. The inference of this resulting relationship is that despite cohesion being a critical shear strength state parameter, it cannot be correlated with the slope of the critical state line.
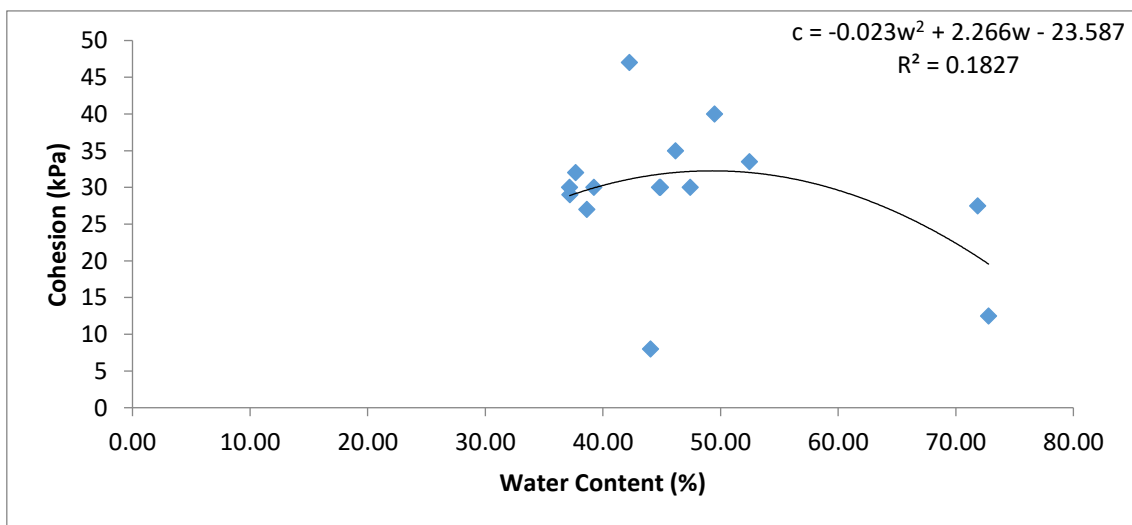
Figure 5-15: Effects of water content on soil cohesion

On consideration of tillage and traction practices , the peak cohesion corresponding to optimum water content of 45 % was 30.7 kPa and this is believed to represent the maximum cohesive force holding the soil particles together. It is at this point that tillage operations intervention on the soil appears appropriate and perhaps result into optimal friability without inimical damage to soil structural matrix. Similarly, maximum traction on operating tillage machinery may be achieved upon conversion of the cohesive strength (30.7 kPa) established. Thus, operating tillage machinery on vertisols with water content beyond 45 % may not only exacerbate slippage and consequential destruction of soil structural matrix but also result in less traction and low work ouput/field capacity. The above assumptions may not however hold due to low R^2 value of 0.1827 between cohesion and water content.

As the case in cohesion parameter, friction parameter increased and peaked at slightly above 3^0 as illustrated in Figure 5.16. The peak friction point occurred at a water content of 45 %. Further increment in water content resulted in continuous drop in angle of internal friction due to reduction in interlocking bonds and frictional resistance of particles at their point of contacts.

A quadratic relation between soil frictional component and water content with a low R^2 value of 0.2185 showed that the friction component, though a critical state parameter, cannot be correlated with the slope of the critical state line and further revealed the minimal friction component in the studied soils.
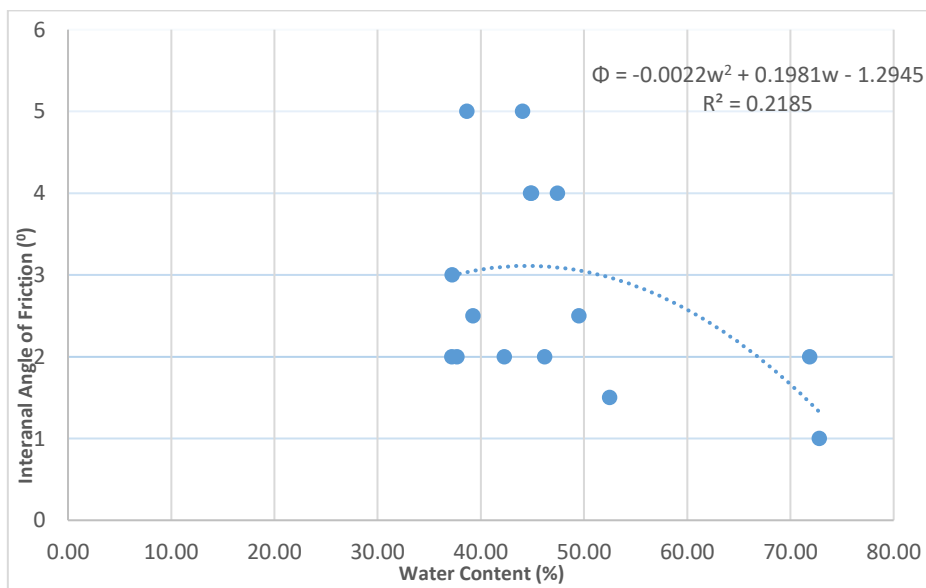
Figure 5-16: Effects of water content on soil internal angle of friction

5.4   Summary of Findings

All tested samples exhibited a three-pattern deformation characteristic in three zones i.e elastic/recoverable zone, maximum shear stress zone and continuous deformation/failure stress zone. Within elastic/recoverable deformation zone, apredictive model in equation 4.1 adequately correlated deviatoric stress (q) and strain (ε). Elastic/recoverable deformation in test samples occurred within a strain span of 0 to 5 %. Similarly, maximum shear stress and failure stress deformation zones were observed within strain ranges of 10 to 15 % and beyond 15 % respectively. Specimen failures were observed through bulging at the base that pointed to plastic flow mode failure pattern. The mean water contents increased with the profile depths. On the other hand, mean shear strengths decreased with increasing profile depths principally due to increased amount of water with depths.

The mean cohesive strengths of all specimens decreased with increase in mean water content. This was likely due to thickening of water films around the particles and at some point, the effects of water change from cohesion to lubrication making it easier for soil particles to slip past each other. Magnitudes of frictional components were generally small in all the profile depths.

6.0   CONCLUSIONS AND RECOMMENDATIONS

6.1   Conclusions

The study established that:

1.   A three-pattern deformation characteristic occurred in vertisols when subjected to loading from working tillage machinery. A model of resultant induced deviatoric stresses within the three deformation zones at various strain levels satisfactorily predicted the shear stress behaviour of the study soil

2.   Transition zone from an increase to a decline in cohesion and angle of internal friction occurred at a water content of 37.5 %. Corresponding cohesive strength that is likely to represent maximum cohesive force holding soil particles together is 70 kPa at 3^0 frictional angle. Optimal traction with attendant tillage result may be attained here on the study soils

3.   Failure pattern in vertisols due to loading from working tillage machinery occurred in plastic flow mode.

6.2   Recommendations

1.   Selection of appropriate machinery for use in tillage operations on vertisols at Mwea Rice Irrigation Scheme should be guided by the total critical shear stress parameters found out in the study i.e. *C* (70 kPa) and Φ (3^0) at 37.5 % water content.

2.   While the study has established that optimal traction and tillage operations on vertisols at Mwea Rice Irrigation Scheme is likely to be achieved at soil water content of 37.5 %, operation of tillage machinery on vertisols with water content above this threshold should be avoided to minimize inimical slippage and resultant aggregate structural destruction.

3.   Further research should be done to identify, analyze and manipulate other paddy rice soils based parameters in optimization of traction and tillage performances on it.

7.0   REFERENCES

Abu-Hamdeh, N.H. and Reeder, R.C. (2003). **Measuring and predicting stress distribution under tractive devices in undisturbed soil**. Biosystems Engineering 85 (2003) 493-502.

Ahmad, H. and Mermut, A. (1996). **Development in Soil Science** 24 (1996) 1- 41.

Alakukku, L. (1996). **Persistence of soil compaction due to high axle load traffic - Long-term effects on the properties of fine-textured and organic soils**. Soil and Tillage Research 37 (1996) 223-238.

Alam, S. and Chowdhary, G.R. (2007). **Soil Engineering in Theory and Practice**. Volume II, 2nd Edition , CBS Publishers & Distributors, New Delhi.

Alam, S. (2002). **Soil Engineering in Theory and Practice**. Volume I, 4th Edition, CBS Publishers & Distributors, New Delhi.

Alexandrou, A. and Earl, R. (1995). **In situ determination of the pre-compaction stress of a soil.** Journal of Agricultural Engineering Research 61 (1995) 67-72.

Al-Jalil, H.F., Khdair, A. and Mukahal, W. (2001). **Design and performance of an adjustable three-point hitch dynamometer**. Soil and Tillage Research 62 (2001)153-156.

Aluko, O.B. and Chandler, H.W. (2004). **Characterisation and modelling of brittle fracture in two-dimensional soil cutting.** Biosystems Engineering 88 (2004) 369-381.

Aluko, O.B. and Seig, D.A. (2000). **An experimental investigation of the characteristics of and conditions for brittle failure in two-dimensional soil cutting**. Soil and Tillage Research 57 (2000) 143-157.

Arpad, K. (1974). **Handbook of Soil Mechanics**. 2nd Edition, Elsevier Scientific Publishing Company, Amsterdam.

Arvidsson, J. (1997). **Soil Compaction in Agriculture – From Soil Stress to Plant Stress**. Doctoral Thesis. Agraria 41, Swedish University of Agricultural Sciences, Uppsala, Sweden.

Arvidsson, J. and Andersson, S. (1997). **Determination of soil displacement by measuring the pressure of a column of liquid**. Proceedings of the 14th International Conference of ISTRO, Puławy, Poland, pp. 47-50.

Arvidsson, J. and Dexter, A.R. (2002). **Tillage. Course in agricultural soil mechanics**. Swedish University of Soil Sciences, Uppsala, Sweden.

Atkinson, J. (2007). **The Mechanics of Soils and Foundation**. 2nd Edition, Taylor and Francis, 270 Madison Avenue, New York.

Atkinson, J. (1993). **An Introduction to the Mechanics of Soils and Foundations through Critical State Soil Mechanics**. McGraw-Hill International Series in Civil Engineering, London, 337 pp.

Atkinson, K.H. and Bransby, P.L. (1978). **The Mechanics of Soils – An Introduction to Critical State Soil Mechanics**. McGraw-Hill, London, 375 pp.

Bailey, A.C. and Johnson, C.E. (1989). **A soil compaction model for cylindrical stress states.** Transactions of the American Society of Agricultural Engineers 32, 822-825.

Bailey, A.C., Johnson, C.E. and Nichols, T.A. (1988). **Soil stress state determination under wheel loads.** Transactions of the American Society of Agricultural Engineers 31, 1309-1314.

Bailey, A.C., Johnson, C.E. and Schafer, R.L. 1986. **A model for agricultural soil compaction**. Journal of Agricultural Engineering Research 33 (1986) 257-262.
Bailey, A.C., Johnson, C.E. and Schafer, R.L. (1984). **Hydrostatic compaction of agricultural soils.** Transactions of the ASAE 27 (4): 925-955.

Bakker, D.M., Harris, H.D. and Wong, K.Y. (1995). **Measurement of stress path under agricultural vehicles and their interpretation in critical state space**. Journal of Agricultural Engineering 61 (1995) 247-260.

Barzegar, A.R., Hashemi, A.M., Herbert, S.J. and Asoodar, M.A. (2004). **Interactive effects of tillage system and soil water content on aggregate size distribution for seedbed preparation in Fluvisols in southwest Iran.** Soil and Tillage Research 78 (2004) 45-52.

Baumgartl, T. and Köck, B. (2004). **Modelling volume change and mechanical properties with hydraulic models**. Soil Science Society of America Journal 68 (2004) 57-65.

Berhanu, D. (1985). **The Vertisols of Ethiopia: their properties, classification and management**. Fifth Meeting of the Eastern African Sub-Committee for Soil Correlation and Land Evaluation.

Berli, M. (2001). **Compaction of Agricultural Subsoils by Tracked Heavy Construction Machinery.** Doctoral Thesis. ETH Diss. No. 14132, Swiss Federal Institute of Technolgy, ETH Zurich, Switzerland, 105 pp.

Berndt, R. D. and Coughlan, K. J. (1977). **The nature of changes in bulk density with water content in a cracking clay**. Australian Journal of Soil Research 15 (1977) 27-37.

Berntsen, R. and Berre, B. (2002). **Soil fragmentation and the efficiency of tillage implements**. Soil and Tillage Research 64 (2002) 137-147.

Bhagat, R.M. and Acharya, C.L. (1988). **Soil water dynamics during wheat growth under different soil management practices**. Journal of Indian Society of Soil Science 36 (1988) 389-396.

Bhagat, R.M. (1990). **Effect of tillage and residue management on hydrothermal regime, nutrient uptake and yield of wheat in a river deposit**. Soil and Tillage Research 17 (1990) 315-326.

Bhagat, R.M., Bhardwaj, A.K., Sharma, P.K. and Pradeep, K. (2003**). Long term effect of residue management on soil physical properties, water use and yield of rice in north-western India.** Journal of Indian Society of Soil Science 51 (2003) 111-117.

Bhagat, R.M., Sharma, P.K. and Verma, T.S. (1994). **Tillage and residue management effects on soil physical properties and rice yields in north western Himalayan soils**. Soil and Tillage Research 29 (1994) 323-334.

Bhagat, R.M., Sharma, P. K. and Verma, T.S. (1995). **Soil structural improvements with addition of Lantana camara biomass in rice-wheat cropping**. Soil Use and Management 11 , 199-203.

Birkás, M., Jolankai, M., Gyuricza, C. and Percze, A. (2004). **Tillage effects on compaction, earthworms and other soil quality indicators in Hungary**. Soil and Tillage Research 78 (2004) 185-196.

Bishop, A.W. (1959). **The principle of effective stress**. Teknisk Ukeblad 106 (39), 859-863.

Blunden, B.G., McBride, R.A., Daniel, H. and Blackwell, P.S. (1994). **Compaction of an earthy sand by rubber tracked and tyred vehicles**. Australian Journal of Soil Research 32 (1994) 1095-1108.

Braunack, M.V., McPhee, J.F. and Dexter, A.R. (1999). **The effect of initial soil water content and tillage implements on seedbed formation**. Soil and Tillage Research 20 (1999) 5-17.

Brink, A.B., Partridge, A. and Williams, A. A. B. (1980). **Soil Survey for Engineering**. Oxford University Press.

Britto, A.M. and Gunn, M.J. (1987). **Critical State Soil Mechanics via Finite Elements**. Ellis Horwood, Chichester, 488 pp.

Brown, H.J., Cruse, R.M., Erbach, D.C. and Melvin S.W. (1992). **Tractive device effects on soil physical properties.** Soil and Tillage Research 22 (1992) 41-53.

Burt, E.C., Wood, R.K. and Bailey, A.C. (1992). **Some comparison of average to peak soil-tire contact pressures.** Transactions of the American Society of Agricultural Engineers 35, 401-404.

Bryan, D., Eagle, D. and Finney, B. (1986). **Soil Management**. 4th Edition, Farming Press Ltd.

Chengshun, X., Xin, W., Xinyue, L., Fuchu, D.and Shuang, J. (2018). **Experimental study of residual strength and the index of shear strength characteristics of clay soil**. Journal of Engineering Geology 233 (2018) 183 – 190.

Chi, L. and Kushwaha, R.L. (1989). **Finite element analysis of forces on a plane soil blade**. Canadian Agricultural Engineering 31(2) (1989) 135-140.

Chi, L., Kushwaha, R.L. and J. S. (1993). **An elasto-plastic constitutive model for agricultural cohesive soil**. Canadian Agricultural Engineering 35(4) (1993) 245-251.

Chunlai, Z., Xuesong,W., Xueyong, Z., Jinlu, T., Bo, L., Jifeng, L., Ligiang, K., Hong, C. and Yonggiu, W. (2018). **Estimation of surface shear of undisturbed soils in the eastern part of northern China's erosion area**. Soil and Tillage Research 178 (2018) 1-10.

Cooper, B. R. and Georges, J .E .W. (1982). **Importance of sugar-cane in the management of clay soils in Trinidad.** Tropical Agriculture (Trinidad) *59,* 183-188.

Dawidowski, J.B. and Koolen, A.J. 1994. **Computerized determination of the precompression stress in compaction testing of field core samples**. Soil and Tillage Research 31 (1994) 277-282.

Dawidowski, J.B., Morrison, J.E. and Snieg, M. (2001). **Measurement of soil layer strength with plate sinkage and uniaxial confined methods**. Transactions of the American Society of Agricultural Engineers 44 (2001) 1059-1064.

Dawidowski, J.B., Worona, M. and Hencel, A. (1988). **The determination of plow draught from soil penetration resistance**. Proceedings of the 11th International Conference of ISTRO on Tillage and Traffic in Crop Production, Edinburgh, Scottland, Vol. 2 (1988) 457-462.

Défossez, P. and Richard, G. (2002). **Models of soil compaction due to traffic and their evaluation.** Soil and Tillage Research 67 (2002) 41-64.

Desbiolles, J.M.A., Godwin, R.J., Kilgour, J. and Blackmore, B.S. (1997). **A novel approach to the prediction of tillage tool draught using a standard tine**. Journal of Agricultural Engineering 66 (1997) 295-309.

Dexter, A.R. (2004a). **Soil physical quality: Part I. Theory, effects of soil texture, density, and organic matter, and effects on root growth**. Geoderma 120, 201-214.

Dexter, A.R. (2004b). **Soil physical quality: Part II. Friability, tillage, tilth and hard-setting**. Geoderma 120, 215-225.

Dexter, A.R. (2004c). **Soil physical quality: Part III. Unsaturated hydraulic conductivity and general conclusions about S-theory**. Geoderma 120, 227-239.

Dexter, A.R. (2002). **Soil mechanical notes. Course in agricultural soil mechanics,** Swedish University of Soil Sciences, Uppsala, Sweden.

Dexter, A.R. (1988). **Advances in characterization of soil structure**. Soil and Tillage Research 11 (1988) 199-238

Dexter, A.R. (1979). **Prediction of soil structures produced by tillage**. Journal of Terramechanics 16 (1979) 117-127.

Dexter, A.R. and Bird, N.R.A. (2001). **Methods for predicting the optimum and the range of water contents for tillage based on the water retention curve**. Soil and Tillage Research 57 (2001) 203-212.

Dexter, A.R., Horn, R. and Kemper, W.D. (1988). **Two mechanisms for age-hardening of soil.** Journal of Soil Science 39 (1988) 163-175.

Dexter, A.R. and Kroesbergen, B. (1985). **Methodology for determination of tensile strength of soil aggregates**. Journal of Agricultural Engineering 31 (1985) 139-147.

Dexter, A.R. and Tanner, D.W. (1973). **The response of unsaturated soils to isotropic stress**. Journal of Soil Science 24 (1973), 491-502.

Dexter, A.R. and Tanner, D.W. (1974). **Time dependence of compressibility for remoulded and undisturbed soils**. Journal of Soil Science 25 (1974) 153-164. Dias Junior, M.S. & Pierce F.J. (1995). **A simple procedure for estimating preconsolidation pressure from soil compression curves**. Soil Technology 8, 139-151.

Diserens, E. & Steinmann, G. (2002). **Calculation of pressure distribution in moist arable soils in Eastern Switzerland: a simple model approach for the practice**. Environmental Geomechanics, EPFL Lausanne, Switzerland, pp. 413-421.

Dorthe, H., Andre, A., Jose, M., Rainer, H., Huner, F. and Alexander, Z. (2018). **Soil functions and in situ stress distribution in subtropical soils as affected by land use vehicle type, tire inflation pressure and plant residue removal**. Soil and Tillage Research 184 (2018) 78 – 92.

Dudal, R. and Eswaran, H. (1988). "**Distribution properties and classification of vertisols,**" **In vertisols: their distribution, properties, classification and management.** Technical Monograph 18 (1988) 1 - 22.

Earl, R. (1997). **Assessment of the behaviour of field soils during compaction**. Journal of Agricultural Engineering 68 (1997) 147-157.

Eswaran, H., Beinroth, F.H., Reich, P. F. and Quandt, L.A. (199). **Vertisols : their properties, classification, distribution and management**. USDA Natural Resources Conservation Service, Washington DC (1999).

Etana, A. and Håkansson, I. (1994). **Swedish experiments on the persistence of subsoil compaction caused by vehicles with high axle load**. Soil and Tillage Research 29 (1994) 167-172

Fox, W. E. (1964). **A study of bulk density and water in a swelling soil**. *Soil Science* 98 (1964) 307316.

Frantisek, B., Petr, P., Adam, P., Jiri, C. and Martin, F. (2022). **Differences in the wheel loads and contact pressure of the in – furrow and on – land rear tractor tyres with mounted and semi – mounted ploughs**. Soil and Tillage Research 215 (2022) 105 – 190.

Gachene, C.K. and Kimaru, G. (2003). **Soil Fertility and Land Productivity**. A Guide for Extension Workers in the Eastern Africa Region.

Gill, W.R. and Vandenberg, G.E. (1968). **Soil Dynamics in Tillage and Traction**. U.S.A. Department of Agriculture, Handbook 316, USA, Washington D.C., cited by Makanga *et al.* (1996).

Gitau, A.N. (2004). **Mechanical Behaviour of a Hardsetting Luvisol Soil.** Ph.D. Thesis. University of Nairobi, Kenya.

Gitau, A.N., Gumbe, L.O. and Biamah, E.K. (2006). **Influence of Soil Water on Stress-Strain Behaviour of Compacting Soil in Semi – Arid Kenya.** Soil and Tillage Research 89 (2006) 144 – 154.

Godwin, R.J. (2003). **A review of the effect of tillage implement geometry on soil failure and implement forces**. In: Proceedings of the 16th International Conference of ISTRO on Soil Management for Sustainability, 14-18 July 2003, Brisbane, Australia, pp. 471-483.

Godwin, R.J., Seig, D.A. and Allott, M. (1985). **The development and evaluation of a force prediction model for agricultural discs.** In: Proceedings of the International Conference on Soil Dynamics, Auburn, AL, USA, pp. 250-265.

Godwin, R.J., Seig, D.A. and Allott, M. (1987). **Soil failure and force prediction for soil engaging discs.** Soil Use and Management 3 (1987) 106-114. 70.

Godwin, R.J. and Spoor, G. (1977). **Soil failure with narrow tines**. Journal of Agricultural Engineering 22 (1977) 213-228.

Godwin, R.J., Spoor, G. & Soomro, M.S. (1984). **The effect of tine arrangement on soil forces and disturbance**. Journal of Agricultural Engineering 30 (1984) 47-56.

Government of Kenya, Ministry of Water and Irrigation. (2021). **Annual Report**. National Irrigation Authority (2021).

Gupta, S.C. and Larson, W.E. (1982). Chapter 10 - **Predicting soil mechanical behaviour during tillage**. In: Predicting Tillage Effects on Soil Physical Properties and Processes. American Society of Agronomy, Special Publications 44 (1982) 151-178.

Gysi, M., Maeder, V. and Weisskopf, P. (2001). **Pressure distribution underneath tires of agricultural vehicles.** Transactions of the American Society of Agricultural Engineers 44 (2001) 1385-1389.

Hammel, K. (1994). **Soil stress distribution under lugged tires**. Soil and Tillage Research 32 (1994) 163-181.

Hettiaratchi, D.R.P. (1997). **Prediction of soil forces acting on concave agricultural discs**. Journal of Agricultural Engineering 68 (1997) 51-62.

Hettiaratchi, D.R.P. (1988). **Theoretical soil mechanics and implement design**. Soil and Tillage Research 11 (1988) 325-347.

Horn, R. (1990b). **Structure effects on strength and stress distribution in arable soils**. In: Proceedings of the International Summer Meeting of the American Society of Agricultural Engineers, June 24-27, 1990, Columbus, Ohio, pp. 8-20.

Igor, D., Barbara, S., Szergej, V. and Marta, B. (2019). **The effects of various tillage treatments on soil physical properties, earthworm abundance and crop yield in Hungary**. Soil and Tillage Research 194 (2019) 104334.

International Soil Reference and Information Centre (ISRIC), **Annual Report,** 2020 – 2021.

Joab, O. W., Macharia, J.N.K. and Sijali, I. V. (2013). **Prioritised vertisol management options in Mwea**. Kenya Agricultural Research Institute. Report.

John, B.L., Turnquist, P.K., Smith, D.W. and Hoki, M. (1989). **Tractors and Their Power Units**, Van Nostrand Reinhold International Co. Ltd.

Johnson, C. E., Schafer, R. L. and Elkin, C. B. (1982). **Prescribing tillage for clay soils**, Tropical Agriculture (Trinidad) 59 (1982) 92 - 96.

Joseph, E.B. (1984). **Physical and GeoTechnical Properties of Soils**. McGraw – Hill, Inc.

Kamara, C. S. and Haque, I. (1987a). **The characteristics of Vertisols at ILCA's research and outreach sites in Ethiopia**. PSD Working Document No. B5. International Livestock Centre for Africa (ILCA), Addis Ababa, Ethiopia.

Kamara, C. S. and Haque, I. (1987b). **Studies on the field capacity of a Udic Vertisol**. International Conference on Measurement of Soil and Plant Water Status, Utah State University, Logan, Utah, 6-10 July 1987. Utah State University Press, Logan, Utah, USA. Vol. 1, pp. 47-58.

Karmar, S.J., Sharma, and Kushwaha, R.L. (2004). **Critical State Elasto – Plastic Constitutive Models for Soil Failure in Tillage – A Review**. Canadian Biosystems Engineering 46 (2004) 2.19 – 2.23.

Kenya Agricultural and Livestock Research Organization (KALRO), **Kenya Soil Suurvey,** Nov 2019.

Khan, F.U., Tahir, A.R. and Yule, I.J. (1999). **Impact of different tillage practices and temporal factor on soil moisture content and soil bulk density**. International Journal of Agriculture & Biology 1 (1999) 163-166.

Kirby, J.M. (1989). **Measurements of the yield surfaces and critical state of some unsaturated agricultural soils**. Journal of Soil Science 40 (1989) 167-182 .

Kirby, J.M. (1991). **Strength and deformation of agricultural soil: measurement and practical significance.** Soil Use and Management 7 (1991) 223-229.

Kirby, J.M. (1999a). **Soil stress measurement: Part 1. Transducer beneath a circular loaded area.** Journal of Agricultural Engineering 72 (1999) 151-160.

Kirby, J.M. (1999b). **Soil stress measurement: Part 2. Transducer in a uniform stress field**. Journal of Agricultural Engineering *72 (1999)* 141-149.

Kirby, J.M., Blunden, B.G. and Trein, C.R. (1997). **Simulating soil deformation using a critical-state model: II. Soil compaction beneath tyres and tracks**. European Journal of Soil Science 48 (1997) 59-70.

Koolen, A.J. (1974). **A method for soil compactibility determination**. Journal of Agricultural Engineering 19 (1974) 271-278.

Koolen, A.J. and Kuipers, H. (1983). **Agricultural Soil Mechanics***:* Advanced Series in Agricultural Sciences 13 (1983) pp 241.

Kosuke, H., Hisayoshi, I., Hidetoshi, M., Teruhito, M., Mayuko, A. and Yuta, S. (2021). **Effect of hardpan on the vertial distribution of water stress in a converted paddy field**. Soil and Tillage Research 214 (2021) 105161.

Kothari, C.R. (2004). **Research Methodology- Methods and Techniques**. 2nd Revised Edition, New Age International Publishers Ltd, New Delhi.

Kushwaha, R.L. and J. Shen. (1994). **The application of plasticity in soil constitutive modeling**. ASAE Paper 941072 (1994).

Lade, P.V. and R.B. Nelson.(1984). **Incrementalization procedure for elasto-plastic constitutive model with multiple, intersecting yield surface**. International Journal for Numerical and Analytical Methods in Geomechanics 8 (1984) 311-323.

Lambe, T.W. and Robert, V.W. (1979). *Soil Mechanics, SI Version*, John Wiley & Sons , New York.

Lambe, T.W. and Whitman, R.V. (1979*).* **Soil Mechanics, SI Version**. John Wiley & Sons.

Loraine, D., Mathia, S., Francois, P., Patrick, V., Thomas, K., Lars, J. and Mathieu, Z. (2020). **Construction of modern wide, low – inflation pressure tyres per se does not affect soil stress**. Soil and Tillage Research 204 (2020) 104708.

Marsili, A., Servadio, P., Pagliai, M. and Vignozzi, N. (1998). **Changes of some physical properties of a clay soil following passage of rubber- and metal-tracked tractors**. Soil and Tillage Research 49 (1998), 185-199.

McIntyre, D. S. (1984). **The physics of volume change in cracking clay soils**.

Ministry of Agriculture, (2010). **The Kenya Agricultural Sector Data Compendium**. Volume 2 – Crops Statistics.

Miriti, J.M., Kironchi, G., Esilaba, A.O., Gachene, C.K.K., Heng, L.K. and Mwangi, D.M. (2013). **The effects of tillage systems on soil physical properties and water conservation in a sandy loam soil in Eastern Kenya**. Journal of Soil Science and Environmental Management 4 (2013) 146-154.

Mouazen, A.M. and Ramon, H. (2002). **A numerical-statistical hybrid modelling scheme for evaluation of draught requirements of a subsoiler cutting a sandy loam soil, as affected by moisture content, bulk density and depth.** Soil and Tillage Research 63 (2002) 155-165.

Muchene, F.M. and Gachene. C.K. (1988). **Properties, Management and Classification of Vertisols in Kenya.** Proceedings of 5th Meeting for the Eastern African Sub – Committee for Soil.

Muir, W.D., Mackenzie, N.L. and Chan, A.H.C. (1992). **Predictive Soil Mechanics.** Proceedings of the Wroth Memorial Symposium, St. Catherine's College, Oxford, pg 496 – 512.

Müller, L., Schindler, U. Fausey, N.R. and Lal, R. (2003). **Comparison of methods for estimating maximum soil water content for optimum workability**. Soil and Tillage Research 72 (2003) 9-20.

Nyle, C.M. (1984). **The Nature and Properties of Soil**. 9th Edition, Macmillan Publishing, New York.

Ojeniyi, S.O. and Dexter, A.R. (1979). **Soil factors affecting the macrostructures produced by tillage**. Transactions of the American Society of Agricultural Engineers 22 (1979) 339-343.

Okello, J.A., Dwyer, M.J. and Cottrell, F.B. (1994). **The tractive performance of rubber tracks and a tractor driving wheel tyre as influenced by design parameters**. Journal of Agricultural Engineering 59 (1994) 33-43.

Onwualu, A.P. and Watts, K.C. (1998). **Draught and vertical forces obtained from dynamic soil cutting by plane tillage tools**. Soil and Tillage Research 48 (1998) 239-253.

O'Sullivan, M.F. and Robertson, E.A.G. (1996). **Critical state soil parameters from intact samples of two agricultural topsoils**. Soil and Tillage Research 39 (1996) 161-173.

Pagliai, M., Marsili, A., Servadio, P., Vignozzi, N. and Pellegrini, S. (2003). **Changes in some physical properties of a clay soil in Central Italy following the passage of rubber tracked and wheeled tractors of medium power.** Soil and Tillage Research 73 (2003) 119-129.

Peter, B. O. and Carmen, M.U. (2021). **A meta – analysis of the impact of traffic – induced compaction on soil physical properties and grain yield**. Soil and Tillage Research 211 (2021) 105019.

Roscoe, K.H., A.N. Schofield and C.P. Wroth. (1958). **On the yielding of soils**. Géotechnique 8 (1958) 22-53.

Schofield, A.N. and C.P. Wroth. (1968). **Critical State Soil Mechanics**. London, England: McGraw-Hill.

Shuihong, Yao, Xiaolong, T. and Bin, Z. (2015). **Effects of rice straw incorporating and tillage depth on soil puddlability and mechanical properties during rice growth period**. Journal of Soil and Tillage Research 146 (2015), Part B, pp: 125 – 132.

Strudley, M.W., Green, T.R. and Ascough, J.C. (2008). **Tillage effects on soil hydraulic properties in space and time: State of the science**. Soil and Tillage Resources 99 (2008) 4-48.

Temesgen et al., (2022). **Vertisols infiltrate rate and model performance evaluation of various land use condition durting Southern Ethiopia's dry season**. Journal of Digital Food, Energy & Water Systems (JD – FEWS) 3 (2022) 16 - 28.

Temga et al., (2019). **Characteristics, classification and genesis of vertisols under seasonally contracted climate in the Lake Chad Basin, Central Africa**. Journal of African Earth Sciences 150 (2019) 176 - 193.

Thomas, K. (2004). **Soil Compaction and Soil Tillage – Studies in Agricultural Soil Mechanics.** Unpublished Ph.D. thesis . Uppsala, Sweden. Department of Soil Sciences, Swedish University of Agricultural Sciences.

Thomas, K., Maria, S., Tino, C., Rainer, H. and Dani, O. (2019). **Effects of vehicular traffic on soil compaction**. Soil and Tillage Research 194 (2019) 104293.

Unger, P.W., Cassel, D.K. and Allen, R. (1991). **Tillage implements disturbance effects on soil properties related to soil and water conservation: a literature review**. Soil and Tillage Resources 19 (1991):363-82.

Venkatranman, C. (2006). **Geotechnical Engineering**. 3rd Edition, New Age International Publishers Ltd, New Delhi.

Yule D F. (1984). **Volumetric calculations in cracking clay soils**. In: J W McGarity, E H Hoult and H B So (eds), **The properties and utilization of cracking clay soils. Reviews in Rural Science No. 5**. University of New England, Armidale, NSW, Australia. pp. 136-140.

Yule D F and Ritchie J T. (1980a). **Soil shrinkage relationships of Texas Vertisols**. I. Small cores. Journal of the Soil Science Society of America 44 (1980)1285-1291.

Yule D F and Ritchie J T. (1980b). **Soil shrinkage relationships of Texas Vertisols**. II. Large cores. Journal of the Soil Science Society of America 44 (1980)1291-1295.

Zhang, J. and R.L. Kushwaha. (1998). **Dynamic analysis of a tillage tool**: Part I – Finite element method. Canadian Agricultural Engineering 40(4) (1998) 287-292.

Appendix A: Deviatoric stress-strain trends for WMD1, WMD2 and WMD3
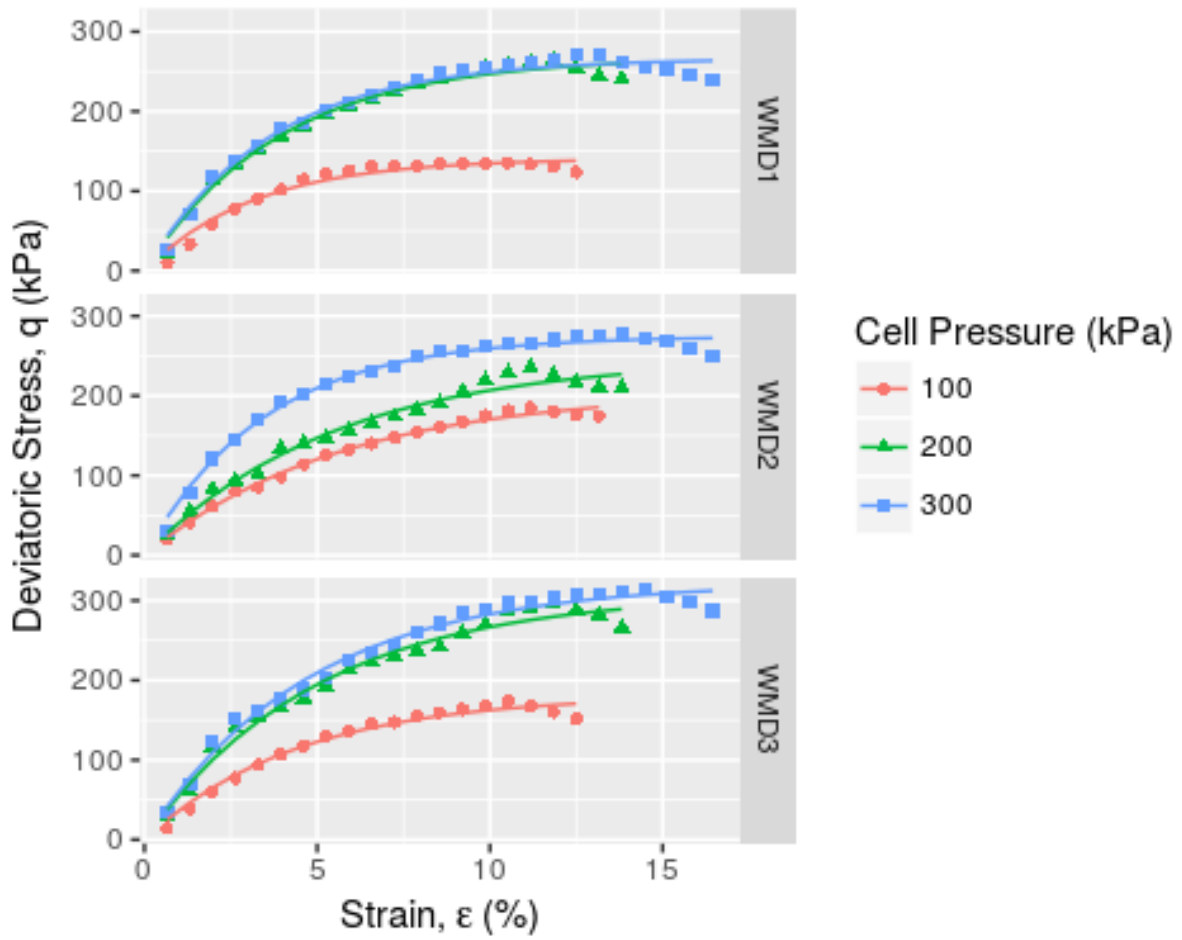
Appendix C: Deviatoric stress-strain trends for THD1, THD2 and THD3
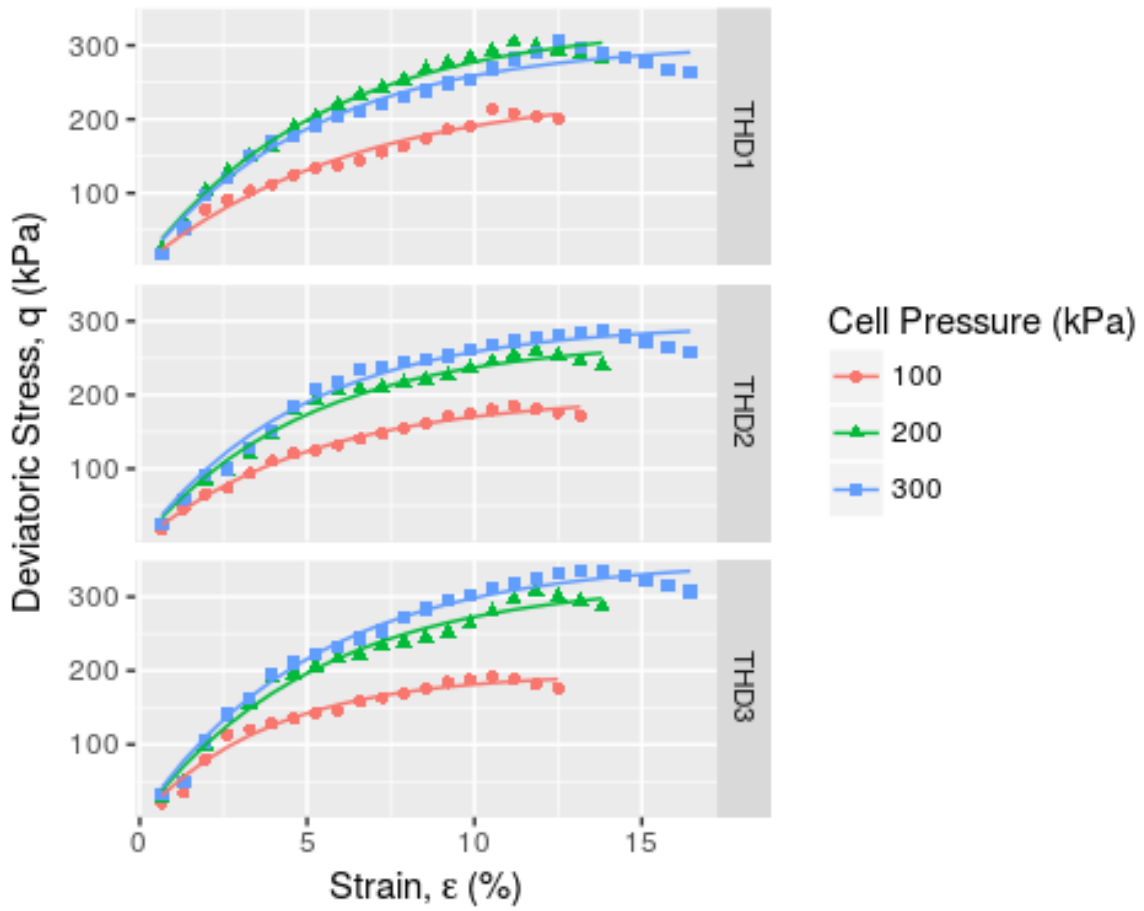
Appendix D: Samples failure conditions data

Table D1 : Failure conditions for KRD1

Moisture Content (w) %	34.60	34.60	34.60	34.60 (Mean)
Failure Conditions Data	**KRD$_1$(i)**	**KRD$_1$(ii)**	**KRD$_1$(iii)**	
Cell Pressures σ_3 (kPa)	100	200	300	
Deviator Stress σ_d (kPa)	136.16	211.45	216.29	
Axial Stress σ_1(kPa)	236.16	411.45	516.29	
Axial Strain ε (%)	9.21	9.21	10.53	
Shear Strength Parameters				
Cohesion (C) kPa/kN/m^2	110			
Internal Angle of Friction (φ)	0^0			
Failure Mode:	Lateral Bulging on the lower side			

Table D2 : Failure conditions for WMD1

Moisture Content (w) %	34.80	34.80	34.80	34.80 (Mean)
Failure Conditions Data	**WMD$_1$(i)**	**WMD$_1$(ii)**	**WMD$_1$(iii)**	
Cell Pressures σ_3 (kPa)	100	200	300	
Deviator Stress σ_d (kPa)	135.76	264.43	271.20	
Axial Stress σ_1(kPa)	235.76	464.43	571.20	
Axial Strain ε (%)	10.53	11.84	13.16	
Shear Strength Parameters				
Cohesion (C) kPa/kN/m^2	131			
Internal Angle of Friction (φ)	0^0			
Failure Mode:	Lateral Bulging on the lower side			

Table D3 : Failure conditions for MWD1

Moisture Content (w) %	35.01	35.62	35.47	35.37 (Mean)
Failure Conditions Data	**MWD$_1$(i)**	**MWD$_1$(ii)**	**MWD$_1$(iii)**	
Cell Pressures σ_3 (kPa)	100	200	300	
Deviator Stress σ_d (kPa)	211.55	261.31	274.27	
Axial Stress σ_1(kPa)	311.55	461.31	574.27	
Axial Strain ε (%)	11.18	11.84	13.16	
Shear StrengthParameters				
Cohesion (C) kPa/kN/m^2	110			
Internal Angle of Friction (φ)	4^0			
Failure Mode:	Lateral Bulging on the lower side			

Table D4 : Failure conditions for TBD1

Moisture Content (w) %	35.39	35.71	35.75	35.62 (Mean)
Failure Conditions Data	**TBD$_1$(i)**	**TBD$_1$(ii)**	**TBD$_1$(iii)**	
Cell Pressures σ_3 (kPa)	100	200	300	
Deviator Stress σ_d (kPa)	213.12	295.53	321.12	
Axial Stress σ_1(kPa)	313.12	495.53	621.12	
Axial Strain ε (%)	11.18	11.84	12.50	
Shear Strength Parameters				
Cohesion (C) kPa/kN/m^2	109			
Internal Angle of Friction (φ)	7^0			
Failure Mode:	Lateral Bulging on the lower side			

Table D5 : Failure conditions for THD1

Moisture Content (w) %	35.29	35.54	35.62	35.48 (Mean)
Failure Conditions Data	**THD$_1$(i)**	**THD$_1$(ii)**	**THD$_1$(iii)**	
Cell Pressures σ_3 (kPa)	100	200	300	
Deviator Stress σ_d (kPa)	213.12	304.01	307.22	
Axial Stress σ_1(kPa)	313.12	504.01	607.22	
Axial Strain ε (%)	10.53	11.18	12.50	
Shear Strength Parameters				
Cohesion (C) kPa/kN/m^2	153			
Internal Angle of Friction (φ)	0^0			
Failure Mode:	Lateral Bulging on the lower side			

Table D6 : Failure conditions for KRD2

Moisture Content (w) %	35.9	35.9	35.9	35.9 (Mean)
Failure Conditions Data	**KRD$_2$(i)**	**KRD$_2$(ii)**	**KRD$_2$(iii)**	
Cell Pressures σ_3 (kPa)	100	200	300	
Deviator Stress σ_d (kPa)	148.80	237.12	258.31	
Axial Stress σ_1(kPa)	248.80	437.12	558.31	
Axial Strain ε (%)	10.53	11.18	13.16	
Shear Strength Parameters				
Cohesion (C) kPa/kN/m^2	94			
Internal Angle of Friction (φ)	5^0			
Failure Mode:	Lateral Bulging on the lower side			

Table D7 : Failure conditions for WMD2

Moisture Content (w) %	36	36.75	36.53	36.43 (Mean)
Failure Conditions Data	**WMD$_2$(i)**	**WMD$_2$(ii)**	**WMD$_2$(iii)**	
Cell Pressures σ_3 (kPa)	100	200	300	
Deviator Stress σ_d (kPa)	184.91	235.06	276.75	
Axial Stress σ_1(kPa)	284.91	435.06	576.75	
Axial Strain ε (%)	11.18	11.18	13.82	
Shear Strength Parameters				
Cohesion (C) kPa/kN/m^2	50			
Internal Angle of Friction (φ)	10^0			
Failure Mode:	Lateral Bulging on the lower side			

Table D8 : Failure conditions for MWD2

Moisture Content (w) %	36.41	36.13	36.73	36.42 (Mean)
Failure Conditions Data	**MWD$_2$(i)**	**MWD$_2$(ii)**	**MWD$_2$(iii)**	
Cell Pressures σ_3 (kPa)	100	200	300	
Deviator Stress σ_d (kPa)	184.91	241.09	277.66	
Axial Stress σ_1(kPa)	284.91	441.09	577.66	
Axial Strain ε (%)	11.18	11.84	14.47	
Shear StrengthParameters				
Cohesion (C) kPa/kN/m^2	65			
Internal Angle of Friction (φ)	10^0			
Failure Mode:	Lateral Bulging on the lower side			

Table D9 : Failure conditions for TBD2

Moisture Content (w) %	36.69	36.73	36.87	36.76 (Mean)
Failure Conditions Data	**TBD$_2$(i)**	**TBD$_2$(ii)**	**TBD$_2$(iii)**	
Cell Pressures σ_3 (kPa)	100	200	300	
Deviator Stress σ_d (kPa)	180.21	256.65	284.99	
Axial Stress σ_1(kPa)	280.21	456.65	584.99	
Axial Strain ε (%)	11.18	11.84	13.16	
Shear Strength Parameters				
Cohesion (C) kPa/kN/m^2	90			
Internal Angle of Friction (φ)	7^0			
Failure Mode:	Lateral Bulging on the lower side			

Table D10 : Failure conditions for THD2

Moisture Content (w) %	36.55	36.39	36.91	36.62 (Mean)
Failure Conditions Data	**THD$_2$(i)**	**THD$_2$(ii)**	**THD$_2$(iii)**	
Cell Pressures σ_3 (kPa)	100	200	300	
Deviator Stress σ_d (kPa)	184.91	258.20	288.92	
Axial Stress σ_1(kPa)	284.91	458.20	588.92	
Axial Strain ε (%)	11.18	11.84	13.82	
Shear Strength Parameters				
Cohesion (C) kPa/kN/m^2	75			
Internal Angle of Friction (φ)	10^0			
Failure Mode:	Lateral Bulging on the lower side			

Table D11 : Failure conditions for KRD3

Moisture Content (w) %	36.4	36.4	36.4	36.4 (Mean)
Failure Conditions Data	**KRD$_3$(i)**	**KRD$_3$(ii)**	**KRD$_3$(iii)**	
Cell Pressures σ_3 (kPa)	100	200	300	
Deviator Stress σ_d (kPa)	146.39	235.15	255.49	
Axial Stress σ_1(kPa)	246.39	435.15	555.49	
Axial Strain ε (%)	10.53	11.84	13.82	
Shear Strength Parameters				
Cohesion (C) kPa/kN/m^2	75			
Internal Angle of Friction (φ)	8^0			
Failure Mode:	Lateral Bulging on the lower side			

Table D12 : Failure conditions for WMD3

Moisture Content (w) %	36.84	36.70	36.90	36.81 (Mean)
Failure Conditions Data	**WMD$_3$(i)**	**WMD$_3$(ii)**	**WMD$_3$(iii)**	
Cell Pressures σ_3 (kPa)	100	200	300	
Deviator Stress σ_d (kPa)	175.65	225.53	270.87	
Axial Stress σ_1(kPa)	275.65	425.53	570.87	
Axial Strain ε (%)	10.53	11.84	14.47	
Shear Strength Parameters				
Cohesion (C) kPa/kN/m^2	55			
Internal Angle of Friction (φ)	10^0			
Failure Mode:	Lateral Bulging on the lower side			

Table D13 : Failure conditions for MWD3

Moisture Content (w) %	37.25	37.77	37.19	37.40 (Mean)
Failure Conditions Data	**MWD$_3$(i)**	**MWD$_3$(ii)**	**MWD$_3$(iii)**	
Cell Pressures σ_3 (kPa)	100	200	300	
Deviator Stress σ_d (kPa)	180.05	240.42	225.93	
Axial Stress σ_1(kPa)	280.05	440.42	525.93	
Axial Strain ε (%)	11.18	11.84	13.82	
Shear StrengthParameters				
Cohesion (C) kPa/kN/m^2	45			
Internal Angle of Friction (φ)	13^0			
Failure Mode:	Lateral Bulging on the lower side			

Table D14 : Failure conditions for TBD3

Moisture Content (w) %	37.46	37.64	37.84	37.65 (Mean)
Failure Conditions Data	**TBD$_3$(i)**	**TBD$_3$(ii)**	**TBD$_3$(iii)**	
Cell Pressures σ_3 (kPa)	100	200	300	
Deviator Stress σ_d (kPa)	179.86	252.31	282.50	
Axial Stress σ_1(kPa)	279.86	452.31	582.50	
Axial Strain ε (%)	10.53	11.84	13.82	
Shear Strength Parameters				
Cohesion (C) kPa/kN/m^2	85			
Internal Angle of Friction (φ)	8^0			
Failure Mode:	Lateral Bulging on the lower side			

Table D15 : Failure conditions for THD3

Moisture Content (w) %	37.16	37.60	37.94	37.57 (Mean)
Failure Conditions Data	**THD$_3$(i)**	**THD$_3$(ii)**	**THD$_3$(iii)**	
Cell Pressures σ_3 (kPa)	100	200	300	
Deviator Stress σ_d (kPa)	182.60	253.98	286.54	
Axial Stress σ_1(kPa)	282.60	453.98	586.54	
Axial Strain ε (%)	10.53	11.84	13.82	
Shear Strength Parameters				
Cohesion (C) kPa/kN/m^2	75			
Internal Angle of Friction (φ)	9^0			
Failure Mode:	Lateral Bulging on the lower side			

Table D16 : Failure conditions for KRU1

Moisture Content (w) %	83.41	67.56	67.40	72.79 (Mean)
Failure Conditions Data	**KRU$_1$(i)**	**KRU$_1$(ii)**	**KRU$_1$(iii)**	
Cell Pressures σ$_3$ (kPa)	100	200	300	
Deviator Stress σ$_d$ (kPa)	24.83	23.51	39.72	
Axial Stress σ$_1$(kPa)	124.83	223.51	339.72	
Axial Strain ε (%)	13.33	11.18	6.08	
Shear Strength Parameters				
Cohesion (C) kPa/kN/m^2	12.5			
Internal Angle of Friction (φ)	1^0			
Failure Mode:	Lateral Bulging on the lower side			

Table D17 : Failure conditions for WMU1

Moisture Content (w) %	80.33	66.84	68.38	71.85 (Mean)
Failure Conditions Data	WMU1(i)	WMU1(ii)	WMU1(iii)	
Cell Pressures σ3 (kPa)	100	200	300	
Deviator Stress σd (kPa)	65	67.23	78.35	
Axial Stress σ1(kPa)	165	267.23	378.35	
Axial Strain ε (%)	7.89	5.92	11.18	
Shear Strength Parameters				
Cohesion (C) kPa/kN/m2	27.5			
Internal Angle of Friction (φ)	20			
Failure Mode:	Bend/Shear			

Table D18 : Failure conditions for MWU1

Moisture Content (w) %	48.36	50.75	49.38	49.49 (Mean)
Failure Conditions Data	**MWU$_1$(i)**	**MWU$_1$(ii)**	**MWU$_1$(iii)**	
Cell Pressures σ$_3$ (kPa)	100	200	300	
Deviator Stress σ$_d$ (kPa)	80.20	87.75	110.51	
Axial Stress σ$_1$(kPa)	180.20	287.75	410.51	
Axial Strain ε (%)	7.24	7.89	7.89	
Shear StrengthParameters				
Cohesion (C) kPa/kN/m^2	40			
Internal Angle of Friction (φ)	2.5^0			
Failure Mode:	Bend/Shear			

Table D19 : Failure conditions for TBU1

Moisture Content (w) %	44.84	49.44	47.96	47.41 (Mean)
Failure Conditions Data	**TBU$_1$(i)**	**TBU$_1$(ii)**	**TBU$_1$(iii)**	
Cell Pressures σ_3 (kPa)	100	200	300	
Deviator Stress σ_d (kPa)	81.02	89.71	112.13	
Axial Stress σ_1(kPa)	181.02	289.71	412.13	
Axial Strain ε (%)	7.24	8.55	7.89	
Shear StrengthParameters				
Cohesion (C) kPa/kN/m^2	30			
Internal Angle of Friction (φ)	4^0			
Failure Mode:	Bend/Shear			

Table D20 : Failure conditions for THU1

Moisture Content (w) %	45.12	44.33	45.25	44.9 (Mean)
Failure Conditions Data	**THU$_1$(i)**	**THU$_1$(ii)**	**THU$_1$(iii)**	
Cell Pressures σ_3 (kPa)	100	200	300	
Deviator Stress σ_d (kPa)	81.25	91.97	113.76	
Axial Stress σ_1(kPa)	181.25	291.97	413.76	
Axial Strain ε (%)	7.89	8.55	7.89	
Shear StrengthParameters				
Cohesion (C) kPa/kN/m^2	30			
Internal Angle of Friction (φ)	4^0			
Failure Mode:	Bend/Shear			

Table D21 : Failure conditions for KRU2

Moisture Content (w) %	44.84	43.75	43.52	44.04 (Mean)
Failure Conditions Data	**KRU$_2$(i)**	**KRU$_2$(ii)**	**KRU$_2$(iii)**	
Cell Pressures σ_3 (kPa)	100	200	300	
Deviator Stress σ_d (kPa)	37.38	41.50	65	
Axial Stress σ_1(kPa)	137.38	241.5	365	
Axial Strain ε (%)	7.89	5.92	7.89	
Shear Strength Parameters				
Cohesion (C) kPa/kN/m^2	8			
Internal Angle of Friction (φ)	5^0			
Failure Mode:	Lateral Bulging on the lower side			

Table D22 : Failure conditions for WMU2

Moisture Content (w) %	46.38	67.80	43.21	52.46 (Mean)
Failure Conditions Data	**WMU$_2$(i)**	**WMU$_2$(ii)**	**WMU$_2$(iii)**	
Cell Pressures σ_3 (kPa)	100	200	300	
Deviator Stress σ_d (kPa)	69.72	72.53	81.83	
Axial Stress σ_1(kPa)	169.72	272.53	381.83	
Axial Strain ε (%)	5.92	6.58	7.24	
Shear Strength Parameters				
Cohesion (C) kPa/kN/m^2	33.5			
Internal Angle of Friction (φ)	1.5^0			
Failure Mode:	Lateral Bulging on the lower side			

Table D23 : Failure conditions for MWU2

Moisture Content (w) %	47.57	46.67	44.29	46.18 (Mean)
Failure Conditions Data	**MWU$_2$(i)**	**MWU$_2$(ii)**	**MWU$_2$(iii)**	
Cell Pressures σ_3 (kPa)	100	200	300	
Deviator Stress σ_d (kPa)	75.82	75.29	83.47	
Axial Stress σ_1(kPa)	175.82	275.29	383.47	
Axial Strain ε (%)	6.58	7.24	7.24	
Shear StrengthParameters				
Cohesion (C) kPa/kN/m^2	35			
Internal Angle of Friction (φ)	2^0			
Failure Mode:	Lateral Bulging on the lower side			

Table D24 : Failure conditions for TBU2

Moisture Content (w) %	43.97	45.51	44.96	44.81 (Mean)
Failure Conditions Data	**TBU$_2$(i)**	**TBU$_2$(ii)**	**TBU$_2$(iii)**	
Cell Pressures σ_3 (kPa)	100	200	300	
Deviator Stress σ_d (kPa)	81.83	91.01	110.51	
Axial Stress σ_1(kPa)	181.83	291.01	410.51	
Axial Strain ε (%)	7.24	7.89	7.89	
Shear Strength Parameters				
Cohesion (C) kPa/kN/m^2	30			
Internal Angle of Friction (φ)	4^0			
Failure Mode:	Lateral Bulging on the lower side			

Table D25 : Failure conditions for THU2

Moisture Content (w) %	42.52	41.95	42.30	42.26 (Mean)
Failure Conditions Data	**THU$_2$(i)**	**THU$_2$(ii)**	**THU$_2$(iii)**	
Cell Pressures σ_3 (kPa)	100	200	300	
Deviator Stress σ_d (kPa)	83.47	109.72	117.01	
Axial Stress σ_1(kPa)	183.47	309.72	417.01	
Axial Strain ε (%)	7.24	8.55	7.89	
Shear Strength Parameters				
Cohesion (C) kPa/kN/m^2	47			
Internal Angle of Friction (φ)	2^0			
Failure Mode:	Lateral Bulging on the lower side			

Table D26 : Failure conditions for KRU3

Moisture Content (w) %	36.52	37.07	37.92	37.17 (Mean)
Failure Conditions Data	**KRU₃(i)**	**KRU₃(ii)**	**KRU₃(iii)**	
Cell Pressures σ_3 (kPa)	100	200	300	
Deviator Stress σ_d (kPa)	66.63	71.80	74.49	
Axial Stress σ_1(kPa)	166.63	271.8	374.49	
Axial Strain ε (%)	7.89	8.55	9.21	
Shear Strength Parameters				
Cohesion (C) kPa/kN/m²	30			
Internal Angle of Friction (φ)	2^0			
Failure Mode:	Lateral Bulging on the lower side			

Table D27 : Failure conditions for WMU3

Moisture Content (w) %	36.88	37.49	37.24	37.20 (Mean)
Failure Conditions Data	**WMU₃(i)**	**WMU₃(ii)**	**WMU₃(iii)**	
Cell Pressures σ_3 (kPa)	100	200	300	
Deviator Stress σ_d (kPa)	71.80	76.38	90.02	
Axial Stress σ_1(kPa)	171.8	276.38	390.02	
Axial Strain ε (%)	8.55	7.89	7.24	
Shear Strength Parameters				
Cohesion (C) kPa/kN/m²	29			
Internal Angle of Friction (φ)	3^0			
Failure Mode:	Lateral Bulging on the lower side			

Table D28 : Failure conditions for MWU3

Moisture Content (w) %	38.31	37.13	37.60	37.68 (Mean)
Failure Conditions Data	**MWU₃(i)**	**MWU₃(ii)**	**MWU₃(iii)**	
Cell Pressures σ_3 (kPa)	100	200	300	
Deviator Stress σ_d (kPa)	73.13	78	90.84	
Axial Stress σ_1(kPa)	173.13	278	390.84	
Axial Strain ε (%)	7.89	7.89	7.24	
Shear StrengthParameters				
Cohesion (C) kPa/kN/m²	32			
Internal Angle of Friction (φ)	2^0			
Failure Mode:	Lateral Bulging on the lower side			

Table D29 : Failure conditions for TBU3

Moisture Content (w) %	38.75	39.12	39.83	39.23 (Mean)
Failure Conditions Data	**TBU₃(i)**	**TBU₃(ii)**	**TBU₃(iii)**	
Cell Pressures σ_3 (kPa)	100	200	300	
Deviator Stress σ_d (kPa)	73.94	77.45	91.01	
Axial Stress σ_1(kPa)	173.94	277.45	391.01	
Axial Strain ε (%)	7.89	8.55	7.89	
Shear Strength Parameters				
Cohesion (C) kPa/kN/m²	30			
Internal Angle of Friction (φ)	2.5^0			
Failure Mode:	Lateral Bulging on the lower side			

Table D30 : Failure conditions for THU3

Moisture Content (w) %	39.56	38.67	37.69	38.64 (Mean)
Failure Conditions Data	**THU$_3$(i)**	**THU$_3$(ii)**	**THU$_3$(iii)**	
Cell Pressures σ_3 (kPa)	100	200	300	
Deviator Stress σ_d (kPa)	76.92	88.74	110.51	
Axial Stress σ_1(kPa)	176.92	288.74	410.51	
Axial Strain ε (%)	7.24	8.55	7.89	
Shear Strength Parameters				
Cohesion (C) kPa/kN/m^2	27			
Internal Angle of Friction (φ)	5^0			
Failure Mode:	Lateral Bulging on the lower side			

Appendix E: Deviatoric stress – strain trends for undisturbed soil samples - WMU1, WMU2 and WMU3
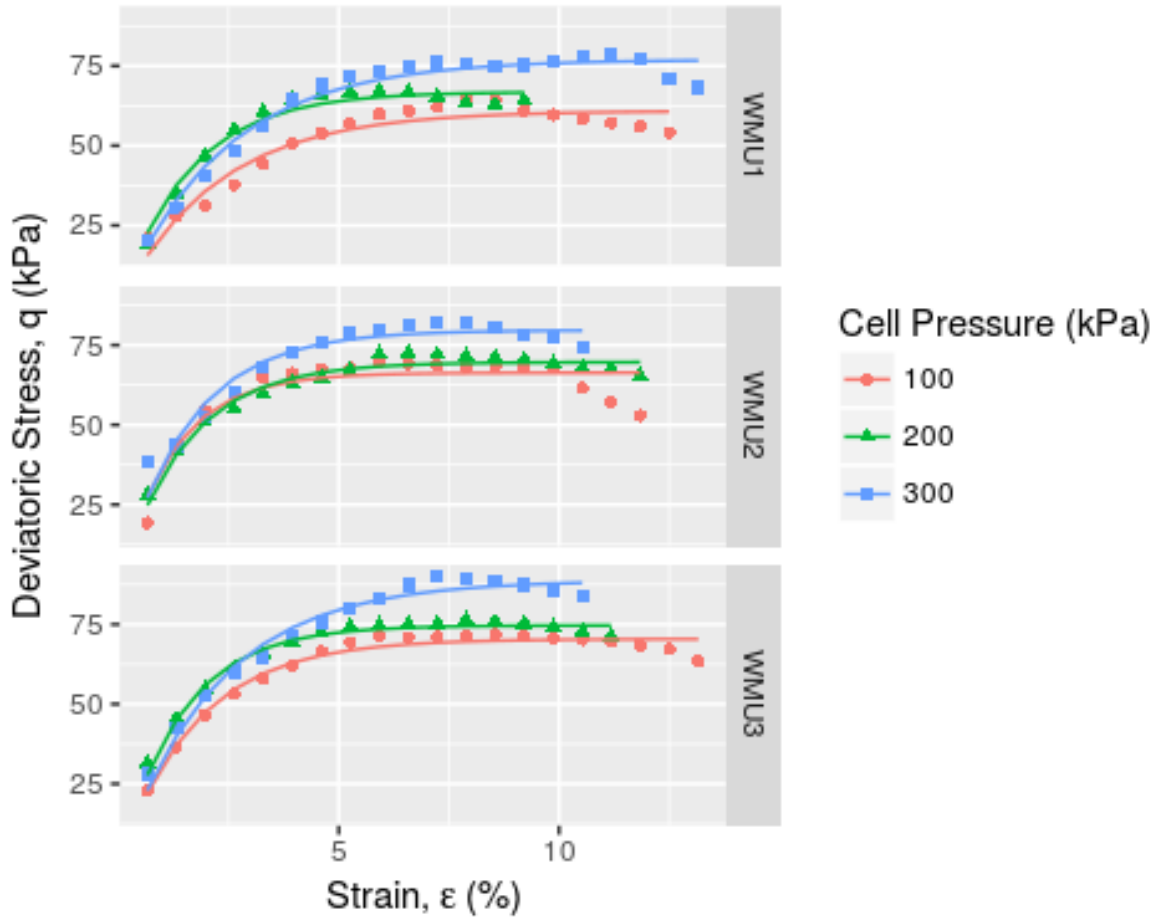
Appendix F: Deviatoric stress – strain trends for undisturbed soil samples - KRU1, KRU2 and KRU3
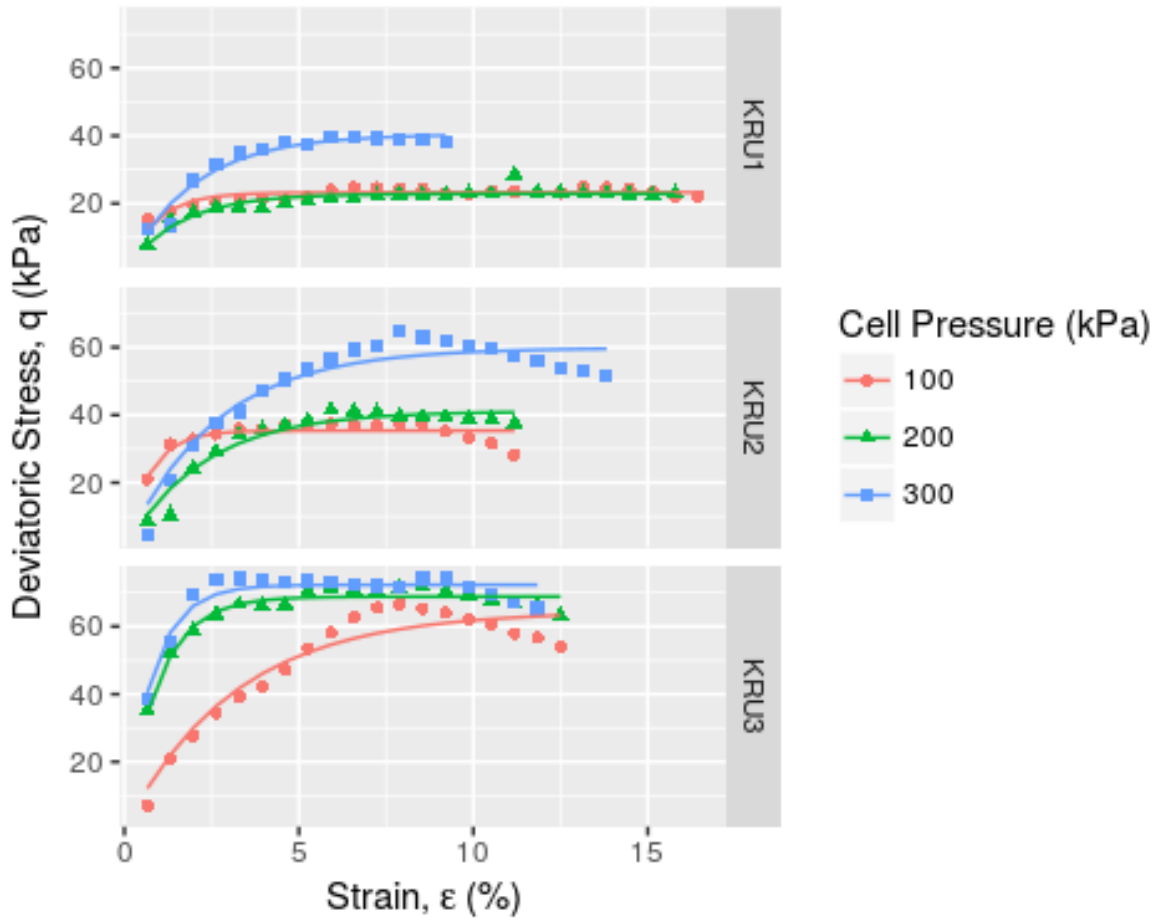
Appendix G: Deviatoric stress – strain with model parameters A and B Data

Appendix G1 : **Deviatoric stress – axial strain curves with model parameters A and B (standard errors in brackets) in recoverable, peak shear strength and residual/failure stress zones in the middle soil profile depth range (20 – 40 cm) at varying total confining stresses for disturbed samples**

Samples in (20 – 40 cm Depth) Middle Profile	Total Confining Stresses (kPa)	Non-linear recoverable deformation zone			Peak shear strength (kPa)	Residual/failure stress (kPa)
		A (kPa)	B	r^2		
KRD	100	156 (3.92)	0.269 (0.019)	0.984	150	150
WMD	100	205 (4.85)	0.176(0.009)	0.992	190	190
MWD	100	183 (4.67)	0.283(0.022)	0.968	190	190
TBD	100	190(6.40)	0.186(0.014)	0.981	190	190
THD	100	199(4.59)	0.193(0.010)	0.989	190	190
KRD	200	239(4.47)	0.282(0.016)	0.983	240	240
WMD	200	247(8.92)	0.181(0.015)	0.974	240	230
MWD	200	239(11.02)	0.215(0.026)	0.932	240	230
TBD	200	278(8.35)	0.177(0.012)	0.983	250	250
THD	200	274(7.63)	0.200(0.014)	0.982	250	250
KRD	300	261(3.69)	0.257(0.012)	0.984	252	250
WMD	300	274(2.79)	0.288(0.011)	0.989	270	250
MWD	300	276(2.78)	0.292(0.011)	0.988	280	250
TBD	300	284(5.23)	0.248(0.015)	0.978	290	270
THD	300	296(6.85)	0.205(0.013)	0.977	290	290

Table G2 : Deviatoric stress – axial strain curves with model parameters A and B (standard errors in brackets) in recoverable, peak shear strength and residual/failure stress zones in the bottom soil profile depth range (40 – 60 cm) at varying total confining stresses for disturbed samples

Samples in (40 – 60 cm Depth) Bottom Profile	Total Confining Stresses (kPa)	Non-linear recoverable deformation zone			Peak shear strength (kPa)	Residual/failure stress (kPa)
		A (kPa)	B	r^2		
KRD	100	178 (4.19)	0.235 (0.014)	0.989	160	160
WMD	100	181(5.65)	0.226(0.018)	0.981	180	170
MWD	100	201 (5.62)	0.212(0.014)	0.986	180	180
TBD	100	205(5.88)	0.206(0.014)	0.987	200	200
THD	100	196(5.69)	0.258(0.021)	0.972	190	190
KRD	200	244(3.71)	0.281(0.014)	0.986	240	240
WMD	200	309(8.51)	0.199(0.014)	0.980	290	260
MWD	200	242(9.44)	0.225(0.024)	0.944	240	240
TBD	200	315(12.07)	0.188(0.017)	0.966	280	280
THD	200	321(10.02)	0.189(0.014)	0.979	300	300
KRD	300	275(3.39)	0.247(0.009)	0.988	260	260
WMD	300	322(5.28)	0.209(0.010)	0.985	300	280
MWD	300	330(6.15)	0.207(0.011)	0.980	300	300
TBD	300	338(6.52)	0.206(0.011)	0.979	330	300
THD	300	349(6.89)	0.192(0.010)	0.985	310	310

Table G3 : Deviatoric stress – axial strain curves with model parameters A and B (standard errors in brackets) in recoverable, peak shear strength and residual/failure stress zones in the top soil profile depth range (0 – 20 cm) at varying total confining stresses for undisturbed samples

Samples in (0 – 20 cm Depth) Top Profile	Total Confining Stresses (kPa)	Non-linear recoverable deformation zone			Peak shear strength (kPa)	Residual/failure stress (kPa)
		A (kPa)	B	r^2		
KRU	100	23 (0.295)	1.14 (0.123)	0.718	20	20
WMU	100	60.90 (1.43)	0.45(0.044)	0.918	62.5	62.5
MWU	100	75.18 (0.91)	0.727(0.055)	0.932	75	75
TBU	100	73.48(1.70)	0.607(0.079)	0.839	80	75
THU	100	73.37(1.99)	0.514(0.071)	0.841	75	70
KRU	200	22.84(0.40)	0.645(0.066)	0.839	20	20
WMU	200	66.86(1.09)	0.626(0.043)	0.974	64	64
MWU	200	77.22(1.98)	0.844(0.147)	0.702	78	78
TBU	200	82.26(1.69)	0.737(0.095)	0.817	90	80
THU	200	84.16(1.92)	0.525(0.061)	0.873	90	80
KRU	300	40.44(1.08)	0.514(0.051)	0.950	40	40
WMU	300	76.99(1.18)	0.424(0.027)	0.966	75	75
MWU	300	98.27(1.94)	0.568(0.061)	0.868	100	100
TBU	300	99.02(1.89)	0.587(0.062)	0.865	110	100
THU	300	101.36(2.03)	0.538(0.056)	0.876	110	105

Table G4 : Deviatoric stress – axial strain curves with model parameters A and B (standard errors in brackets) in recoverable, peak shear strength and residual/failure stress zones in the bottom soil profile depth range (40 – 60 cm) at varying total confining stresses for undisturbed samples

Samples in (40 – 60 cm Depth) bottom Profile	Total Confining Stresses (kPa)	Non-linear recoverable deformation zone			Peak shear strength (kPa)	Residual/failure stress (kPa)
		A (kPa)	B	r^2		
KRU	100	64.52 (2.48)	0.32 (0.039)	0.926	60	60
WMU	100	70.41 (0.74)	0.57 (0.029)	0.969	70	70
MWU	100	70.26 (1.06)	0.57 (0.042)	0.939	70	70
TBU	100	70.37 (1.32)	0.56 (0.052)	0.911	70	70
THU	100	70.10 (1.53)	0.60 (0.068)	0.865	70	70
KRU	200	68.83 (0.61)	1.04 (0.064)	0.936	70	70
WMU	200	74.68 (0.61)	0.70 (0.029)	0.981	75	75
MWU	200	74.41 (0.80)	0.65 (0.035)	0.971	75	75
TBU	200	73.80 (0.78)	0.66 (0.034)	0.972	73	73
THU	200	84.58 (1.10)	0.55 (0.032)	0.971	80	80
KRU	300	72.29 (0.81)	1.24 (0.104)	0.893	72	72
WMU	300	88.79 (1.39)	0.45 (0.026)	0.978	87.5	87.5
MWU	300	87.57 (1.38)	0.48 (0.029)	0.973	84	84
TBU	300	86.56 (1.01)	0.60 (0.031)	0.976	90	80
THU	300	105.28 (2.68)	0.42 (0.037)	0.953	105	105

Appendix H: Definitions of Terminologies

Adhesion: Attraction between molecular forces of dissimilar materials.

Anistropic Consolidation: Consolidation of a test sample under stresses in which the vertical effective stress is different from the horizontal effective stress.

Atterberg Limits (AL): Water content at the boundaries between adjacent soil states

Axial Stress: Vertical stress on the test specimen due to axial load applied or summation of deviatoric and confining stresses.

Back Pressure: Is pressure applied to a pore fluid within a test sample.

Cohesion: Is the intermolecular attraction between particles of similar materials.

Compaction: Rapid compression due to application of momentary pressure (loading).

Confining Pressure : All round pressure on test specimen within a triaxial cell.

Consolidation: Is the gradual compression or reduction in volume of soil mass caused by application of a sustained pressure and due principall to expulsion of water from soil voids and accompanid by a transfer of pressure from pore water to the soil solids.

Deviatoric Stress: Is the axial stress less confining stress.

Effective Stress : Difference between the total stress (pressure) and pore pressure.

Failure: A state in which shear resistance is exceeded or when stresses or strains reach critical or limiting value.

Fully Saturated Soil: Soil in which the void space are filled with water.

Isotropic Consolidation: Consolidation of test specimen under the influence of an all round hydrostatic pressure in which vertical effective stress and horizontal effective are equal.

Liquid Limit (LL): Water content at which soil passes from plastic state to liquid state.

Optimum Water Content for Tillage (OPT): Is the moisture content of soil at which tillage produce the largest number of small aggregates.

Partly Saturated Soil: Soil in which the void spaces are filled with air and water.

Plasticity: Being deformed without rupture and without elastic rebound and without noticeable change in volume.

Plasticity Limit (PL): Water content at which soil passes from plastic state to semi solid state.

Pore Water Pressure: Pressure of water contained in the void spaces of the soil

Puddling: Wet tillage/wet ploughing.

Shrinkage Limit (SL): Water content at which soil tends to pass from semi solid to solid state.

Slip: Soil displacement that occurs during conversion of soil strength into traction.

Soil: A three phase system consisting of solid particles, water and air in varying proportion.

Soil Structure: Is the arrangement of soil particles in a soil mass.

Soil Texture : Is the size and relative proportion of sand, silt and clay in a soil mass.

Tillage: Physical manipulation of soil with appropriate implement to loosen surface soil layer.

Total Stress : Actual stress in a soil masss due to the application of a specific pressure or force.

Traction: Driving force/forward thrust developed by the wheels or tracks of a tractive equipment in contact with soil.

Vertical Stress: The stress applied to test sample in the vertical direction.

Yielding: Permanent deformation/plastic deformation.